

ABSTRACT

Title of dissertation: HYDROGENIC SPIN QUANTUM COMPUTING
 IN SILICON AND DAMPING AND DIFFUSION
 IN A CHAIN-BOSON MODEL

Andrew J. Skinner, Doctor of Philosophy, 2006

Dissertation directed by: Professor Bei-Lok Hu
 Department of Physics

We propose an architecture for quantum computing with spin-pair encoded qubits in silicon. Electron-nuclear spin-pairs are controlled by a DC magnetic field and electrode-switched on and off hyperfine interaction. This digital processing is insensitive to tuning errors and easy to model. Electron shuttling between donors enables multi-qubit logic. These hydrogenic spin qubits are transferable to nuclear spin-pairs, which have long coherence times, and electron spin-pairs, which are ideally suited for measurement and initialization. The architecture is scaleable to highly parallel operation.

We also study the open-system dynamics of a few two-level systems coupled together and embedded in a crystal lattice. In one case, superconducting quantum interference devices, or SQUIDS, exchange their angular momenta with the lattice. Some decaying oscillations can emerge in a lower energy subspace with a longer coherence time. In another case, the exchange coupling between spins-1/2 is strained by lattice distortions. At a critical point energy level crossing, four well-spaced spins

dissipate collectively. This is partially true also for the two- or three-SQUID-chain.

These collective couplings can improve coherence times.

HYDROGENIC SPIN QUANTUM COMPUTING IN SILICON
AND
DAMPING AND DIFFUSION IN A CHAIN-BOSON MODEL

by

Andrew J. Skinner

Dissertation submitted to the Faculty of the Graduate School of the
University of Maryland, College Park in partial fulfillment
of the requirements for the degree of
Doctor of Philosophy
2006

Advisory Committee:

Professor Bei-Lok Hu, Chair
Professor Michael Coplan
Professor Theodore Jacobson
Professor Bruce Kane
Professor William Phillips
Professor Victor Yakovenko

© Copyright by
Andrew J. Skinner
2006

ACKNOWLEDGMENTS

This milestone would not have been reached without the influence and support of a large number of people.

Among many excellent and inspiring mentors I would like especially to thank: Bill Wootters for revealing the foundations of quantum physics; Thomas Murdock for cultivating my critical thinking and leadership skills; Edmond Roelof for inspiring me to be a scientist, and a mathematical one; Ted Jacobson for teaching me quantum mechanics and geometrical methods; Sam Lomonaco for frequent interesting discussions and mathematical instruction; and Bruce Kane for challenging and collegial research and his never-ending moral support.

Michael Coplan first invited me to the University of Maryland and fostered my hands-on skills, from research electronics to machine tools and drafting. I used his textbook on building scientific apparatus to design, patent, and produce the Welkin[®] pencil which inscribed every equation in this work.

It was a joy to work with Bruce Kane and Michael Davenport on our proposal for hydrogenic spin quantum computing in silicon. I especially enjoyed my time at the Laboratory for Physical Science and am grateful to Marc Manheimer and his colleagues for their patient financial support. Jane Hessing cheerfully managed my affairs with the University and deserves special mention for the encouragement she offered me at difficult moments.

I am very grateful to Eugene Chudnovsky for his friendly and helpful advice on the SQUID-phonon coupling, and to Frederick Strauch, Philip Johnson, and Sanjiv Shresta for their instruction on the inductive and capacitive couplings between SQUIDs. Oleg Tchernyshyov also deserves credit for his kind counsel on spin-chains and their coupling to phonons.

I am deeply indebted to Bei-Lok Hu for his generous interest in the chain-boson model and my career, and especially for his candid and very valuable advice about my physics and its presentation.

Among my fellow students, Peter Weingartner deserves credit for teaching me technical elegance: from Unix and C to LaTeX and postscript. Thanks also go to Dave Wren for partnering with me in our research electronics class and to Brian Dorland and Joseph Howard for progressing with me from the Midcourse Space Experiment to graduate studies in physics. Dan Sullivan at the Laboratory for Physical Science kindly appreciated my foundational and mathematical leanings in physics. Friendly chats with Arthur Cole about physics graduate school and the rest of world helped keep me sane, as did the rock climbing and mountaineering with Matt Esson, the flying of model rockets with Sean Belouin, and the piloting of R/C gliders with Bradford Behr. I am especially grateful to Brad for his constant enthusiasm and confidence in my various endeavors, and for his and his wife Virginia's hospitality during my time as an itinerant student of physics.

My in-laws deserve special credit for their unquestioning support, which has carried me over many obstacles and helped my own family to blossom, and for being such interesting and genuinely good people. My step-father has also been keenly

aware of and responsive to the hurdles I have encountered.

I am grateful to my brother and sister for their encouragement and for being such wonderful role models; in them I see the generous spirit of my father and the sensible optimism of my mother. Words cannot express my gratitude to my father, who with boundless energy engaged me in interesting projects and adventures, and my mother, who sacrificed so much and so many years later still helped me through the toughest times of this project with logistical and moral support. I am especially proud of my mother for her cheerful perseverance in science, politics, and life.

Finally, I owe my deepest gratitude to my wife for her loving and patient support, her inspirational awareness and balance, and for giving me such beautiful and cheerful children who are surely our greatest accomplishment.

TABLE OF CONTENTS

1	Introduction	1
1.1	Solid State Encoded Qubits	1
1.2	Overview	3
1.3	Hydrogenic Spin Quantum Computing	3
1.4	The Chain-Boson Model	5
1.5	Key Results	9
2	Hydrogenic Spin Quantum Computing in Silicon: a Digital Approach	11
2.1	Abstract	11
2.2	Introduction to the Kane Quantum Computer	12
2.3	Encoding of Logical Qubits	13
2.4	Digital Hyperfine Control	15
2.5	Electron Shuttling	16
2.6	The Model Hamiltonian and its Invariant Subspaces	18
2.7	Resonant Hyperfine Stepping	19
2.8	Single Qubit Gates	24
2.9	Two Qubit Gates	27
2.10	Gate Times and Errors	34
2.11	Tuneable Fidelity	35
2.12	The Nuclear Spin-Pair Quantum Memory	37
2.13	Readout, Initialization, and Refrigeration	38
2.14	Conclusion	39
2.15	Appendix: Subtleties of Resonant Hyperfine Stepping	41
2.15.1	Relative Phases Between Invariant Subspaces	41
2.15.2	Distinction from Electron Spin Resonance	44
3	Damping and Diffusion of a Few Coupled SQUIDs in a Phonon Bath	46
3.1	Abstract	46
3.2	Introduction	46
3.3	The Unbiased SQUID	51
3.4	The Heisenberg SQUID Chain	52
3.5	The Harmonic Phonon Bath	54
3.6	The Chain-Bath Coupling	55
3.7	The Formalism	58
3.8	The Coefficients	60
3.8.1	The Bath Correlator	61
3.8.2	The Spectral Densities	64
3.8.3	The Markov Approximation	67
3.9	The Born-Markov Master Equation	70
3.10	The Four Generators	72
3.10.1	The Renormalization	73
3.10.2	The Anomalous Diffusion	75

3.10.3	Renormalizing the Chain	76
3.10.4	The Damping and Diffusion	78
3.11	Numerical Simulations	81
3.12	Discussion	82
3.13	Conclusion	83
4	Damping and Diffusion of A Heisenberg Few-Spin Chain in a Phonon Bath	86
4.1	Abstract	86
4.2	Introduction	86
4.3	The Heisenberg Spin Chain	89
4.4	The Harmonic Phonon Bath	92
4.5	The Chain-Bath Coupling	93
4.6	The Formalism	95
4.7	The Coefficients	96
4.7.1	The Bath Correlator	96
4.7.2	The Markov Approximation	98
4.8	The Four Generators	100
4.8.1	The Renormalization	101
4.8.2	The Anomalous Diffusion	102
4.8.3	The Damping and Diffusion	103
4.9	Numerical Simulations	104
4.10	Discussion	106
4.11	Conclusion	107
5	Summary	109
5.1	P donor spins in Si	109
5.2	The Chain-Boson Model	110
5.3	Relevance	112
	Bibliography	113

Chapter 1

Introduction

1.1 Solid State Encoded Qubits

A quantum computer comprising many two-level systems, or “qubits,” could, in principle, evolve a superposition of many different bit-strings into an entangled state in which “input” and “output” registers are correlated according to the input and output values of a desired function. The computer’s unitary evolution is, in effect, parallel processing the different inputs. The entangled state contains correlations which are stronger than what can be explained classically. They are strong enough that global properties of the function, such as its period, can be obtained exponentially faster than in a classical computation.

Proposals for quantum computation in the solid state stand to benefit from the rapid advances in semiconductor electronics and are potentially scalable to large arrays of qubits controlled by gate electrodes. Example qubits include electron spins in quantum dots [1], P donor spins in Si [2], Cooper-Pair Boxes [3], and SQUIDS [4, 5].

The implementation and precise control of a register of quantum bits are formidable technical challenges. A good design seeks to minimize difficulties in construction and operation. Sometimes it helps to “encode” each logical qubit, e.g. $\alpha |0\rangle + \beta |1\rangle$, in multiple physical qubits, for example in a pair of spins-1/2 with

$|0\rangle \equiv (|\uparrow\downarrow\rangle - |\downarrow\uparrow\rangle)/\sqrt{2}$ and $|1\rangle \equiv (|\uparrow\downarrow\rangle + |\downarrow\uparrow\rangle)/\sqrt{2}$. Encoding often results in reduced constraints on computer design [6, 7].

Another issue is the qubits' unavoidable coupling to environmental noises which can destroy the quantum information and thwart the computation. The loss of the quantum information is generally called “decoherence.” When perturbed by a weak coupling to the environment, most superpositions decay into random statistical mixtures of stationary states. This is caused by fluctuations in the controlling fields as well as the absorption and (possibly spontaneous) emission of quanta. Quantum error prevention techniques have been proposed to lower the error rates below a threshold 1 error per 10^4 or 10^5 gate operations so that quantum error correction techniques can then realize the power of quantum computation [8].

Qubit encoding is also the key ingredient in quantum error correction, by providing a redundancy with which to diagnose and correct errors [9], and quantum error prevention, by storing the logical qubit in a decoherence-free subspace [10, 11, 12]. These subspaces can arise from the symmetries of a collective coupling to the environment, in which the physical qubits are so close together that each couples, in effect, to the same environmental variable as the others.

1.2 Overview

This dissertation has two main components. In the first we propose an architecture for encoded quantum computation using P donor spins in Si. The encoding has nothing to do with quantum error correction or prevention; instead it facilitates

the use of digital control and electron shuttling. These in turn solve a variety of problems with the original design [2] for unencoded quantum computation with P donor spins in Si. The proposal is detailed extensively in chapter 2 and concisely in [13].

In the second, unrelated, component we develop two models for the decoherence of a chain of a few coupled qubits: coupled SQUIDs exchanging their angular momenta with a crystal lattice (chapter 3); and spins whose exchange coupling is strained by lattice distortions (chapter 4). We find that some or all of the benefits of a collective coupling to the environment can be obtained, even for distant physical qubits, if we arrange a critical level of interaction between the physical qubits. We also find that, in the SQUID chain, some decaying oscillations can emerge in a lower energy subspace with a longer coherence time; there are two equally-spaced pairs of energies, and a superposition of the upper two eigenstates relaxes coherently.

1.3 Hydrogenic Spin Quantum Computing

Donor nuclear spins in silicon are especially good solid state qubits because of their long coherence times. They can in principle be controlled by hyperfine-tuned magnetic resonance techniques and coupled by the electron exchange interaction when carefully tuned surface gate voltages properly position the donors' electrons [2]. However, this "exchange mediation" is restricted to nearest neighbor interactions and is extremely difficult to control [14, 15]; the coupling strength is very sensitive to the electrons' positions, exhibiting rapid oscillations due to Si band structure

[16, 17]. Precise tuning of the hyperfine interaction will also be difficult. In this work we present an alternative donor spin architecture which tolerates tuning errors and overcomes nearest neighbor restrictions.

Our proposal relies on the “encoding” of each logical qubit, $\alpha|0\rangle + \beta|1\rangle$, in the $J_z = 0$ subspace of a pair of spins: $|0\rangle \equiv (|\uparrow\downarrow\rangle - |\downarrow\uparrow\rangle)/\sqrt{2}$ and $|1\rangle \equiv (|\uparrow\downarrow\rangle + |\downarrow\uparrow\rangle)/\sqrt{2}$. When the two spins are donor nuclei the qubit benefits from their long coherence times. On the other hand, measurements are facilitated when the two spins are electrons [18, 19]. Following Levy, who proposed Heisenberg-only quantum computing with distinct magnetic moments in a static magnetic field [20, 6, 21], we will show that when the two spins are an electron and its donor nuclear spin (“a hydrogenic spin qubit”) the qubits are easier to control and can be coupled, well beyond their nearest neighbors, with electron shuttling.

In the hydrogenic spin qubit the electron and donor nuclear spins are coupled by the hyperfine interaction. The ground state coupling for P donors in Si, $H_A = A\vec{\sigma}_e\vec{\sigma}_n$, is ideally suited to quantum computing because its strength, determined by the electron-donor overlap, $|\psi(0)|^2$, is a quadratic, and thus insensitive, function of any small perturbing electric field. We can use a surface “A-gate” voltage to draw the electron off the nucleus, effectively switching off the coupling ($H_A \rightarrow 0$) to a regime which is similarly insensitive to tuning errors. We therefore propose a digital approach [1], in which the hyperfine interaction is switched on and off in a globally applied static magnetic field to implement single qubit logic.

Electron spin coherence distances of over 100 μm have been demonstrated [22], so single electron shuttling [23] to remote donor sites is a good candidate for enabling

two-qubit interaction. Arrays of “S-gate” electrodes between qubits are thus used to shuttle individual electrons from site to site. Two qubits become entangled when the hyperfine interaction is applied between the electron of one qubit and the nucleus of another. This is analogous to ion-trap proposals in which ions, and thus their quantum information, can be transported from one local trap to another [24, 25]. This transport is considerably more efficient than a bucket brigade series of nearest neighbor interactions and can circumvent misbehaved donor sites.

1.4 The Chain-Boson Model

The spin-boson model [26] has been widely applied towards a better understanding of the environment’s effect on qubit coherence. In the spin-boson model, a two-level system is coupled to an environment of oscillators which model a heat bath, such as is often used in studies of quantum Brownian motion [27, 28]. Because of the coupling, the system becomes entangled with the bath. When averaged over environmental outcomes, the system typically loses coherence and thermalizes.

In light of qubit encoding schemes and the desire to process and protect quantum information, it is necessary to study the decoherence of multiple qubits. In the chain-boson model one embeds a chain of qubits in a bosonic bath so that the qubits experience a location-dependent interaction with the bath variables.

For a system comprising a register of qubits, two types of system-bath coupling have already been extensively considered. The simplest is a collective coupling, in which each qubit couples to the same environmental variable as the rest. This

is appropriate to scenarios where the qubits are spaced closer together than the relevant wavelengths of the bath, i.e. those corresponding to the qubits' transition frequencies. The symmetries of the collective coupling can lead, with certain system Hamiltonians, to decoherence free subspaces [11, 29, 12] and Dicke superradiance [30, 31].

The other commonly used type of system-bath coupling is the independent coupling model, in which each qubit couples to its own bath, separate from the baths used for the other qubits. This is an appropriate model for qubits spaced farther apart than the relevant wavelengths of the bath. And in the context of solid state qubits, a significant source of noise is the voltage leads that control the qubits. With one lead per qubit, the independent baths model is a natural assumption. The independent coupling model has been used to study the decoherence during two-qubit logic gates [32, 33] as well as the entanglement rate for coupled qubits [34].

When there is one voltage lead controlling multiple qubits, one typically uses the collective coupling model, as each qubit is experiencing the same electronic noise. A likely scenario for a pair of qubits is an independent lead for each qubit as well as one common lead. For this case, the disentangling and decohering of the qubits has been considered [35]. Several works compare the collective and independent bath scenarios for coupled qubits [36, 37, 38, 39]. Fine-tuning the inter-qubit coupling to protect against collective dissipation has also been studied [40]. In comparison, the optimum qubit-qubit coupling was examined for the case of independent dissipation [41, 42].

Most studies fall into these two categories, whether the qubits are coupled together or not. But for *uncoupled* qubits there has been careful consideration of the intermediate scenario, in which the qubits are neither far apart nor close together [43, 44, 45]. The relaxation and decoherence rates depend on $\vec{k} \cdot \vec{R}$, where \vec{R} connects the qubits and the \vec{k} are the bath wavevectors that interact with the qubits. These results make an elegant transition between the two limiting cases of qubits close together and far apart. In the intermediate scenario the bath can induce entanglement between uncoupled qubits [46], as can also happen with a collective coupling to the bath [47].

In this dissertation, an essential point is that in a chain of *coupled* qubits the inter-qubit couplings can play a crucial role in determining which are the relevant bath wavevectors and thus whether the qubits couple collectively or independently to the bath. In our models, there is a critical point energy level crossing at which some transition frequencies are so slow that $\vec{k} \cdot \vec{R} \ll 1$ even though the qubits may be far apart with respect to the uncoupled qubits' transition frequencies. At the critical point the chain can obtain some or all of the benefits of a collective coupling to the bath. Another result is the possibility for decaying quantum oscillations to emerge in a lower energy subspace with an improved coherence time. We believe this phenomenon is related to some prior research on automatic quantum error correction [48].

There have been some other works whose equations include the intermediate regime for coupled qubits [49, 50] but the role of the inter-qubit coupling in determining the relevant bath wavevectors and their relation to the inter-qubit distance

is not evident.

1.5 Key Results

We propose that hydrogenic spin qubits and coherent single electron shuttling can enable a silicon-based quantum computer featuring digital hyperfine control insensitive to tuning errors, a long-lived nuclear spin memory, a projective readout scheme, and qubit refrigeration in which 50% of the qubits can be initialized at high temperature. The computer is scalable to highly parallel operation because digital shuttling of electrons overcomes nearest neighbor restrictions. Donors can be irregularly spaced and far apart, allowing for large gate electrodes, and malfunctioning donor sites can be diagnosed and avoided. These many benefits motivate further research on the coherent shuttling and measurement of electron spins, extremely pure Si fabrication, encoding and error-correction techniques, optimal control sequences, and the spin-orbit and dipole-dipole interactions during realistic electrode driven switching and shuttling.

We also develop a chain-boson model for the open-system dynamics, in the Born-Markov approximation, of coupled qubits embedded in a bosonic bath and experiencing a location-dependent coupling to the environment. Our master equation shows how to renormalize the chains and how the coefficients of damping and diffusion lead to relaxation, decoherence, and thermalization, as well as the possibility for decaying oscillations to emerge in a lower energy subspace (this can occur, for example, in our SQUID-chain model). By including a location-dependent coupling

to the bath, we see a way to use inter-qubit couplings to protect quantum information. They can provide a critical point energy level crossing at which some or all of the benefits of a collective coupling may be obtained. In the exchange-strained spin-chain, for example, a non-degenerate subspace becomes decoherence-free.

Chapter 2

Hydrogenic Spin Quantum Computing in Silicon: a Digital Approach

This chapter's work was a collaboration with Michael Davenport under the supervision of Dr. Bruce Kane. A concise report has already been published [13].

2.1 Abstract

We suggest an architecture for quantum computing in which pairs of electron and donor nuclear spins in silicon act as qubits. Levy first proposed Heisenberg control of qubits encoded in spin-1/2 pairs with distinct Landé g-factors in a magnetic field [20]. We specialize this idea to P donors in Si. Voltage pulses to electrodes above donor sites turn the hyperfine interaction on and off. This digital hyperfine processing is insensitive to tuning errors, minimizes the number and variation of physical parameters and is easy to model. Pulses to electrodes between sites shuttle electrons from donor to donor to enable multi-qubit logic. These “hydrogenic spin” qubits are transferable to nuclear spin-pairs, which have long coherence times, and electron spin-pairs, which are ideally suited for measurement and initialization by a projective measurement of singlet vs. triplet charge configuration beneath a single electron transistor. The architecture is scalable to highly parallel operation. The clock rate and magnetic field can be tuned for optimal fidelity, adjusting for vagaries in the pulse shape and strength. Simulated one and two qubit gates take less than

$5 \mu\text{s}$ and have errors less than 10^{-5} even for fractional variations of field or frequency as large as 10^{-5} .

2.2 Introduction to the Kane Quantum Computer

A quantum computer comprising many two-level systems, or “qubits,” exhibits coherent superpositions (the incompatibility of certain observables) and entanglement (strong correlations between qubits). These quantum features may be harnessed to solve problems which are essentially impossible for a classical computer, such as the factorization of large integers or the simulation of many-body quantum systems [8]. Solid state implementations stand to benefit from the rapid advances in semiconductor electronics and are potentially scalable to large arrays of qubits controlled by gate electrodes.

Donor nuclear spins in silicon are especially good solid state qubits because of their long coherence times. In Kane’s original proposal for a spin based solid state quantum computer [2] the donor nuclear spins serve as qubits, hyperfine-tuned magnetic resonance is used to control individual qubits, and adjacent qubits can be coupled by the electron exchange interaction when carefully tuned surface gate voltages properly position the donors’ electrons. There are many advantages to the Kane proposal. It leverages modern semiconductor technologies and the nuclear spin qubits are well isolated from interaction with the environment.

There are also a number of disadvantages. The exchange-mediated qubit coupling requires the qubits to be in close and regular proximity under nanometer

sized electrodes, and qubit interaction is restricted to nearest-neighbor coupling. The electron mediated interaction strength, effected by “J” gate electrodes between donors, is extremely difficult to control [14, 15]; its strength is very sensitive to the electrons’ positions, exhibiting rapid oscillations due to Si band structure [16, 17]. the hyperfine interaction, effected by “A” gate electrodes above donors, must be tuned precisely to resonance with an AC magnetic field which will, in turn, heat the computer; and readout by singlet vs. triplet charge configuration is not projective (because the triplet outcome is ambiguous). In this work we present an alternative donor spin architecture which tolerates tuning errors and overcomes nearest neighbor restrictions.

2.3 Encoding of Logical Qubits

Any successful implementation of a quantum computer will likely take advantage of error-correction schemes [8] and/or decoherence-free subspaces [11, 29, 51]. In the context of spin based quantum computing, researchers have proposed encoding each logical qubit in multiple spins. We are led to consider the ramifications of simple encoding schemes in the Kane quantum computer.

Indeed, other proposals for encoded spin based quantum computing do away with magnetic resonance and exchange mediation, using only spin-spin interaction. DiVincenzo et. al. showed how to do this with the exchange interaction by encoding each qubit in three spins [7, 52, 53]. By including a static magnetic field, Levy proposed Heisenberg-only quantum computing for qubits encoded in the $J_z = 0$

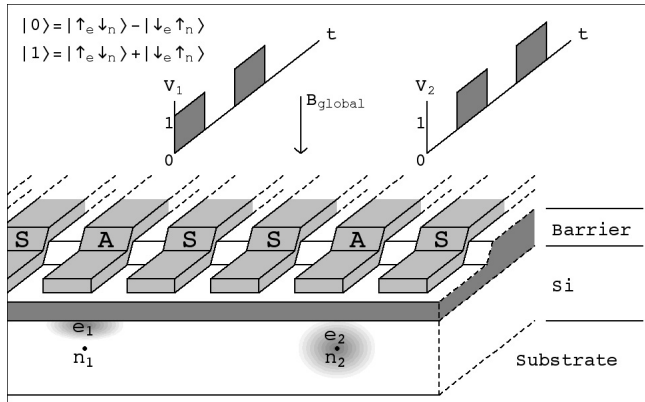


Figure 2.1: Schematic of the proposed architecture. Each qubit is encoded in the spins of an electron and its donor nucleus. “A-gates” above donor sites switch the electron-donor overlap, and thus the hyperfine interaction, while “S-gates” shuttle electrons from donor to donor. “Bit trains” of voltage pulses control the computer. In this instance: the “ e_1n_1 ” qubit evolves solely due to a uniform magnetic field while hyperfine interaction within the e_2n_2 qubit is applied for a single qubit operation. One clock cycle later: e_1n_1 will experience hyperfine interactions while e_2n_2 will not.

subspace of two spins with different magnetic moments [20, 6]. Benjamin specialized Levy’s idea to square pulses of various strengths and durations [21].

Our proposal relies on the “encoding” of each logical qubit, $\alpha|0\rangle + \beta|1\rangle$, in the $J_z = 0$ subspace of a pair of spins: $|0\rangle \equiv (|\uparrow\downarrow\rangle - |\downarrow\uparrow\rangle)/\sqrt{2}$ and $|1\rangle \equiv (|\uparrow\downarrow\rangle + |\downarrow\uparrow\rangle)/\sqrt{2}$. When the two spins are donor nuclei the qubit benefits from their long coherence times. On the other hand, measurements are facilitated when the two spins are electrons [18, 19]. Following Levy, who proposed Heisenberg-only quantum computing with distinct magnetic moments in a static magnetic field [20, 6, 21], we will show that when the two spins are an electron and its donor nuclear spin (“a hydrogenic spin qubit”) the qubits are easier to control and can be coupled, well beyond their nearest neighbors, with electron shuttling.

2.4 Digital Hyperfine Control

In the hydrogenic spin qubit the electron and donor nuclear spins are coupled by the hyperfine interaction. The ground state coupling for P donors in Si, $H_A = A \vec{\sigma}_e \cdot \vec{\sigma}_n$ with $A = 121.517 \pm 0.021$ neV [54], is ideally suited to quantum computing because its strength, determined by the electron-donor overlap, $|\psi(0)|^2$, is a quadratic, and thus insensitive, function of any small perturbing electric field. Here $\vec{\sigma} \equiv (\sigma^x, \sigma^y, \sigma^z)$ are the Pauli operators, labeled by the spin on which they operate.

As depicted in Figure 2.1, we can use a surface “A-gate” voltage to draw the electron off the nucleus, effectively switching off the coupling ($H_A \rightarrow 0$) to a regime which is similarly insensitive to tuning errors. We can avoid tuning the hyperfine strength if we work with a digital approach [1], in which the interaction is only on or off for a sufficient time to give the desired integrated strength; effectively we are trading tuning complexity for timing complexity. However, at the cost of discretizing the available integrated strengths, we can compose an integrated “on” pulse with a “bit train” of pulses from a pulse-pattern generator.

The hyperfine control generates the electron-donor ($e-n$) spin swap $|0\rangle + |1\rangle \leftrightarrow |0\rangle - |1\rangle$ and we augment this with a globally applied static magnetic field, which generates $|0\rangle \leftrightarrow |1\rangle$. For $\mathcal{O}(1 \text{ mT})$ fields the two generators are of comparable strength and an alternating series of interactions implements single qubit logic in direct analogy with Euler’s theorem for constructing an arbitrary rotation from a sequence of rotations about distinct axes [8].

2.5 Electron Shuttling

We also want to overcome the restriction to nearest-neighbor coupling and the difficulties of exchange mediation. Electron spin coherence distances of over $100\ \mu\text{m}$ have been demonstrated [22], so single electron shuttling [23] to remote donor sites is a good candidate for enabling two-qubit interaction. As shown in Figure 2.2, arrays of “S-gate” electrodes between qubits are thus used to shuttle individual electrons from site to site. This is analogous to ion-trap proposals in which ions, and thus their quantum information, can be transported from one local trap to another [24, 25]. This transport is considerably more efficient than a bucket brigade series of nearest neighbor interactions and can circumvent donor sites which have been diagnosed as unreliable for hydrogenic spin quantum computing, due to contamination or poor donor placement or any other undetermined reason.

Inter-qubit entanglement is necessary for implementing conditional logic operations. Two qubits become entangled when the hyperfine interaction is applied between the electron of one qubit and the nucleus of another. Speaking intuitively, a single qubit operation is being performed on a new qubit whose information is shared *non-locally* by the two qubits being entangled. Actually, as will be explained later, it is much more subtle: the operation causes entanglement *and* decoherence by coupling to an auxiliary subspace *outside* the logical subspace, and a sequence of operations can build up the entanglement while “recohering” the two qubits.

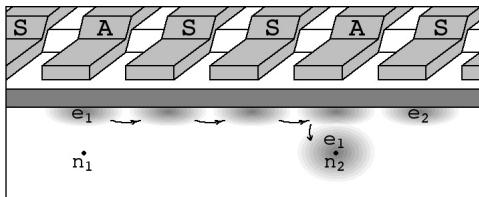


Figure 2.2: Entangling qubits e_1n_1 and e_2n_2 . S-gates displace e_2 and shuttle e_1 to the vicinity of n_2 . The A-gate above n_2 then applies hyperfine interaction, generating a partial e_1-n_2 spin swap within a *new* qubit e_1n_2 ; hyperfine interaction *between* two qubits may be viewed, casually, as a single qubit operation on the new qubit whose information is shared *non-locally* by the two original qubits.

2.6 The Model Hamiltonian and its Invariant Subspaces

The evolution of the electron and donor spins is described by their Hamiltonian,

$$H = \sum_{i,j} A_{ij} \vec{\sigma}_{e_i} \cdot \vec{\sigma}_{n_j} + \sum_i B (g_e \mu_B \sigma_{e_i}^z - g_n \mu_N \sigma_{n_i}^z).$$

The second term, H_B , sums the contribution from all donors and their electrons, with respective magnetic moments $g_n \mu_N$ and $g_e \mu_B$, in the vertical magnetic field B assumed parallel to a (100) lattice plane. It augments the hyperfine contact term, H_A , which is a sum of interactions between electron-donor pairs. Interaction between the i th electron and the j th donor is either off ($A_{ij} = 0$) or on ($A_{ij} = A$). We assume instantaneous switching and neglect the hydrogenic spin-orbit and dipole-dipole interactions (which are zero for the ground state and for sufficiently large r but finite in between) as well as any randomness in the contact strength during the switch. For P donors in Si the ground and first excited orbitals are separated by ≈ 15 meV corresponding to a period of 0.044 ps; a more realistic adiabatic switch takes $\mathcal{O}(3$ ps) which is still fast compared to the hyperfine interaction. Any remaining

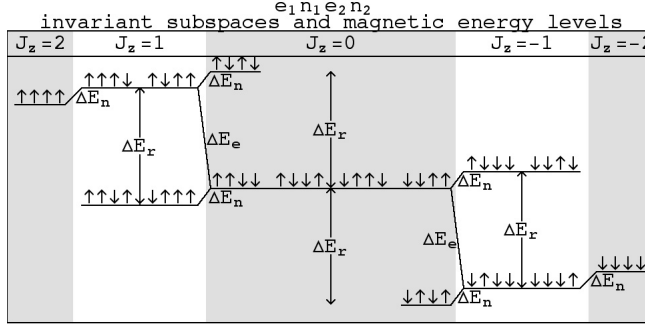


Figure 2.3: Magnetic energy levels and invariant subspaces of a two-qubit computer. Flipping a single electron or single nuclear spin changes the energy by ΔE_e or ΔE_n respectively and takes the state to another subspace. Within an invariant subspace, simultaneous electron and donor spin flips change the energy by $\Delta E_r = \Delta E_e + \Delta E_n$.

hydrogenic spin-orbit and dipole-dipole effects are coherent and can in principle be compensated by sophisticated control sequences or pulse shaping [55, 56], although we do not consider them here. Similarly, we neglect the spin-orbit effect at the interface [57] because, for controlled shuttling of individual spins in Si, it is small, coherent, and, with further research, characterizable and correctable.

The state space of spins is decomposable into invariant subspaces labeled by the z component of the total spin; up and down spins are stationary states of H_B while electron-donor spin swaps, generated by H_A , preserve the number of up vs. down spins. Within each invariant subspace flipping an electron spin, which changes the energy by $\Delta E_e = 2Bg_e\mu_B$ has a compensatory nuclear spin flip, which changes the energy by a further $\Delta E_n = 2Bg_n\mu_N$, and the magnetic energy splittings are thus integer multiples of $\Delta E_r = \Delta E_e + \Delta E_n$. Transitions between subspaces require the flipping of one spin or the other and thus there exist nonresonant shifts ΔE_e and ΔE_n between subspaces. As a specific example Figure 2.3 shows the magnetic energy levels and invariant subspaces of a two-qubit computer.

2.7 Resonant Hyperfine Stepping

It is desirable to generate pure hyperfine evolution even though the magnetic field is, in fact, always present. Hyperfine interaction in the magnetic field, $e^{-i(H_B+H_A)t/\hbar}$, is a far cry from independent hyperfine interaction $e^{-iH_A t/\hbar}$; we are actually veering “off course” from our desired unitary evolution. To make matters worse, the magnetic field and hyperfine interaction do not commute, which means that our course correction cannot be as simple as reversing, for a finite θ pulse, the magnetic field coupling:

$$e^{-iH_A t/\hbar} \neq e^{+iH_B t/\hbar} e^{-i(H_B+H_A)t/\hbar}.$$

However, for a short time step Δt the course correction is very good despite the non-commutativity. In fact, by a variant of the Cambell-Baker-Hausdorf formula [8], we can make a short Δt hyperfine step with an error $\mathcal{O}(\Delta t^3)$ by making $\Delta t/2$ corrections before and after:

$$e^{+iH_B \Delta t/2\hbar} e^{-i(H_B+H_A)\Delta t/\hbar} e^{+iH_B \Delta t/2\hbar} = e^{-iH_A \Delta t/\hbar} + \mathcal{O}(\Delta t^3)$$

We can thus compose a finite t pulse of hyperfine evolution with a large number, a , of these short $\Delta t = t/a$ steps of hyperfine *and* magnetic evolution corrected, on the fly, by time-reversed $\Delta t/2$ steps of solely magnetic interaction. This composition is the essence of the the Trotter formula [8],

$$e^{-iH_A t/\hbar} \approx (e^{+iH_B \Delta t/2\hbar} e^{-i(H_A+H_B)\Delta t/\hbar} e^{+iH_B \Delta t/2\hbar})^a.$$

Although the magnetic and hyperfine steps do not commute, the remaining $\mathcal{O}(\Delta t^3)$ error of each short step also shrinks with a decreasing magnetic field (the non-

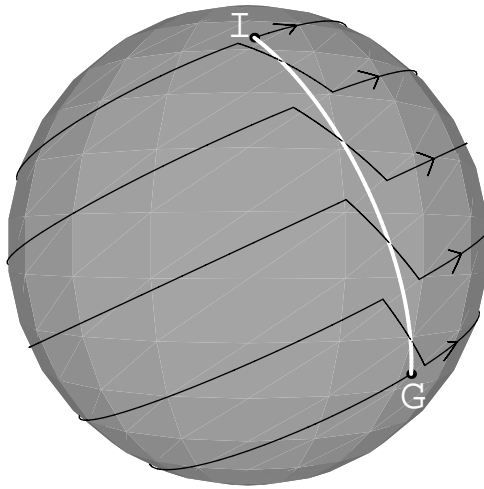


Figure 2.4: Unitary hyperfine evolution implemented by resonant hyperfine stepping in a magnetic field. The desired hyperfine evolution from I to G, sketched on a cartoon of the unitary group manifold, is non-trivial because the magnetic field and hyperfine interaction do not commute. We proceed in smaller steps, sandwiched between small course corrections made with almost full laps of magnetic evolution.

commutivity, $[H_A, H_B]$, scales with B). In other words, we can achieve good fidelity with sufficiently short Δt steps and a sufficiently weak field.

Within each invariant subspace the time-reversed magnetic steps are achieved by incomplete periods of magnetic evolution. A full period is determined by the energy splitting: $T_B = h/\Delta E_r$ (see Figure 2.3). We need only wait for $T_B - \Delta t/2$ to achieve the magnetic correction step. In analogy with magnetic resonance techniques we thus proceed by resonant stepping; for each period of magnetic evolution there is a short step of $H_A + H_B$. This technique is illustrated in Figure 2.4 which shows a cartoon of the unitary group manifold (not to scale and with fewer dimensions!) and a desired hyperfine evolution from the identity, I, to a goal transformation, G. The cartoon shows four steps, each effectively preceeded and succeeded by $\Delta t/2$ corrections. The result is true hyperfine evolution within each invariant subspace.

The use of digital bit trains from a pulse pattern generator considerably simplifies the timing of these operations. We define a bit pulse (one clock cycle) to be $\Delta t/2$; each digital hyperfine step, Δt , is thus a “two-bit pulse.” For example, we divide the fixed hyperfine period, $T_A = h/4A = 8.50847$ ns, into 96 clock cycles by setting the frequency at $f = 11.2829$ GHz; given this frequency we then divide the magnetic period T_B into 256 clock cycles by choosing a field strength of $B = 1.57171$ mT. Within an invariant subspace, generating pure hyperfine evolution is now as simple as turning off certain A-gate voltages (so that the hyperfine interaction is turned on) for 2 clock cycles out of every 256.

The encoded qubits reside in the $J_z = 0$ invariant subspace. We can thus construct logic operations from finite ϕ pulses of magnetic evolution, $(B, \phi) \equiv$

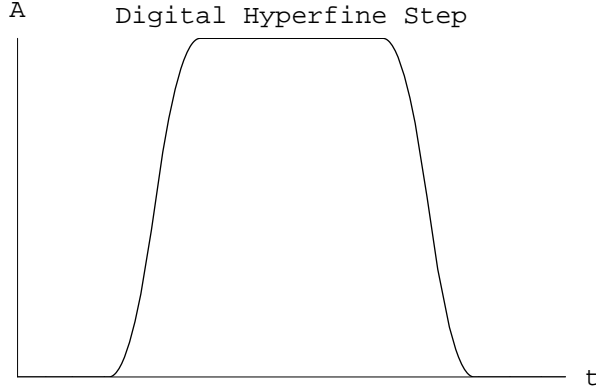


Figure 2.5: Schematic of a digital hyperfine step. It need not be perfectly square; it’s simply an integrated step in the right direction. In fact, a gradual turn-on and turn-off is necessary for adiabatic evolution of the electron wavefunction whose “on-again then off-again” overlap with the nucleus switches the hyperfine strength. A reasonable step is 177.26 ps with 30 ps rise and fall times.

$e^{-iH_B\phi T_B/h}$, and θ pulses of pure hyperfine evolution, $(A, \theta) \equiv e^{-iH_A\theta T_A/h}$, implemented with resonant hyperfine stepping.

The beauty of this approach is in its simplicity. There is no tuning of the hyperfine interaction; the purely digital approach means it is either on or off for the an integrated pulse which is comprised of an integer number of two-bit pulses between single laps around the group.

In fact, we need not even know the exact strength and shape of the digital hyperfine step (Figure 2.5). Instead, it can be viewed as a small integrated step in the right direction. These steps are supposed to be the same for all applied qubit interactions all the time; qubits’ donor sites not satisfying this criterion are diagnosed and simply not used for quantum computation. We composed our hyperfine interactions with $a = 48$ laps per 2π pulse; each Δt step was 177.26 ps. We have been assuming that the electron-donor overlap is modulated adiabatically by the

A gate electrode above the donor. For P donors in Si the ground and first excited states are separated by approximately $15 \text{ meV} \approx 22.8 \text{ THz}$ so gate voltage rise and fall times on the order of a few picoseconds should be adequately slow; 30 ps is even more reasonable.

As an added benefit, resonant hyperfine stepping also maintains the stroboscopic synchronization with an isolated qubit precessing in the global magnetic field. Each step-plus-lap combination matches one full lap for an isolated qubit; whatever the composed duration of the effective hyperfine pulse may be, it will take an integer number of magnetic periods, T_B .

2.8 Single Qubit Gates

Within a qubit the hyperfine interaction splits the degeneracy of the logical basis states $|0\rangle = (|\uparrow_e\downarrow_n\rangle - |\downarrow_e\uparrow_n\rangle)/\sqrt{2}$ and $|1\rangle = (|\uparrow_e\downarrow_n\rangle + |\downarrow_e\uparrow_n\rangle)/\sqrt{2}$ while the vertical magnetic field splits $|\uparrow_e\downarrow_n\rangle$ and $|\downarrow_e\uparrow_n\rangle$. There are thus two independent Hamiltonians for unitary evolution of the qubit: the magnetic field, generating $|0\rangle \leftrightarrow |1\rangle$, and hyperfine interaction, generating the e - n spin swap $|0\rangle+|1\rangle \leftrightarrow |0\rangle-|1\rangle$. Following Benjamin, these interactions can be visualized as generating Bloch Sphere rotations. States simply precess about the x and z axes under the magnetic field and hyperfine interaction respectively. We can implement any single qubit gate by sequences of such rotations [8]

To be more explicit, consider the Hamiltonian for an electron, with magnetic moment $g_e\mu_B$, and its donor, with magnetic moment $g_n\mu_n$, in an applied magnetic

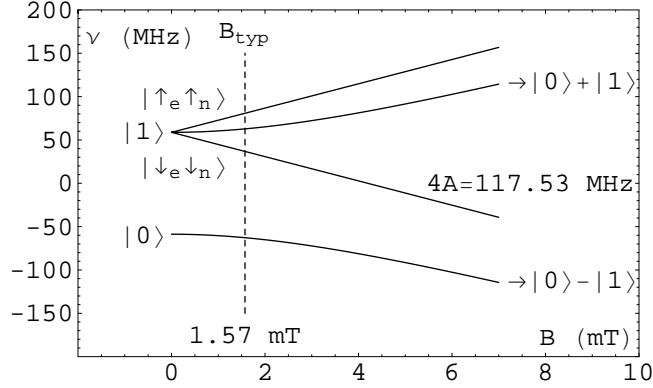


Figure 2.6: Eigenvalues and Eigenkets of an en spin-pair. The hyperfine interaction splits $|0\rangle$ and $|1\rangle$, generating $|0\rangle + |1\rangle \leftrightarrow |0\rangle - |1\rangle$, while the magnetic field splits $|0\rangle + |1\rangle$ and $|0\rangle - |1\rangle$, generating $|0\rangle \leftrightarrow |1\rangle$. Arbitrary single qubit operations can be composed of sequences of these “Bloch Sphere rotations.” A typical magnetic field strength is 1.57 mT.

field B with hyperfine interaction strength A proportional to the donor overlap of the electron wavefunction:

$$H = A\vec{\sigma}^e \cdot \vec{\sigma}^n + B(g_e\mu_B\sigma_z^e - g_n\mu_n\sigma_z^n) + AI$$

The inconsequential absolute energy shift, AI , will help manifest the generators of Bloch Sphere rotations. In our $\{|\uparrow_e\uparrow_n\rangle, |0\rangle, |1\rangle, |\downarrow_e\downarrow_n\rangle\}$ basis this Hamiltonian takes the matrix form

$$\begin{pmatrix} 2A + B(g_e\mu_B - g_n\mu_n) & 0 & 0 & 0 \\ 0 & -2A & B(g_e\mu_B + g_n\mu_n) & 0 \\ 0 & B(g_e\mu_B + g_n\mu_n) & 2A & 0 \\ 0 & 0 & 0 & 2A - B(g_e\mu_B - g_n\mu_n) \end{pmatrix}$$

Note the center two-by-two block matrix. In the two dimensional logical subspace with basis $\{|0\rangle, |1\rangle\}$ the single qubit Hamiltonian comprises $B(g_e\mu_B + g_n\mu_n)\sigma_x - 2A\sigma_z$. We thus have our choice of two generators: $H_B \equiv B(g_e\mu_B + g_n\mu_n)\sigma_x$, as-

Gate	Matrix	Composition
X	$\begin{pmatrix} 0 & 1 \\ 1 & 0 \end{pmatrix}$	$(B, \frac{3\pi}{2})(A, \pi)(B, \frac{\pi}{2})(A, \pi)$
Y	$\begin{pmatrix} 0 & -i \\ i & 0 \end{pmatrix}$	$(B, \frac{3\pi}{2})(A, \pi)(B, \frac{\pi}{2})$
Z	$\begin{pmatrix} 1 & 0 \\ 0 & -1 \end{pmatrix}$	(A, π)
S	$\begin{pmatrix} 1 & 0 \\ 0 & i \end{pmatrix}$	$(A, \frac{3\pi}{2})$
H	$\frac{1}{\sqrt{2}} \begin{pmatrix} 1 & 1 \\ 1 & -1 \end{pmatrix}$	$(B, \frac{3\pi}{2})(A, \frac{3\pi}{2})(B, \frac{\pi}{2})(A, \pi)$
L	$\frac{1}{\sqrt{2}} \begin{pmatrix} 1 & -1 \\ 1 & 1 \end{pmatrix}$	$(B, \frac{3\pi}{2})(A, \frac{3\pi}{2})(B, \frac{\pi}{2})$

Table 2.1: Some single qubit gates and their composition using B and A rotations.

sociated with the magnetic field, and $H_A \equiv -2A\sigma_z$, associated with the hyperfine interaction between the first and second spins (the subscripts designate the interacting spins). Since an arbitrary single qubit unitary operation, up to an overall phase, can be viewed as a rotation about some axis, and any rotation can be composed of rotations about the x and z axes [8], H_B and H_A are sufficient for generating any single qubit gates, such as those in Table 2.1.

Our compositions always total an integer number of $(B, 2\pi)$ rotations. This is because we want our perspective to remain synchronized with the other qubits

which are constantly evolving under the influence of the global magnetic field; we are adopting a *stroboscopic* picture in which our desired gate is completed when an isolated qubit, precessing about its Bloch Sphere x -axis, completes a full rotation. For example, rather than implementing an X gate with (B, π) we use $(B, \frac{3\pi}{2})(A, \pi)(B, \frac{\pi}{2})(A, \pi)$. (Our hyperfine interactions, such as (A, π) , maintain the same stroboscopic synchronization because they are implemented with resonant hyperfine stepping.) We find such a composition for an arbitrary single qubit gate G by numerically solving the angles for an alternating series of σ_x and σ_z rotations,

$$G = (\sigma_z, \theta_n)(\sigma_x, \theta_{n-1}) \dots (\sigma_z, \theta_2)(\sigma_x, \theta_1)$$

subject to the stroboscopic constraint for which the total pulse time implements a full period of magnetic evolution giving the identity transformation: $I = (\sigma_x, \theta_1 + \theta_3 + \dots + \theta_{n-1})$. Typically, no more than four rotations are needed.

2.9 Two Qubit Gates

Entanglement is a crucial ingredient in canonical two qubit logic gates such as the Controlled-Z and Controlled-Not, shown here in the two qubit logical basis of states $\{|00\rangle, |01\rangle, |10\rangle, |11\rangle\}$:

$$CZ = \begin{pmatrix} 1 & 0 & 0 & 0 \\ 0 & 1 & 0 & 0 \\ 0 & 0 & 1 & 0 \\ 0 & 0 & 0 & -1 \end{pmatrix} \quad CNOT = \begin{pmatrix} 1 & 0 & 0 & 0 \\ 0 & 1 & 0 & 0 \\ 0 & 0 & 0 & 1 \\ 0 & 0 & 1 & 0 \end{pmatrix}$$

We create such entanglement when the hyperfine interaction is applied, after shuttling, between the electron of one qubit and the nucleus of another. Figure 2.2 shows hyperfine interaction between two qubits. One may casually consider the entangling of two qubits as the manipulation of a *new* qubit containing information shared *non-locally* by the two original qubits.

The two qubit interactions are actually much more subtle because they couple logical states to auxiliary states outside of the computational basis. Thus the two qubits temporarily decohere during the entangling operations. However, it is possible, by a sequence of operations, to build up the entanglement while “recohering” the qubits with evolution back into the logical subspace.

The coupling to the auxiliary subspace takes place because hyperfine interactions generate $e-n$ spin swaps. In the context of two spin-pair qubits there is a four spin system, $e_1 n_1 e_2 n_2$. Swapping e_1 and n_2 generates $|\uparrow_{e_1} \downarrow_{n_1} \uparrow_{e_2} \downarrow_{n_2}\rangle \leftrightarrow |\downarrow_{e_1} \downarrow_{n_1} \uparrow_{e_2} \uparrow_{n_2}\rangle$ and $|\downarrow_{e_1} \uparrow_{n_1} \downarrow_{e_2} \uparrow_{n_2}\rangle \leftrightarrow |\uparrow_{e_1} \uparrow_{n_1} \downarrow_{e_2} \downarrow_{n_2}\rangle$. Similarly, swapping n_1 and e_2 generates $|\uparrow_{e_1} \downarrow_{n_1} \uparrow_{e_2} \downarrow_{n_2}\rangle \leftrightarrow |\uparrow_{e_1} \uparrow_{n_1} \downarrow_{e_2} \downarrow_{n_2}\rangle$ and $|\downarrow_{e_1} \uparrow_{n_1} \downarrow_{e_2} \uparrow_{n_2}\rangle \leftrightarrow |\downarrow_{e_1} \downarrow_{n_1} \uparrow_{e_2} \uparrow_{n_2}\rangle$. The auxiliary space is thus spanned by $|\uparrow_{e_1} \uparrow_{n_1} \downarrow_{e_2} \downarrow_{n_2}\rangle$ and $|\downarrow_{e_1} \downarrow_{n_1} \uparrow_{e_2} \uparrow_{n_2}\rangle$

The two qubit scenario makes use of five available generators. The three local generators are the magnetic field, B , and two hyperfine interactions: within the first qubit, A_{11} , and within the second qubit, A_{22} .

$$H_B = g_e \mu_B B (\sigma_z^{e_1} + \sigma_z^{e_2}) - g_n \mu_n B (\sigma_z^{n_1} + \sigma_z^{n_2})$$

$$A_{11} = A \vec{\sigma}^{e_1} \cdot \vec{\sigma}^{n_1} \quad A_{22} = A \vec{\sigma}^{e_2} \cdot \vec{\sigma}^{n_2}$$

The non-local generators are the other two possible hyperfine interactions: between

the first electron and second nucleus, A_{12} , and between the second electron and first nucleus, A_{21} .

$$A_{12} = A\vec{\sigma}^{e_1} \cdot \vec{\sigma}^{n_2} \quad A_{21} = A\vec{\sigma}^{e_2} \cdot \vec{\sigma}^{n_1}$$

The logical and auxiliary states span the six dimensional $J_z = 0$ subspace of the sixteen dimensional Hilbert space of our four spins. This six dimensional subspace is invariant under the group action of our five available Hamiltonians; while logical states may couple to auxiliary states, none couple outside the $J_z = 0$ invariant subspace. In our

$$\{|\uparrow_{e_1}\uparrow_{n_1}\downarrow_{e_2}\downarrow_{n_2}\rangle, |00\rangle, |01\rangle, |10\rangle, |11\rangle, |\downarrow_{e_1}\downarrow_{n_1}\uparrow_{e_2}\uparrow_{n_2}\rangle\}$$

basis the non-local generators' matrices reveal the coupling to the auxiliary states (the first and last rows and columns):

$$A_{12} = A \begin{pmatrix} 0 & 1 & -1 & -1 & 1 & 0 \\ 1 & 1 & 0 & 0 & -1 & 1 \\ -1 & 0 & 1 & -1 & 0 & 1 \\ -1 & 0 & -1 & 1 & 0 & 1 \\ 1 & -1 & 0 & 0 & 1 & 1 \\ 0 & 1 & 1 & 1 & 1 & 0 \end{pmatrix} \quad A_{21} = A \begin{pmatrix} 0 & 1 & 1 & 1 & 1 & 0 \\ 1 & 1 & 0 & 0 & -1 & 1 \\ 1 & 0 & 1 & -1 & 0 & -1 \\ 1 & 0 & -1 & 1 & 0 & -1 \\ 1 & -1 & 0 & 0 & 1 & 1 \\ 0 & 1 & -1 & -1 & 1 & 0 \end{pmatrix}$$

A logical SWAP operation can be realized very simply by successive $e-n$ spin

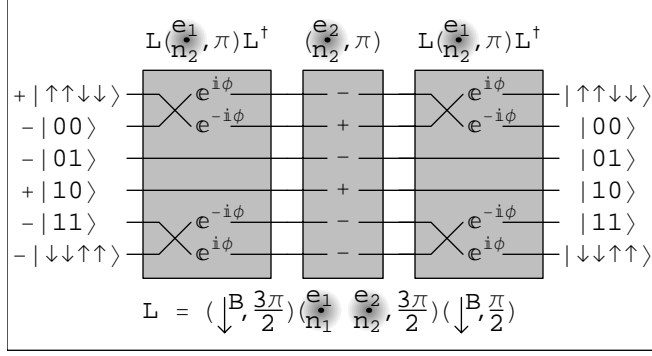


Figure 2.7: A Controlled Z gate. Up to local transformations, an $e-n$ spin swap *between* two qubits swaps logical and auxiliary states. Levy proposed sandwiching a local operation between two such logical-auxiliary swaps [20].

swaps:

$$SWAP = (A_{11} + A_{22}, \pi)(A_{12} + A_{21}, \pi) = \begin{pmatrix} 0 & 0 & 0 & 0 & 0 & 1 \\ 0 & 1 & 0 & 0 & 0 & 0 \\ 0 & 0 & 0 & 1 & 0 & 0 \\ 0 & 0 & 1 & 0 & 0 & 0 \\ 0 & 0 & 0 & 0 & 1 & 0 \\ 1 & 0 & 0 & 0 & 0 & 0 \end{pmatrix}.$$

The CZ and CNOT are more difficult. But it turns out that in an $e-n$ spin swap between the electron of the first qubit and the nucleus of the second (A_{12}, π), up to a local basis change L , the $|00\rangle$ and $|11\rangle$ states are swapped with the auxiliary states $|\uparrow_{e_1}\uparrow_{n_1}\downarrow_{e_2}\downarrow_{n_2}\rangle$ and $|\downarrow_{e_1}\downarrow_{n_1}\uparrow_{e_2}\uparrow_{n_2}\rangle$ respectively. Another π pulse of hyperfine interaction reverses the swap. As illustrated in Figure 2.7, Levy proposed sandwiching a single qubit gate between two such logical-auxiliary swaps, realizing, up to local operations, a CZ and CNOT [20].

The CZ and CNOT can thus be obtained as follows:

$$L = (B, \frac{3\pi}{2})(A_{11} + A_{22}, \frac{3\pi}{2})(B, \frac{\pi}{2})$$

$$L^\dagger = (B, \frac{3\pi}{2})(A_{11} + A_{22}, \frac{\pi}{2})(B, \frac{\pi}{2})$$

$$CZ = (A_{11}, \pi)L(A_{12}, \pi)L^\dagger(A_{22}, \pi)L(A_{12}, \pi)L^\dagger$$

$$H_2^\dagger = (A_{22}, \pi)(B, \frac{3\pi}{2})(A_{22}, \frac{\pi}{2})(B, \frac{\pi}{2})$$

$$CNOT = H_2^\dagger CZ H_2^\dagger$$

Note that we have redefined L to be two simultaneous local transformations ($L = L_1 \otimes L_2$) and that the Hadamard, H_2^\dagger , is performed on the second, not the first qubit (we use H_2^\dagger instead of H_2 because it is faster, in this architecture, than implementing H_2).

A very important lesson drawn from the CZ is that single qubit gates develop a relative phase between the logical and auxiliary subspaces; it's crucial for obtaining the CZ. Even the logical-auxiliary swaps developed $e^{\pm i\phi}$ phases, due to the local

transformations L and L^\dagger . The matrix form for the magnetic Hamiltonian is

$$H_B = B(g_e\mu_B + g_n\mu_n) \begin{pmatrix} 0 & 0 & 0 & 0 & 0 & 0 \\ 0 & 0 & 1 & 1 & 0 & 0 \\ 0 & 1 & 0 & 0 & 1 & 0 \\ 0 & 1 & 0 & 0 & 1 & 0 \\ 0 & 0 & 1 & 1 & 0 & 0 \\ 0 & 0 & 0 & 0 & 0 & 0 \end{pmatrix}$$

which, in the logical subspace, is $\sim \sigma_x^1 + \sigma_x^2$ (each qubit precesses about its x -axis independently). The single qubit hyperfine generators are

$$A_{11} = 2A \begin{pmatrix} 1 & 0 & 0 & 0 & 0 & 0 \\ 0 & -1 & 0 & 0 & 0 & 0 \\ 0 & 0 & -1 & 0 & 0 & 0 \\ 0 & 0 & 0 & 1 & 0 & 0 \\ 0 & 0 & 0 & 0 & 1 & 0 \\ 0 & 0 & 0 & 0 & 0 & 1 \end{pmatrix} \quad A_{22} = 2A \begin{pmatrix} 1 & 0 & 0 & 0 & 0 & 0 \\ 0 & -1 & 0 & 0 & 0 & 0 \\ 0 & 0 & 1 & 0 & 0 & 0 \\ 0 & 0 & 0 & -1 & 0 & 0 \\ 0 & 0 & 0 & 0 & 1 & 0 \\ 0 & 0 & 0 & 0 & 0 & 1 \end{pmatrix}$$

which, again in the logical subspace, are $\sim \sigma_z^1$ and $\sim \sigma_z^2$ respectively (each generates a z -axis rotation of its relevant qubit).

A useful way to think about an e - n spin swap is as a transfer of our quantum information into a different encoding scheme. For example, consideration of the (A_{12}, π) pulse of interaction between the first electron and the second donor reveals a faster CZ and CNOT. The π pulse generates an e - n spin swap between e_1 and n_2 . Specifically, the interaction generates $|\uparrow_{e_1}\downarrow_{n_1}\uparrow_{e_2}\downarrow_{n_2}\rangle \leftrightarrow |\downarrow_{e_1}\downarrow_{n_1}\uparrow_{e_2}\uparrow_{n_2}\rangle$ and

$|\downarrow_{e_1}\uparrow_{n_1}\downarrow_{e_2}\uparrow_{n_2}\rangle \leftrightarrow |\uparrow_{e_1}\uparrow_{n_1}\downarrow_{e_2}\downarrow_{n_2}\rangle$; whatever information was encoded in $e_1n_1e_2n_2$ is now encoded in $n_2n_1e_2e_1$.

Considering e_1n_1 as a data qubit and e_2n_2 as an unentangled ancilla, we see that the data qubit is now encoded in the n_2n_1 donor spin-pair. Alternatively, an e_2n_2 data qubit has been transferred, with the use of an unentangled ancilla e_1n_1 , into an e_2e_1 electron spin-pair.

Sandwiched within the entangling CZ, between the π pulses of A_{12} , there is a sequence of operations $L^\dagger(A_{22}, \pi)L$ which are local with respect to the $e_1n_1e_2n_2$ encoding. We can see that the sandwiched local operations generate the entanglement when viewed from the $n_2n_1e_2e_1$ encoding (from this perspective they are *non-local* operations). The $e_1n_1e_2n_2$ equivalent sequence is

$$(B, \frac{3\pi}{2}) \underbrace{(A_{12} + A_{21}, \frac{3\pi}{2})(B, \frac{\pi}{2})(A_{21}, \pi)(B, \frac{3\pi}{2})(A_{12} + A_{21}, \frac{\pi}{2})}_{N} (B, \frac{\pi}{2})$$

in which the underbrace highlights the entangler N and from which we obtain a faster CZ, requiring two-thirds of the original time, composed of fewer elementary operations, and giving better fidelity:

$$CZ = L(B, \frac{3\pi}{2})N(B, \frac{\pi}{2})L^\dagger.$$

With N it is possible to show, also, that a faster and better CNOT is

$$CNOT = (L_1 \otimes Z_2)N(L_1 \otimes Z_2)^\dagger,$$

in which single qubit operations,

$$(L_1 \otimes Z_2) = (B, \frac{3\pi}{2})(A_{11} + A_{22}, \pi)(A_{11}, \frac{\pi}{2})(B, \frac{\pi}{2}),$$

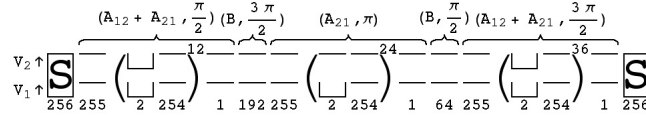


Figure 2.8: Operations time line for an entangler. Between shuttling operations represented schematically by an “S,” the diagram depicts a sequence of on-or-off A-gate voltages; the bottom line of the figure shows their duration in clock cycles. Hyperfine interaction is on whenever the voltage is off. The magnetic field is always on.

augment the entangler. This gate construction refines Levy’s original [20] but it may not be optimal. Figure 2.8 depicts the actual sequence of A-gate voltages that implements the entangler, N. The two A gate voltages above the donors, V_1 and V_2 , are almost always on; the electrons are drawn away from their donors and there is no hyperfine interaction. Every so often the voltage above a donor is turned off for two clock cycles; the donor attracts the electron, turning on a two-bit pulse of hyperfine interaction. Repeating these hyperfine steps every 256 clock cycles, in resonance with the magnetic laps, generates a finite pulse of high fidelity hyperfine evolution. Shuttling each electron to the other’s donor can presumably take only ns, but is delayed to 256 clock cycles to maintain the stroboscopic synchronization with isolated qubits. Most of the time is spent on the $\pi/2$, π , and $3\pi/2$ pulses of hyperfine evolution, requiring 12, 24, and 36 step-plus-lap combinations respectively. The $3\pi/2$ and $\pi/2$ pulses of magnetic evolution require only 192 and 64 clock cycles respectively.

2.10 Gate Times and Errors

Digital processing with resonant hyperfine stepping takes discrete steps around the unitary group. Shorter hyperfine steps and a weaker magnetic field reduce the errors. However, commercially available pulse pattern generators are limited to approximately 12 GHz (hence our choice of $f = 11.2829$ GHz). Furthermore, the preponderance of magnetic periods (one for each small hyperfine step) means that a computation slows with weaker field. There is thus a trade-off between fidelity and speed.

Our choice of $B = 1.57171$ mT yields a complete spin swap (the architecture's fundamental process) in $0.57\mu\text{s}$. When ideally implemented with resonant hyperfine stepping, its expected error (defined to be the average probability of incorrectly transforming an initial, arbitrary, two-qubit basis of states) is less than 2.1×10^{-7} . The CNOT is our most complicated gate and can be ideally implemented with an expected error of at most 0.9×10^{-6} in $3.22\mu\text{s}$.

But it is unrealistic to presume exact values for the frequency, field, and hyperfine strength. There may also be variations of hyperfine and/or field strength from one donor site to the next. Indeed, although isotope purification can remove most Si^{29} from the crystal, the remaining impurities cause field variations (although these fluctuate so slowly that spin-echo techniques may be applicable). Another complication is that the Landé factor for the electron, g_e , could vary by as much as 10^{-3} between the donor and the Si-barrier interface [54].

We have studied the sensitivity to these parameters by the explicit simula-

tion of canonical one- and two-qubit logic gates. The threshold theorem [8] for quantum computation concludes that efficient quantum computing, obtained with error-correction techniques, is possible when logic gate errors are less than 10^{-5} . We found that this threshold is obtainable with relative variations in frequency, field, and hyperfine strength as large as 10^{-5} , 10^{-5} , and 5×10^{-4} , respectively. The sensitivity to local variations in these parameters is approximately the same. The fidelity is comparatively insensitive to the hyperfine strength because our gate compositions are predominantly magnetic. Finally, the architecture can tolerate 5×10^{-3} variations in g_e between the donor and the interface.

2.11 Tuneable Fidelity

The use of discrete stepping “coarse-grains” the attainable unitary transformations. Canonical gates lie on a very coarse “grid” of multiples of $\pi/4$ steps (not a coordinate grid, since $[H_B, H_A] \neq 0$, but simply a set of discrete transformations obtainable by finite steps). The computer must be configured to operate on this grid; f_0 and B_0 are restricted to those values that compose gates in integer steps. For example, $(a_{2\pi} = 48, b_{2\pi} = 256)$ realizes a fine grid of $(A_{ij}, \pi/24)$ and $(M, \pi/128)$ transformations.

It may be that the calculated field and frequency for this $(a_{2\pi}, b_{2\pi})$ configuration are only approximations and that the ideal f_0 and B_0 are slightly different. As shown in Figures 2.5 and 2.9 the hyperfine step strength and shape may be such that the discrete steps do not land on the goal transformation, G. Tuning the

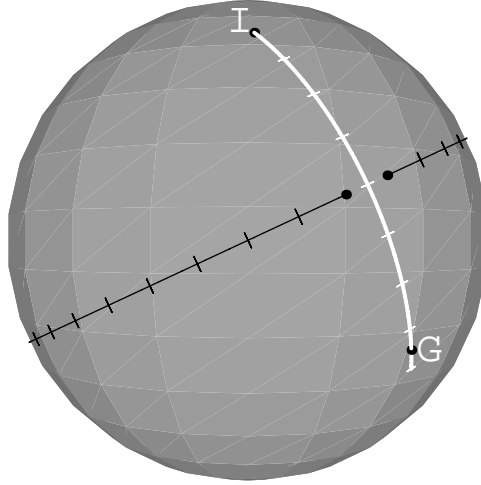


Figure 2.9: Tuning the fidelity. Step sizes can be adjusted, by tuning the clock frequency and magnetic field strength, until discrete steps attain our goal G.

clock frequency will adjust the step size until G is obtained in an integer number of hyperfine steps. Similarly, the magnetic field can be tuned until the magnetic lap around the group is obtained in an integer number of clock cycles.

2.12 The Nuclear Spin-Pair Quantum Memory

A π pulse of hyperfine interaction, (A_{ij}, π) , between two qubits generates a complete spin swap between the electron of one qubit and the donor of the other. Considered as a switch to a new encoding scheme, this hyperfine “data bus” transfers one qubit into a nuclear spin-pair and the other into an electron spin-pair. For example, an en data qubit, with the use of an $e_A n_A$ “ancilla,” can be transferred, by resonant hyperfine stepping, into an $n_A n$ nuclear spin-pair qubit, as is shown in

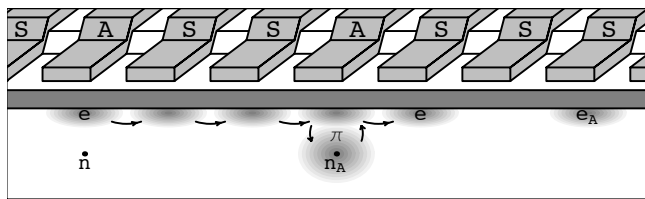


Figure 2.10: Ancilla Facilitated Hyperfine “Data Bus” to a nuclear spin-pair quantum memory. A π pulse of hyperfine interaction between an en qubit and an unentangled ancilla qubit $e_A n_A$ (specifically an $e-n$ spin swap between e and n_A) has transferred en into an $n_A n$ storage qubit.

Figure 2.10. Retrieval simply requires another π pulse to repeat the spin swap.

The relatively weak nuclear magnetic moment gives the nuclear spin a long decoherence time which makes the nuclear spin-pair qubit a natural quantum memory. Since the two nuclear spins have the same magnetic moments, their ($J_z = 0$) qubit does not respond to the magnetic field. Furthermore, if the data and ancilla were unentangled before the swap then the data (now encoded in the nuclear spin-pair) and ancilla (now encoded in the electron spin-pair) remain unentangled, so decoherence or collapse of the electron spin-pair will not degrade the memory. (In the Appendix to this chapter we show that the qubit’s transfer succeeds even when the ancilla is outside its logical subspace; relative phases developed between invariant subspaces, by resonant hyperfine stepping, are absorbed solely into the ancilla).

2.13 Readout, Initialization, and Refrigeration

As illustrated in Figure 2.11, the data qubit can, alternatively, be transferred into an electron spin-pair to facilitate measurement by various proposed methods

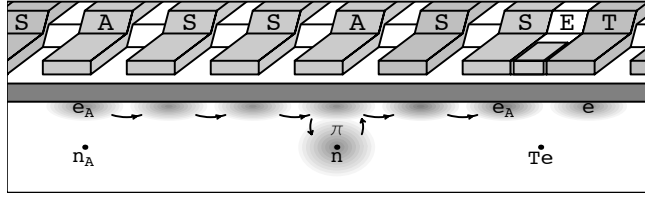


Figure 2.11: Projective Read-Out. An $e-n$ spin swap between spins e_A and n has transferred the en qubit into an ee_A read-out qubit above the Tellurium double donor and beneath the SET, which will detect the singlet vs. triplet charge configuration.

to distinguish singlets and triplets. For an electron spin-pair known to reside in the logical subspace, these are effectively $|0\rangle = |\text{singlet}\rangle$ vs. $|1\rangle = |\text{triplet}, S_z = 0\rangle$ projective qubit measurements. For example, a Single Electron Transistor (SET) is capable of very sensitive charge configuration measurements; above a donor it can detect electrode driven charge density fluctuations associated with the electron spin-pair singlet [18]. Alternatively, in a quantum dot the electrons' spin determines the tunneling of spin-polarized currents [19].

After measurement the collapsed electron spin-pair can be transferred back into an electron-donor pair via another spin swap. This provides a way to initialize the computer at high temperature (e. g., 1 K). Readout collapses an electron spin-pair into a singlet or triplet. The singlet outcome, $|\uparrow_{e_1}\downarrow_{e_2}\rangle - |\downarrow_{e_1}\uparrow_{e_2}\rangle$, is immediately convertible, via a spin swap, to $|0\rangle$. The triplet outcome, $|\uparrow_{e_1}\uparrow_{e_2}\rangle, |\uparrow_{e_1}\downarrow_{e_2}\rangle + |\downarrow_{e_1}\uparrow_{e_2}\rangle$, or $|\downarrow_{e_1}\downarrow_{e_2}\rangle$, can be recycled, as depicted in Figure 2.12, through a single qubit $|0\rangle \leftrightarrow |1\rangle$ operation sandwiched between spin swaps, for another chance to obtain a useful singlet. (In the Appendix to this chapter we show that this cascaded measurement prevails despite relative phases developed between invariant subspaces.) At high

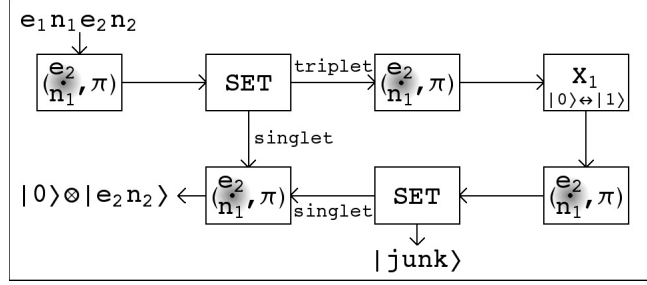


Figure 2.12: Qubit Initialization and Sorting. A singlet outcome is immediately convertible into $|0\rangle$ while the triplet outcome can be recycled through a sequence of operations into another chance for a useful singlet.

temperature 50% of the electron-donor pairs will obtain $|0\rangle$, and by electron shuttling the successful 50% can be “pooled” into the working part of the computer in analogy with Kane’s original proposal for on-chip spin refrigeration [58].

2.14 Conclusion

Consideration of a simple encoding scheme for the Kane quantum computer has led to a modified architecture which overcomes many obstacles to the original proposal. Resonant hyperfine stepping provides digital control with an extremely well defined and stable parameter; there is no tuning of the hyperfine strength and there is no qubit specific tuning; we can optimize the fidelity of the entire computer by tuning the clock frequency (and thus the bit pulse width) of the bit trains. Effectively, we have replaced the AC magnetic field with a digital electric field.

Digital shuttling of electrons removes the need for the complicated and difficult exchange mediated coupling and overcomes the nearest neighbor restrictions. It also makes the computer easier to fabricate since the donors can be irregularly spaced and further apart, allowing for larger gate electrodes, and malfunctioning donor sites

can be diagnosed and ignored, provided there is enough S gate capability to shuttle other qubits' electrons around the misbehaving donor.

There is a natural data-bus to a nuclear spin-pair quantum memory or electron spin-pairs for projective measurement beneath a Single Electron Transistor. The availability of a projective measurement means we can initialize 50% of the qubits at higher temperatures, and electron shuttling can then pool initialized qubits into the working part of the computer. These many benefits were obtained at the cost of coupling to an auxiliary subspace outside the logical subspace. Therefore the fidelity depends crucially on tuning the clock frequency and the global magnetic field. We have investigated the sensitivity of the computer and found that “five nine’s fidelity” is attainable even for relative variations in field and frequency as large as 10^{-5} .

This work was supported by the National Security Agency. AJS is grateful for helpful discussions with S. Lomonaco.

2.15 Appendix: Subtleties of Resonant Hyperfine Stepping

Resonant hyperfine stepping yields high fidelity hyperfine evolution within our $J_z = 0$ invariant subspace but not in the full Hilbert space of N spins because relative phases develop between invariant subspaces. Also, despite the obvious analogy with electron spin resonance, the resonant hyperfine stepping does not generate the same evolution as would be obtained in “encoded qubit resonance,” in which a period of sinusoidal hyperfine interaction is applied for each magnetic lap around the group.

2.15.1 Relative Phases Between Invariant Subspaces

The relative phases develop because some magnetic energy level differences between invariant subspaces are not resonant with the energy differences that exists within the $J_z = 0$ invariant subspace. For example, in Figure 2.3, there are five invariant subspaces for four spins. Within any one of these invariant subspaces the magnetic energy levels are split by integer multiples of $E_r = 2B(g_e\mu_B + g_n\mu_n)$ (flipping an electron spin, which changes the energy by $\pm 2Bg_e\mu_B$ has a compensatory nuclear spin flip, which changes the energy by a further $\pm 2Bg_n\mu_n$) and resonant hyperfine stepping works as designed. On the other hand, distinct invariant subspaces are separated by relative energies (such as $E_n = 2Bg_n\mu_n$ and $E_e = 2Bg_e\mu_B$) which are off resonance; in general, resonant hyperfine stepping implements spin swaps only up to relative phases between invariant subspaces.

Ordinarily, all processing takes place within the $J_z = 0$ invariant subspace. But there are two situations for which we must consider the possibility of off-resonance hyperfine steps: the hyperfine data bus and the qubit initialization scheme.

In the Hyperfine Data Bus

The unentangled ancilla used in the hyperfine data bus may be outside the logical subspace, in which case the four-spin ket projects across invariant subspaces. Specifically, the qubit may be in an arbitrary logical ($J_z = 0$) superposition while the ancilla is in a broader arbitrary superposition:

$$(\alpha |\uparrow_1\downarrow_2\rangle + \beta |\downarrow_1\uparrow_2\rangle) \otimes (a |\uparrow_3\uparrow_4\rangle + b |\uparrow_3\downarrow_4\rangle + c |\downarrow_3\uparrow_4\rangle + d |\downarrow_3\downarrow_4\rangle)$$

This general logical \otimes ancilla ket has components in the $J_z = 1, 0,$ and -1 invariant subspaces. During resonant hyperfine stepping, the $J_z = \pm 1$ subspaces will develop phases $e^{i\phi_{\pm 1}}$ with respect to the $J_z = 0$ subspace. However, on account of their unentangled nature and the fact that the projecting across subspaces originated from the ancilla, not the qubit, these phases can be entirely absorbed into the ancilla. For example, after “swapping” spins 2 and 3 we obtain

$$(\alpha |\uparrow_1\downarrow_3\rangle + \beta |\downarrow_1\uparrow_3\rangle) \otimes (e^{i\phi_1} a |\uparrow_2\uparrow_4\rangle + b |\uparrow_2\downarrow_4\rangle + c |\downarrow_2\uparrow_4\rangle + e^{i\phi_{-1}} d |\downarrow_2\downarrow_4\rangle)$$

The transferred qubit still has components (α, β) in the spin-swapped basis while the ancilla is modified to have components $(e^{i\phi_1} a, b, c, e^{i\phi_{-1}} d)$. This line of reasoning applies also to statistical mixtures. resonant hyperfine stepping correctly implements the hyperfine data bus provided the data spin-pair is logical and is unentangled with the ancilla.

In the Initialization Scheme

With regard to the initialization scheme, we now know that resonant hyperfine stepping will convert the electron spin-pair singlet into $|0\rangle$ regardless of the state of the facilitating ancilla. On the other hand, the ambiguous triplet outcome, when tensored with an arbitrary ancilla, gives a four-spin ket projecting across all five invariant subspaces. This time we cannot simply absorb phases developed between invariant subspaces into components of the ancilla. However, we can do this for each term of the superposition of tensor products, as follows. In general we will begin

with

$$(\alpha |\uparrow_1 \uparrow_2\rangle + \beta(|\uparrow_1 \downarrow_2\rangle + |\downarrow_1 \uparrow_2\rangle) + \gamma |\downarrow_1 \downarrow_2\rangle) \otimes (a |\uparrow_3 \uparrow_4\rangle + b |\uparrow_3 \downarrow_4\rangle + c |\downarrow_3 \uparrow_4\rangle + d |\downarrow_3 \downarrow_4\rangle)$$

which will evolve, under a resonant hyperfine stepping implemented “spin swap” to

$$\alpha |\uparrow_1 \uparrow_3\rangle \otimes |\psi_{24}^1\rangle + \beta(|\uparrow_1 \downarrow_3\rangle + |\downarrow_1 \uparrow_3\rangle) \otimes |\psi_{24}^2\rangle + \gamma |\downarrow_1 \downarrow_3\rangle \otimes |\psi_{24}^3\rangle$$

where $|\psi_{24}^1\rangle$, $|\psi_{24}^2\rangle$, and $|\psi_{24}^3\rangle$ are modified ancilla states which have absorbed phases between invariant subspaces. We can then perform the single qubit X gate to convert $|\uparrow_1 \downarrow_3\rangle + |\downarrow_1 \uparrow_3\rangle$ into $|\uparrow_1 \downarrow_3\rangle - |\downarrow_1 \uparrow_3\rangle$ obtaining

$$\alpha |\uparrow_1 \uparrow_3\rangle \otimes |\phi_{24}^1\rangle + \beta(|\uparrow_1 \downarrow_3\rangle - |\downarrow_1 \uparrow_3\rangle) \otimes |\phi_{24}^2\rangle + \gamma |\downarrow_1 \downarrow_3\rangle \otimes |\phi_{24}^3\rangle$$

where $|\phi_{24}^1\rangle$, $|\phi_{24}^2\rangle$, and $|\phi_{24}^3\rangle$ have absorbed yet more relative phases. This can be now be converted, by one last spin swap, into

$$\alpha |\uparrow_1 \uparrow_2\rangle \otimes |\chi_{34}^1\rangle + \beta(|\uparrow_1 \downarrow_2\rangle - |\downarrow_1 \uparrow_2\rangle) \otimes |\chi_{34}^2\rangle + \gamma |\downarrow_1 \downarrow_2\rangle \otimes |\chi_{34}^3\rangle$$

with $|\chi_{34}^1\rangle$, $|\chi_{34}^2\rangle$, and $|\chi_{34}^3\rangle$ serving again to absorb phases. The subsequent singlet outcome obtains with probability $|\beta|^2$ (the same probability as for the original $|\uparrow\downarrow\rangle + |\downarrow\uparrow\rangle$). This argument also holds for statistical mixtures. The initialization works as intended despite the subtleties of resonant hyperfine stepping.

2.15.2 Distinction from Electron Spin Resonance

Even though the hyperfine interaction strength is always positive we are tempted to imagine the effects of “encoded qubit resonance” (EQR) in which we apply a period of sinusoidal oscillation in the hyperfine strength for each magnetic lap around

the group, in analogy with electron spin resonance (ESR). It turns out that the effective generators of EQR are different from those of resonant hyperfine stepping.

For example, qubit resonance within the first qubit results in an effective generator

$$A_{11}^{EQR} \sim \begin{pmatrix} 0 & 0 & 0 & 0 & 0 & 0 \\ 0 & -1 & 0 & 0 & 0 & 0 \\ 0 & 0 & -1 & 0 & 0 & 0 \\ 0 & 0 & 0 & 1 & 0 & 0 \\ 0 & 0 & 0 & 0 & 1 & 0 \\ 0 & 0 & 0 & 0 & 0 & 0 \end{pmatrix} \neq A_{11} \sim \begin{pmatrix} 1 & 0 & 0 & 0 & 0 & 0 \\ 0 & -1 & 0 & 0 & 0 & 0 \\ 0 & 0 & -1 & 0 & 0 & 0 \\ 0 & 0 & 0 & 1 & 0 & 0 \\ 0 & 0 & 0 & 0 & 1 & 0 \\ 0 & 0 & 0 & 0 & 0 & 1 \end{pmatrix}$$

and thus a U_{11}^{EQR} hyperfine interaction effected by a $\pi/2$ pulse (a π pulse with respect to the logical subspace) of qubit resonance develops a different logical-auxiliary phase than the $U_{11} = (A_{11}, \pi)$ pulse effected by resonant hyperfine stepping.

$$U_{11}^{EQR} = \begin{pmatrix} -i & 0 & 0 & 0 & 0 & 0 \\ 0 & 1 & 0 & 0 & 0 & 0 \\ 0 & 0 & 1 & 0 & 0 & 0 \\ 0 & 0 & 0 & -1 & 0 & 0 \\ 0 & 0 & 0 & 0 & -1 & 0 \\ 0 & 0 & 0 & 0 & 0 & -i \end{pmatrix} \neq U_{11} = \begin{pmatrix} -1 & 0 & 0 & 0 & 0 & 0 \\ 0 & 1 & 0 & 0 & 0 & 0 \\ 0 & 0 & 1 & 0 & 0 & 0 \\ 0 & 0 & 0 & -1 & 0 & 0 \\ 0 & 0 & 0 & 0 & -1 & 0 \\ 0 & 0 & 0 & 0 & 0 & -1 \end{pmatrix}$$

Although the two are identical within the logical subspace, the distinction is important when trying to implement two-qubit operations which make use of the auxiliary subspace. Our gate prescriptions assume the use of resonant hyperfine stepping.

Chapter 3

Damping and Diffusion of a Few Coupled SQUIDS in a Phonon Bath

3.1 Abstract

We develop a master equation, within the Born-Markov approximation, for a few superconducting quantum interference devices (SQUIDS) coupled into a chain and exchanging their angular momenta with a low temperature phonon bath. Our master equation has four generators; we concentrate on the damping and diffusion which together cause relaxation and decoherence. The spectrum of the Heisenberg SQUID chain is such that some decaying oscillations can emerge in a lower energy subspace; for two equally-spaced pairs of energies, a superposition of the upper two eigenstates relaxes coherently. It also presents critical point energy level crossings where even well-spaced large SQUIDS can partially exhibit collective coupling behavior that can dramatically reduce certain relaxation and decoherence rates.

3.2 Introduction

A superconducting quantum interference device (SQUID) can be made from a small strip of aluminum bent into a ring, joined at the ends, and cooled to a milliKelvin temperature. Aluminum is a superconductor and an aluminum oxide layer, where the ends meet, forms a “Josephson Junction” potential barrier. Precise

tuning of an externally imposed magnetic flux can cause coherent quantum oscillations of the current between clockwise “ $|\uparrow\rangle$ ” and counterclockwise “ $|\downarrow\rangle$ ” states. The ground state, $|0\rangle = (|\uparrow\rangle + |\downarrow\rangle)/\sqrt{2}$, and first excited state, $|1\rangle = (|\uparrow\rangle - |\downarrow\rangle)/\sqrt{2}$, span the low-energy dynamics of the device and form a logical basis for a qubit of quantum information, $c_0 |0\rangle + c_1 |1\rangle$.

Many SQUIDs can be coupled together into a chain. The aluminum rings are not actually linked but their proximity allows capacitive and inductive interaction between nearest neighbor SQUIDs [59, 60]. We are principally interested in using the chain to encode and protect quantum information [61]. But chains could propagate excitations, qubits [62, 63, 64, 65], and even entangled (strongly correlated) singlets, $(|\uparrow\downarrow\rangle - |\downarrow\uparrow\rangle)/\sqrt{2}$ [66, 67, 68]. They could also provide long-sought experimental realizations of spin chains which in turn illustrate the correlations and phase transitions of many-body physics. Cooling a chain to its zero-temperature ground state can prepare useful entanglement [69]. Ground state entanglement can vanish abruptly, for example, as spin-spin couplings are adjusted across a critical point [70, 71, 72]. In that case, it is the intermediate energy states that can possess entanglement; their quantum correlations can be evident, at a warmer but not too-high temperature, when mixed sufficiently into the equilibrium state [73, 74].

The instantaneous state of a spin-chain can be described by a density operator $\rho(t) = \sum_n p_n |\psi_n\rangle \langle\psi_n|$ which averages pure states $|\psi_n\rangle \langle\psi_n|$, weighted by their probabilities p_n , into a statistical mixture. In the energy eigenbasis, a diagonal element $\langle\alpha|\rho|\alpha\rangle$ is the probability of obtaining the eigenstate $|\alpha\rangle$, sometimes called the population of $|\alpha\rangle$. An off-diagonal element $\langle\alpha|\rho|\beta\rangle$ results from including su-

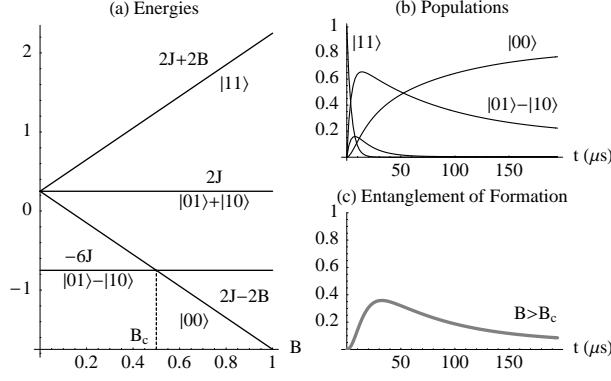


Figure 3.1: A Heisenberg two-SQUID chain above the critical point B_c cooling from $|11\rangle$ to $|00\rangle$. In the process, the states $|01\rangle \pm |10\rangle$ are occupied, resulting in a surge of the entanglement of formation, even though the ground state is separable and the large SQUIDS are dissipating independently. ($8J/h = 1.0\text{GHz}$, $2B/h = 1.5\text{GHz}$, $k_B T/h = 0.3\text{GHz}$, $R = 10\mu\text{m}$, $I = 3\mu\text{A}$, $\rho = 5\text{g/cm}^3$, $c_\perp = 5\text{km/s}$).

perpositions of eigenstates, e. g. $|\psi_1\rangle = c_\alpha |\alpha\rangle + c_\beta |\beta\rangle$; it has an evolving phase, $\langle\alpha|\rho(t)|\beta\rangle = e^{i(E_\alpha - E_\beta)t/\hbar} \langle\alpha|\rho(0)|\beta\rangle$, which indicates the chain's coherent dynamics. For this reason, these off-diagonal terms are called coherences.

The evolving phase of a coherence corresponds directly to oscillations in some physical expectation value. This is because the density operator can be written as a real linear combination of trace-orthogonal Hermitian operators. The coefficients of the expansion are just expectation values, e.g. $\text{Tr}[\rho(t)\sigma^x/2]$ is the (time-dependent) coefficient of σ^x . In the case of a single spin, its density operator is a real linear combination of Pauli operators whose coefficients are the components of the spin's average polarization. Its precession about the z -axis is indicated by an evolving phase, but physically we experience oscillating expectation values for x and y measurements.

For several qubits, observing the oscillations corresponding to an arbitrary

coherence can be complicated; one may implement a rapid unitary transformation of $\rho(t)$ to effectively transform an easier measurement into the one that will observe the oscillations. And many repetitions of the same state-preparation $\rho(0)$, evolution, and measurement are needed for each evolved time t before one can, statistically, observe the coherences in $\rho(t)$ as an oscillating expectation value.

Usually, when a quantum system is “opened-up” to its finite-temperature environment, its energies and eigenstates are perturbed and the new energies and stationary states are viewed as renormalized quantities. Then it equilibrates to a stationary thermal mixture of these eigenstates. The populations are adjusted, or interchanged, until a thermal mixture is obtained, in a process we call relaxation. The coherences will also decay (they must if the equilibrium state is to be stationary). Some of this “decoherence” goes along with the relaxation — adjusting the probabilities of the eigenstates undermines the support for any phase between them — but it can also be caused by pure dephasing, in which the phase’s probability distribution spreads, reducing the (averaged) coherence, without adjusting the populations. The decay of a coherence is, physically, just the decay of the oscillations in an expectation value. It’s absolute value is the decaying envelope of the oscillations.

We consider some open-system effects of the SQUIDS’ coupling to phonons. We suppose the SQUIDS are lithographically etched and deposited into a solid crystal (e.g. of silicon) which, for simplicity, we assume surrounds the chain. In a SQUID’s oscillation between current states, the conservation of total angular momentum requires torsional oscillations of the solid and thus the emission and absorption of phonons; the concomitant phonon-induced decoherence of a single SQUID has al-

ready been calculated [75].

Working from the total Hamiltonian $H = H_S + H_B + V$, describing the SQUIDS, the bath, and their coupling, we apply master equation techniques from the quantum Brownian motion model [76, 28], in the Born-Markov approximation, to a chain of SQUIDS interacting with a phonon heat bath. The resulting generators of the open-system dynamics are associated with four types of coefficients: the renormalization, anomalous diffusion, damping, and diffusion. We use the damping and diffusion to develop a matrix element equation for the populations and coherences. It gives the relaxation and decoherence rates, as well as the possibility for coherent oscillations to move from one subspace, where they are decaying, into a lower energy subspace with a longer decoherence time. A complete network of selection-ruled transitions leads to thermalization. This is usually the case for large well-spaced SQUIDS. For small closely-spaced SQUIDS the network is broken by the degeneracies of their collective coupling to the bath; decoherence and transition rates can scale with the number of SQUIDS or vanish; some subspaces are protected. Finally, at the critical point even the large well-spaced SQUIDS can acquire some of this collective Dicke super- and sub-radiant and super- and sub-decoherent behavior.

3.3 The Unbiased SQUID

The aluminum oxide barrier in the SQUID loop acts as a capacitor upon which charges q and $-q$ can accumulate. When an external magnetic flux threads the loop, the supercurrent of paired-electrons attempts to screen the flux by tunneling

through the thin barrier. The screening flux ϕ is a conjugate variable to the charge q : $[\phi, q] = i\hbar$. In fact, the Josephson Junction physics is such that the individual SQUID Hamiltonian is [77]

$$H_{SQUID} = \frac{q^2}{2C_J} + \frac{\phi^2}{2L} - E_J \cos \left[\frac{2e}{\hbar}(\phi - \Phi_x) \right]$$

where C_J is the junction capacitance, L is the loop inductance, E_J is the Josephson energy, $h/2e$ is the flux quantum, and Φ_x is the externally imposed flux. The $q^2/2C$ term acts like a kinetic energy term while the rest serves as a double-well potential for the flux ϕ . The truncation of the Hamiltonian to a two-level (qubit) system requires a large level separation in each well, so that only the bottom level of one well, $|\uparrow\rangle$, and the other, $|\downarrow\rangle$, are relevant. There remains the possibility of tunneling through the *symmetric* barrier, so the antisymmetric combination $|1\rangle$ has a higher energy than the symmetric $|0\rangle$. The effective result of this truncation scheme for the unbiased double-well is

$$H_{SQUID} \Rightarrow -B\sigma^x$$

with $|\uparrow\rangle$ and $|\downarrow\rangle$ the eigenstates of σ^z . Here B is not the imposed magnetic field. Instead, it is an effective magnetic field (in units of energy) appropriate to the natural precession of our pseudo-spin qubits: coherent quantum oscillations between $|\uparrow\rangle$ and $|\downarrow\rangle$.

We are interested in large SQUIDS of radius $R = 10\mu\text{m}$ with a $3\mu\text{A}$ current oscillating at 1.0 ± 0.5 GHz. Our decoherence model [75] gives decoherence times of a few μs which are not inconsistent with those of recent experiments [4, 78]. On the other hand we will also use small SQUIDS, with $R = 10$ nm and $I = 0.1\mu\text{A}$,

to demonstrate the concept of a collective coupling to the environment even though the small single SQUID decoherence model predicts times which are extraordinarily long, e.g. 10^6 s. The concept of a collective coupling is relevant to the critical point open-system dynamics of the large SQUIDs.

3.4 The Heisenberg SQUID Chain

For its mathematical simplicity and relevance to quantum information processing, we consider the isotropic Heisenberg coupling between nearest neighbor SQUIDs. In principle this can be engineered with a precise balance of inductive and capacitive coupling between nearest-neighbor SQUIDs. However, several of our methods are applicable to other types of coupling. The “antiferromagnetic” ($J > 0$) Heisenberg chain of N SQUIDs evolves by its Hamiltonian,

$$H_S = \sum_{j=1}^N (J \vec{\sigma}_j \cdot \vec{\sigma}_{j+1} - B \sigma_j^x),$$

assuming periodic boundary conditions $\vec{\sigma}_{N+1} \equiv \vec{\sigma}_1$. Here, $\vec{\sigma}_j$ are the Pauli matrices for the j th SQUID, with $|\uparrow\rangle$ and $|\downarrow\rangle$ the eigenstates of σ^z .

The Heisenberg and magnetic sums commute and their respective quantum numbers l and m determine the energy spectrum $\{lJ - mB\}$ (up to some degeneracies not split by J and B). Regardless of N , each eigenstate is a linear combination of states with the same number of $|1\rangle$ vs. $|0\rangle$ qubits ($m \equiv N_0 - N_1$) and is typically entangled, with the exception of the extremal m states $|11\dots\rangle$ and $|00\dots\rangle$. Increasing B relative to fixed J causes energy-level crossings. At a critical value, B_c , the ground state changes from entangled to unentangled.

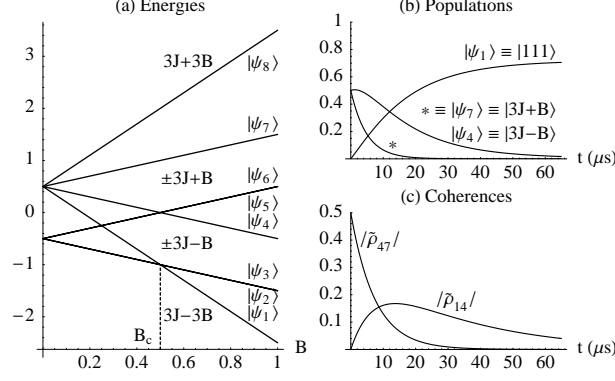


Figure 3.2: Decaying oscillations emerging in a lower energy subspace. Three large SQUIDs dissipating independently. $|\psi_4\rangle + |\psi_7\rangle$ cooling, through a mixture including $|\psi_1\rangle + |\psi_4\rangle$, to $|\psi_1\rangle$. The transitions $|\psi_4\rangle \leftrightarrow |\psi_1\rangle$ and $|\psi_7\rangle \leftrightarrow |\psi_4\rangle$ are resonant ($\Delta_{14} = \Delta_{47}$). $\tilde{\rho}_{47}$, which decays $\sim e^{-\tilde{\Gamma}_{47}t}$, is absorbed into $\tilde{\rho}_{14}$ which decays more slowly $\sim e^{-\tilde{\Gamma}_{14}t}$. It might be easier to start with $|\uparrow\uparrow\uparrow\rangle$, which is sufficiently close to the equal superposition of $|\psi_4\rangle = |001\rangle + |100\rangle + |010\rangle$ and $|\psi_7\rangle = |011\rangle + |110\rangle + |100\rangle$, to prepare the coherence which flows into $\tilde{\rho}_{14}$. ($6J/h = 1.0\text{GHz}$, $2B/h = 1.5\text{GHz}$, $k_B T/h = 0.3\text{GHz}$, $R = 10\mu\text{m}$, $I = 3\mu\text{A}$).

The two-SQUID chain's energies are shown in Figure 3.1; their eigenstates are $|\psi_1\rangle \equiv |00\rangle$, $|\psi_2\rangle \equiv |01\rangle - |10\rangle$, $|\psi_3\rangle \equiv |01\rangle + |10\rangle$, and $|\psi_4\rangle \equiv |11\rangle$. For the three-SQUID chain's energies, shown in Figure 3.2, we use eigenstates

$$\begin{aligned}
 |\psi_1\rangle &\equiv |000\rangle \\
 |\psi_2\rangle &\equiv |001\rangle - |100\rangle \\
 |\psi_3\rangle &\equiv |001\rangle + |100\rangle - 2|010\rangle \\
 |\psi_4\rangle &\equiv |001\rangle + |100\rangle + |010\rangle \\
 |\psi_5\rangle &\equiv |011\rangle - |110\rangle \\
 |\psi_6\rangle &\equiv |011\rangle + |110\rangle - 2|101\rangle \\
 |\psi_7\rangle &\equiv |011\rangle + |110\rangle + |101\rangle \\
 |\psi_8\rangle &\equiv |111\rangle.
 \end{aligned}$$

3.5 The Harmonic Phonon Bath

The harmonic crystal Hamiltonian is composed of phonon modes labelled by wavevector \vec{k} and polarization index s . The phonons are annihilated by $a_{\vec{k}s}$ and created by $a_{\vec{k}s}^\dagger$ and each contributes an energy $\hbar\omega_s(\vec{k})$:

$$H_B = \sum_{\vec{k},s} \hbar\omega_s(\vec{k}) a_{\vec{k}s}^\dagger a_{\vec{k}s} = \sum_n \overbrace{\sum_{\vec{k},s} \hbar\omega_s(\vec{k}) n_{\vec{k}s}}^{E_n} |n\rangle \langle n|.$$

The eigenstates, $|n\rangle$, have a definite number $\langle a_{\vec{k}s}^\dagger a_{\vec{k}s} \rangle = n_{\vec{k}s}$ of phonons in each mode, so that their total energy is $E_n = \sum_{\vec{k},s} \hbar\omega_s(\vec{k}) n_{\vec{k}s}$. The label n stands for the string of phonon numbers for each mode. We make use of

$$\begin{aligned} a_{\vec{k}s} |n\rangle &= \sqrt{n_{\vec{k}s}} |n_{\vec{k}s} - 1\rangle & a_{\vec{k}s}^\dagger |n\rangle &= \sqrt{n_{\vec{k}s} + 1} |n_{\vec{k}s} + 1\rangle \\ \langle n| a_{\vec{k}s}^\dagger &= \sqrt{n_{\vec{k}s}} \langle n_{\vec{k}s} - 1| & \langle n| a_{\vec{k}s} &= \sqrt{n_{\vec{k}s} + 1} \langle n_{\vec{k}s} + 1| \\ H_B |n\rangle &= E_n |n\rangle & e^{\pm iH_B t/\hbar} |n\rangle &= e^{\pm iE_n t/\hbar} |n\rangle \end{aligned}$$

where $|n_{\vec{k}s} \pm 1\rangle$ just means, in the string n of phonon numbers, one more or less phonon in the $\vec{k}s$ mode. For frequencies below a cutoff frequency Λ we assume linear dispersions, $\omega_{1,2}(\vec{k}) = c_\perp |\vec{k}|$ and $\omega_3(\vec{k}) = c_\parallel |\vec{k}|$, for transverse (\perp) and longitudinal (\parallel) polarizations $\hat{e}_s(\vec{k}) = \{\hat{k}_{\perp 1}, \hat{k}_{\perp 2}, \hat{k}_\parallel\}$. The momentum density at site \vec{r} is

$$\vec{\pi}(\vec{r}) = \frac{-i}{\sqrt{V}} \sum_{\vec{k},s} \sqrt{\frac{\hbar\omega_s(\vec{k})\rho}{2}} (a_{\vec{k}s} e^{i\vec{k}\cdot\vec{r}} - a_{\vec{k}s}^\dagger e^{-i\vec{k}\cdot\vec{r}}) \hat{e}_s(\vec{k})$$

with V and ρ the volume and mass density of the crystal.

3.6 The Chain-Bath Coupling

The coupling between the SQUIDS and the crystal arises from the fact that each SQUID's current is formed from the electron band states in the reference frame

co-moving with the lattice sites during the torsional oscillations of the crystal [75]. In the lab frame the electron velocity \vec{v}_e must include the speed $\dot{\vec{u}} = \vec{\pi}/\rho$ of the lattice sites: $\vec{v}_e = \vec{j}/(en_e) + \dot{\vec{u}}$. Here \vec{j} is the current density and e and n_e are the electron charge and number density of the electrons. Their kinetic energy density $n_e \frac{1}{2} m_e |\vec{v}_e|^2$ thus acquires a cross term $\sim \vec{j} \cdot \dot{\vec{u}}$ so that the total Hamiltonian must include an additional $V = (m_e/e) \int d^3r \vec{j} \cdot \dot{\vec{u}}$. From this we derive, following [75], the coupling V_j of an individual SQUID to the crystal and then, because the current density \vec{j} is the sum of the individual densities \vec{j}_j , sum their contributions into the total coupling V .

The first SQUID has a current $I\sigma_1^z$ confined to its ring of cross-sectional area b : $\vec{j}_1 = (I/b)\sigma_1^z \hat{\phi}$ within the ring, $\vec{j}_1 = 0$ elsewhere. Here $\hat{\phi}$ is the azimuthal unit vector in cylindrical coordinates centered on the ring. With

$$\vec{\phi}_{\vec{k}} \equiv \int_0^{2\pi} d\phi \int_{R-\sqrt{b}/2}^{R+\sqrt{b}/2} dr r \int_{-\sqrt{b}/2}^{\sqrt{b}/2} dz \hat{\phi} e^{-i\vec{k}\cdot\vec{r}}$$

the Fourier transform of the $\hat{\phi}$ within the ring, we have

$$V_1 = \frac{m_e I}{e b} \sigma_1^z \frac{-i}{\sqrt{V}} \sum_{\vec{k}_s} \sqrt{\frac{\hbar\omega_s(\vec{k})}{2\rho}} \left(a_{\vec{k}_s} \vec{\phi}_{\vec{k}}^* - a_{\vec{k}_s}^\dagger \vec{\phi}_{\vec{k}} \right) \cdot \hat{e}_s(\vec{k}).$$

In the thin ring approximation, $|\vec{k}|\sqrt{b} \ll 1$, the Fourier transform becomes

$$\vec{\phi}_{\vec{k}} \Rightarrow -i2\pi Rb J_1(|\vec{k}|R \sin \theta) \hat{n}_{\vec{k}},$$

where $J_1(|\vec{k}|R \sin \theta)$ is the first order Bessel function. The polar angle θ is the angle between the \hat{z} -axis of the ring and the wavevector \vec{k} while $\hat{n}_{\vec{k}} \perp \vec{k}$ lies in the plane of the ring. Choosing $\hat{e}_1(\vec{k})$ to lie in the plane of the ring, i.e. $\hat{e}_1(\vec{k}) = \hat{n}_{\vec{k}}$, we obtain

$$V_1 = \gamma \sigma_1^z \sum_{\vec{k}} \sqrt{|\vec{k}R|} J_1(|\vec{k}R| \sin \theta) \left(a_{\vec{k}1} + a_{\vec{k}1}^\dagger \right),$$

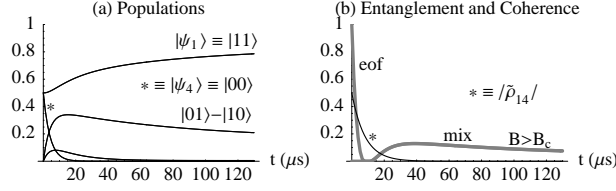


Figure 3.3: Decoherence and Relaxation in two large SQUIDs dissipating independently. $|00\rangle + |11\rangle$ cooling above the critical point. (a) The population dynamics are the same for an equal mixture of $|\psi_1\rangle \equiv |11\rangle$ and $|\psi_4\rangle \equiv |00\rangle$; only the superposition is entangled. (b) The entanglement does not oscillate because any phase between $|00\rangle$ and $|11\rangle$ may be generated locally. It decays faster than the coherence $\tilde{\rho}_{14} \sim e^{-\tilde{\Gamma}_{14}t}$ upon which it depends. Later, the populations mix back in some entanglement. ($8J/h = 1.0\text{GHz}$, $2B/h = 1.5\text{GHz}$, $k_B T/h = 0.3\text{GHz}$, $R = 10\mu\text{m}$, $I = 3\mu\text{A}$).

with coupling constant $\gamma \equiv 2\pi I(m_e/e)\sqrt{R\hbar c_\perp/2\rho V}$.

Note that the only displacements that couple to the SQUID are torsional, $\hat{n}_{\vec{k}} \cdot \vec{k} = 0 \Leftrightarrow \nabla \cdot \vec{u} = 0$, and in-plane, consistent with the conservation of total angular momentum. This is the minimal, required by symmetry, coupling of SQUIDs to the phonon bath.

The other SQUID rings are centered not at $\vec{r} = 0$ but are evenly spaced, a distance d apart, along the \hat{x} -axis. The analysis for each SQUID's coupling to phonons is calculated in its own coordinates \vec{r}_j centered at $\vec{x}_j \equiv d(j-1)\hat{x}$ so that $\vec{r} = \vec{x}_j + \vec{r}_j$. The creation and annihilation operators' phase factors $e^{\pm i\vec{k} \cdot \vec{r}}$ become $e^{\pm i\vec{k} \cdot \vec{x}_j} e^{\pm i\vec{k} \cdot \vec{r}_j}$ while the rest of the calculations, in the \vec{r}_j coordinates, are exactly the same as before. The total coupling is thus

$$V = \gamma \sum_j \sigma_j^z \sum_{\vec{k}} \sqrt{|\vec{k}R|} J_1(k_x R) \left(a_{\vec{k}1} e^{i\vec{k} \cdot \vec{x}_j} + a_{\vec{k}1}^\dagger e^{-i\vec{k} \cdot \vec{x}_j} \right), \quad (3.1)$$

where $J_1(k_x R)$ is shorthand for $J_1(|\vec{k}R| \sin \theta)$.

Writing $V = \gamma \sum_j \mathcal{X}_j \phi_j$ emphasizes the bi-linear form, akin to a quantum

Brownian oscillator's coupling to an oscillator bath, $\sim x\phi$, only here we are summing over several contact-points between the chain and the bath. The chain operators $\mathcal{X}_j \equiv \sigma_j^z$ interact with the bath operators

$$\phi_j \equiv \sum_{\vec{k}} \sqrt{|\vec{k}R|} J_1(k_x R) \left(a_{\vec{k}1} e^{i\vec{k}\cdot\vec{x}_j} + a_{\vec{k}1}^\dagger e^{-i\vec{k}\cdot\vec{x}_j} \right).$$

Note that there are selection rules: $\langle l'm' | \mathcal{X}_j | lm \rangle \sim \delta_{m', m \pm 2}$. The “interaction operator” \mathcal{X}_j flips the j^{th} $|0\rangle$ or $|1\rangle$, giving us a non-zero probability only to obtain an eigenstate with one more $|1\rangle$ or $|0\rangle$. The allowed bath-driven transition frequencies are $\Delta = [\pm 2B + (l - l')J]/\hbar$; any transitions driven between degenerate states are necessarily between distinct l and l' at a crossing of energy levels. For example, the two-SQUID chain's interaction operators are, in its eigenbasis,

$$\mathcal{X}_{1,2} = \frac{1}{\sqrt{2}} \begin{pmatrix} 0 & \mp 1 & 1 & 0 \\ \mp 1 & 0 & 0 & \pm 1 \\ 1 & 0 & 0 & 1 \\ 0 & \pm 1 & 1 & 0 \end{pmatrix}.$$

They present a “network” of selection-ruled transitions: $|\psi_1\rangle \leftrightarrow |\psi_2\rangle$, $|\psi_1\rangle \leftrightarrow |\psi_3\rangle$, $|\psi_2\rangle \leftrightarrow |\psi_4\rangle$, and $|\psi_3\rangle \leftrightarrow |\psi_4\rangle$ with energies $2B$ and $2B \pm 8J$.

3.7 The Formalism

We now apply master equation techniques from the model of quantum Brownian motion [76, 28] to the chain of SQUIDS interacting with their phonon bath.

The unperturbed Hamiltonian $H_0 \equiv H_S + H_B$ defines a standard interaction picture in which the coupling $\tilde{V}(t) = e^{iH_0 t/\hbar} V(t) e^{-iH_0 t/\hbar}$ determines the evolution of

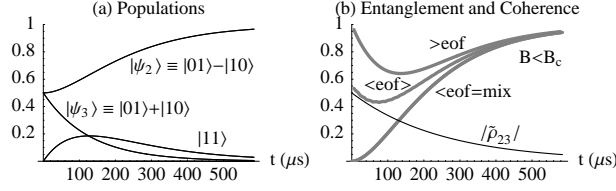


Figure 3.4: Entanglement oscillations in two large SQUIDs dissipating independently. $|01\rangle$ cooling below the critical point. (a) The population dynamics are the same for an equal mixture of $|\psi_2\rangle \equiv |01\rangle - |10\rangle$ and $|\psi_3\rangle \equiv |01\rangle + |10\rangle$. (b) From their initial superposition $|01\rangle$, the evolving phase between $|\psi_2\rangle$ and $|\psi_3\rangle$ drives $\approx 6 \times 10^5$ rapid oscillations of the entanglement of formation (eof); we have plotted a moving average $\langle \text{eof} \rangle$, the upper bound ($>\text{eof}$), and the lower bound ($<\text{eof}$) which is the same as the entanglement of the mixture. Initially, the moving average decays with the coherence $\tilde{\rho}_{23} \sim e^{-\Gamma_{23}t}$ but later pulls away to equilibrate. ($8J/h = 1.0\text{GHz}$, $2B/h = 0.5\text{GHz}$, $k_B T/h = 0.1\text{GHz}$, $R = 10\mu\text{m}$, $I = 3\mu\text{A}$).

the system-bath density operator $\tilde{w}(t)$ to second order as

$$\dot{\tilde{w}}(t) = -\frac{i}{\hbar} [\tilde{V}(t), \tilde{w}(0)] - \frac{1}{\hbar^2} \int_0^t dt' [\tilde{V}(t), [\tilde{V}(t'), \tilde{w}(0)]].$$

(The overdot denotes $\frac{d}{dt}$). Next, we assume the bath is a thermal state $\rho_B = (e^{-H_B/k_B T})/Z_B$ initially uncorrelated with the chain: $\tilde{w}(0) = \rho(0) \otimes \rho_B$. Here T is the temperature and $Z_B = \sum_n e^{-E_n/k_B T}$ is the bath's partition function. We average (trace) over the states of the bath to obtain a preliminary equation of motion for the system:

$$\dot{\tilde{\rho}}(t) = -\frac{\gamma^2}{\hbar^2} \sum_{j,k=1}^N \int_0^t dt' \text{Tr}_B [\tilde{\mathcal{X}}_j(t) \tilde{\phi}_j(t), [\tilde{\mathcal{X}}_k(t') \tilde{\phi}_k(t'), \tilde{w}(0)]] \quad (3.2)$$

where we eliminated the first order term with the $\text{Tr}_B[\tilde{\phi}_j \rho_B] = 0$ that results from summing (tracing), in the bath's energy eigenbasis, over the always-vanishing diagonal matrix elements $\langle n | \tilde{\phi}_j \rho_B | n \rangle = 0$. For example, for $j = 1$ (when $e^{\pm i\vec{k} \cdot \vec{x}_j} = 1$)

we have

$$\mathrm{Tr}_B[\tilde{\phi}_1 \rho_B] = \sum_n \sum_{\vec{k}} \sqrt{|\vec{k}R|} J_1(k_x R) \underbrace{\langle n | (\tilde{a}_{\vec{k}1} + \tilde{a}_{\vec{k}1}^\dagger) | n \rangle}_0 \frac{e^{-E_n/k_B T}}{Z_B} = 0.$$

For a given (j, k) -pair of SQUIDS, the trace of the nested commutators results in four integrals. Since they differ only in the permutation of terms, a representative one is

$$\tilde{\mathcal{X}}_j(t) \underbrace{\int_0^t dt' \tilde{\mathcal{X}}_k(t') \overbrace{\mathrm{Tr}_B[\tilde{\phi}_j(t) \tilde{\phi}_k(t') \rho_B]}^{\nu_{jk}(\tau) - i\mu_{jk}(\tau)}}_{\tilde{\mathcal{V}}_{jk}(t) - i\tilde{\mathcal{U}}_{jk}(t)} \rho(0), \quad (3.3)$$

where the over- and under-braces highlight the time-averaging of the interaction operator $\tilde{\mathcal{X}}_k(t')$, into what we call the noise $\tilde{\mathcal{V}}_{jk}(t)$ and susceptibility $\tilde{\mathcal{U}}_{jk}(t)$ operators, by the kernels $\nu_{jk}(\tau)$ and $\mu_{jk}(\tau)$ that, with $\tau \equiv t - t'$, are the real and imaginary parts of the bath correlator $\mathrm{Tr}_B[\tilde{\phi}_j(t) \tilde{\phi}_k(t') \rho_B]$. In the context of the quantum Brownian oscillator, these noise and susceptibility kernels are sometimes called, respectively, the fluctuation ν and dissipation η [28].

The four integrals for each SQUID-pair, originating from the nested commutators and each contributing a noise and a susceptibility, can be collected to obtain a ‘‘Born’’ (but not yet Born-Markov) master equation (still in the interaction picture, still only valid to second order),

$$\dot{\tilde{\rho}} = -\frac{\gamma^2}{\hbar^2} \sum_{j,k=1}^N \left([\tilde{\mathcal{X}}_j, [\tilde{\mathcal{V}}_{jk}, \tilde{\rho}]] - i[\tilde{\mathcal{X}}_j, \{\tilde{\mathcal{U}}_{jk}, \tilde{\rho}\}] \right), \quad (3.4)$$

where we have used Born’s approximation that replaces $\rho(0)$ with $\tilde{\rho}(t) \approx \rho(0)$.

Born’s approximation adds a self-awareness to the integrated solution for $\tilde{\rho}(t)$; in a small time step dt the instantaneous change $d\tilde{\rho}$ depends not on the initial $\rho(0)$ but on the updated instantaneous $\tilde{\rho}(t)$. We will see that this updating is needed

for the long-time equilibration to thermal equilibrium. The Born master equation, although technically still only valid to second order, is a plausible guess at the longer-time open-system dynamics which, like any other theory, can only be supported by real data or exactly solvable open-systems, like the quantum Brownian oscillator, and may not be valid in every case.

3.8 The Coefficients

The time-averaging into the noise and susceptibility may be done in a basis of energy eigenstates $|\alpha\rangle$ for which $H_S |\alpha\rangle = E_\alpha |\alpha\rangle$ and $\hbar\Delta_{\alpha\beta} \equiv E_\beta - E_\alpha$ is the energy lost in the transition from $|\beta\rangle$ to $|\alpha\rangle$. The averages' matrix elements are

$$\langle\alpha|\tilde{\mathcal{X}}_k|\beta\rangle \int_0^t d\tau (\nu_{jk} - i\mu_{jk}) e^{i\Delta_{\alpha\beta}\tau} \equiv \langle\alpha|\tilde{\mathcal{V}}_{jk}|\beta\rangle - i\langle\alpha|\tilde{\mathcal{U}}_{jk}|\beta\rangle,$$

$$\underbrace{\hspace{10em}}_{(D_{jk}^\Delta(t) + iA_{jk}^\Delta(t)) - i(r_{jk}^\Delta(t) + i\gamma_{jk}^\Delta(t))}$$

where the coefficients of Diffusion, Anomalous diffusion, renormalization, and damping serve to Fourier-sample (at least for $t \rightarrow \infty$) the real and imaginary parts of the bath correlator:

$$D_{jk}^\Delta(t) = \int_0^t d\tau \nu_{jk}(\tau) \cos \Delta\tau \quad A_{jk}^\Delta(t) = \int_0^t d\tau \nu_{jk}(\tau) \sin \Delta\tau$$

$$r_{jk}^\Delta(t) = \int_0^t d\tau \mu_{jk}(\tau) \cos \Delta\tau \quad \gamma_{jk}^\Delta(t) = \int_0^t d\tau \mu_{jk}(\tau) \sin \Delta\tau.$$

Back in the Schrödinger picture, both the chain and bath are evolving by coherent oscillations perturbed by the coupling $V = \gamma \sum_j \mathcal{X}_j \phi_j$. This coupling will have the greatest effect when the oscillations are resonant, and have little effect for off-resonant oscillations. In this sense, the evolution of $\tilde{\mathcal{X}}_k(t')$ (in the interaction picture) is sampling the bath correlations at the transition frequencies allowed by

the selection rules; the noise and susceptibility accumulate these data; and the instantaneous dynamics of $\tilde{\rho}$ depend on them. Each type of coefficient results in its own generator of these open-system dynamics and later we consider in detail their effects.

3.8.1 The Bath Correlator

For now, in order to understand the coefficients, we show that the bath correlator can be written as a frequency integral,

$$\text{Tr}_B[\tilde{\phi}_j(t) \tilde{\phi}_k(t') \rho_B] = \underbrace{\int_0^\infty d\omega J_{jk}(\omega) \coth\left(\frac{\hbar\omega}{2k_B T}\right) \cos(\omega\tau)}_{\nu_{jk}(\tau)} - i \underbrace{\int_0^\infty d\omega J_{jk}(\omega) \sin(\omega\tau)}_{\mu_{jk}(\tau)},$$

characterized by bath spectral densities $J_{jk}(\omega)$. To evaluate the correlator we (again) perform the trace in the bath's energy eigenbasis by summing over the diagonal matrix elements:

$$\begin{aligned} \text{Tr}_B[\tilde{\phi}_j(t) \tilde{\phi}_k(t') \rho_B] &= \sum_n \sum_{\vec{k}, \vec{k}'} \sqrt{|\vec{k}R||\vec{k}'R|} J_1(k_x R) J_1(k'_x R) \\ &\times \langle n | \left(\tilde{a}_{\vec{k}1}(t) e^{i\vec{k}\cdot\vec{x}_j} + \tilde{a}_{\vec{k}1}^\dagger(t) e^{-i\vec{k}\cdot\vec{x}_j} \right) \left(\tilde{a}_{\vec{k}'1}(t') e^{i\vec{k}'\cdot\vec{x}_k} + \tilde{a}_{\vec{k}'1}^\dagger(t') e^{-i\vec{k}'\cdot\vec{x}_k} \right) \frac{e^{-E_n/k_B T}}{Z_B} |n\rangle \\ &= \overbrace{\left(\frac{V}{8\pi^3} \int_0^\infty \frac{d\omega \omega^2}{c_\perp^3} \int_0^\pi d\theta \sin\theta \int_0^{2\pi} d\phi \right)}^{\sum_{\vec{k}} |\vec{k}R| J_1^2(k_x R)} \omega\tau_R J_1^2(\omega\tau_R \sin\theta) \\ &\times \underbrace{\left[\coth\left(\frac{\hbar\omega}{2k_B T}\right) \cos(\omega\tau) - i \sin(\omega\tau) \right]}_{(N_\omega+1)e^{-i\omega\tau} + N_\omega e^{i\omega\tau}} \underbrace{\cos(\omega\tau_{jk} \sin\theta \cos\phi)}_{\Re[e^{\pm i\vec{k}\cdot(\vec{x}_j - \vec{x}_k)}]}. \end{aligned}$$

The steps leading to the second line are as follows. The double sum $\sum_{\vec{k}, \vec{k}'}$ collapses to a single sum $\sum_{\vec{k}}$ (which we convert to a \vec{k} -space integral in spherical coordinates) because the only non-zero cross-terms $\sim \delta_{\vec{k}\vec{k}'}$. They are

$$\langle n | \tilde{a}_{\vec{k}1} e^{i\vec{k}\cdot\vec{x}_j} \tilde{a}_{\vec{k}'1}^\dagger e^{-i\vec{k}'\cdot\vec{x}_k} |n\rangle = (n_{\vec{k}1} + 1) \delta_{\vec{k}\vec{k}'} e^{-i\omega\tau} e^{i\vec{k}\cdot\vec{x}_{jk}}$$

and

$$\langle n | \tilde{a}_{\vec{k}_1}^\dagger e^{-i\vec{k}\cdot\vec{x}_j} \tilde{a}_{\vec{k}'_1} e^{i\vec{k}'\cdot\vec{x}_k} | n \rangle = n_{\vec{k}_1} \delta_{\vec{k}\vec{k}'} e^{i\omega\tau} e^{-i\vec{k}\cdot\vec{x}_{jk}},$$

where the factors $e^{\pm i\omega\tau}$ arise from being in the interaction picture. Here we have abbreviated $\omega_1(\vec{k}) = \omega$ for the angular frequency of the mode with wavevector \vec{k} and transverse-in-plane polarization and written $\vec{x}_{jk} = \vec{x}_j - \vec{x}_k$ for the vector connecting the (j, k) -pair of SQUIDS. We have also used $\tau_R \equiv R/c_\perp$, which is half the time it takes a phonon to traverse a SQUID. We switch the order of the sums, $\sum_n \sum_{\vec{k}} \Rightarrow \sum_{\vec{k}} \sum_n$, and write $N_\omega \equiv \sum_n n_{\vec{k}_1} \frac{e^{-E_n/k_B T}}{Z_B}$ for the thermal-average occupation number. It sums to

$$N_\omega = \frac{\sum_{n_{\vec{k}_1}} n_{\vec{k}_1} e^{-\hbar\omega n_{\vec{k}_1}/k_B T}}{\sum_{n_{\vec{k}_1}} e^{-\hbar\omega n_{\vec{k}_1}/k_B T}} \underbrace{\frac{\prod_{i \neq \vec{k}_1} \sum_{n_i} e^{-\hbar\omega_i n_i/k_B T}}{\prod_{i \neq \vec{k}_1} \sum_{n_i} e^{-\hbar\omega_i n_i/k_B T}}}_1 = 1/(e^{\hbar\omega/k_B T} - 1).$$

Now every function in the bath correlator besides the $e^{\pm i\vec{k}\cdot\vec{x}_{jk}}$ is an even function of \vec{k} . The sum over wavevectors thus selects the $\cos(\vec{k} \cdot \vec{x}_{jk})$ part of $e^{\pm i\vec{k}\cdot\vec{x}_{jk}}$. Because the (j, k) -pair of SQUIDS are positioned on the \hat{x} -axis, we use $k_x = |\vec{k}| \sin \theta \cos \phi$ to obtain $\cos(\vec{k} \cdot \vec{x}_{jk}) = \cos(\omega\tau_{jk} \sin \theta \cos \phi)$, with $\tau_{jk} = d(j - k)/c_\perp$ the phonon transit time between the SQUIDS. Finally, it can be shown that $(2N_\omega + 1) = \coth(\hbar\omega/2k_B T)$ so that we can write

$$(N_\omega + 1)e^{-i\omega\tau} + N_\omega e^{i\omega\tau} = \coth\left(\frac{\hbar\omega}{2k_B T}\right) \cos(\omega\tau) - i \sin(\omega\tau).$$

To complete our analysis of the bath correlator we must integrate over the modes. It is relatively easy to perform the ϕ integration $\int_0^{2\pi} d\phi \cos(\omega\tau_{jk} \sin \theta \cos \phi) = 2\pi J_0(\omega\tau_{jk} \sin \theta)$, while the θ integration

$$\Theta_{jk}(\omega\tau_R) \equiv 2\pi \int_0^\pi d\theta \sin \theta J_1^2(\omega\tau_R \sin \theta) J_0(\omega\tau_{jk} \sin \theta)$$

requires some approximations. But with $\Theta_{jk}(\omega\tau_R)$ we can write the bath correlator as an integral over bath frequencies,

$$\text{Tr}_B[\tilde{\phi}_j(t)\tilde{\phi}_k(t')\rho_B] = \underbrace{\int_0^\infty d\omega J_{jk}(\omega) \coth\left(\frac{\hbar\omega}{2k_B T}\right) \cos(\omega\tau)}_{\nu_{jk}(\tau)} - i \underbrace{\int_0^\infty d\omega J_{jk}(\omega) \sin(\omega\tau)}_{\mu_{jk}(\tau)},$$

characterized by the spectral densities

$$J_{jk}(\omega) = \frac{V}{8\pi^3} \frac{\tau_R}{c_\perp^3} \omega^3 \Theta_{jk}(\omega\tau_R).$$

Technically, the ω integration should have an upper limit corresponding to the maximum wavevector \vec{k} available to the bath. Furthermore, the linear dispersions $\omega_s(\vec{k})$ we assumed for the phonon bath do not necessarily apply to the larger \vec{k} . One can thus introduce a cutoff, or ‘‘Debye,’’ frequency $\Lambda \gg \Delta$ by inserting a factor $e^{-\omega/\Lambda}$ into the ω integrations. This essentially discards from our master equations any high frequency ($\omega \gg \Lambda$) effects of the bath.

3.8.2 The Spectral Densities

It will turn out that the long-time values of the coefficients of damping and diffusion can be obtained from knowing the spectral densities at reasonable chain frequencies Δ , while we will make do without ever actually evaluating the coefficients of renormalization and anomalous diffusion (which would require integrating to higher bath frequencies). At these reasonable Δ we can approximate the spectral densities in two regimes from which we draw our examples: SQUIDs which are far apart ($\Delta\tau_{jk} \gg 1$) and close together ($\Delta\tau_{jk} \ll 1$). In these examples the J and B of the SQUID chain must be set close-to or far-from any level crossings where $\Delta \Rightarrow 0$.

For the single SQUID ($j = k$) θ integration we obtain

$$\frac{\gamma^2 \pi}{\hbar^2 2} J_{jj}(\Delta) = \frac{m_e^2 I^2 (\pi R^2)^2}{3\pi \hbar e^2 4\rho c_{\perp}^5} \Delta^5 \underbrace{{}_pF_q\left(\left\{\frac{3}{2}\right\}, \left\{\frac{5}{2}, 3\right\}, -(\Delta\tau_R)^2\right)}_{3\Theta_{jj}(\Delta\tau_R)/2\pi(\Delta\tau_R)^2}$$

independent of j and with ${}_pF_q$ the generalized hypergeometric function. Here we multiplied by $\frac{\gamma^2 \pi}{\hbar^2 2}$ to get a useful equivalent-rate. Although we use these exact “ ${}_pF_q$ ” rates in our numerical simulations, it is helpful to know that for a “small ring” ($\Delta\tau_R \ll 1$) the single small SQUID equivalent-rate is approximately

$$\frac{\gamma^2 \pi}{\hbar^2 2} J_{jj}^{(S)}(\Delta) \Rightarrow \frac{m_e^2}{3\pi \hbar e^2} \frac{I^2 (\pi R^2)^2}{4\rho c_{\perp}^5} \Delta^5$$

while for a “large ring” ($\Delta\tau_R \gg 1$) the single large SQUID equivalent-rate is approximately

$$\frac{\gamma^2 \pi}{\hbar^2 2} J_{jj}^{(L)}(\Delta) \Rightarrow \frac{\pi m_e^2}{\hbar e^2} \frac{I^2 R}{4\rho c_{\perp}^2} \Delta^2.$$

Next we assume that when $\Delta\tau_{jk} \gg 1$ we can neglect the cross term ($j \neq k$) spectral densities. The assumption relies on the $J_0(\Delta\tau_{jk} \sin \theta)$ kernel of the θ integration oscillating quickly enough between positive and negative values that the integral never accumulates any significant value.

For $\Delta\tau_{jk} \ll 1$, as can happen for “large” SQUIDs at a level crossing where $\Delta \approx 0$ or, regardless of Δ , for a few small SQUIDs spaced only a few small SQUID radii apart, the cross term spectral densities must be considered. It turns out that to first order in $\Delta\tau_{jk}$ we can use the single SQUID $j = k$ rates for the $j \neq k$ cross terms. $\Delta\tau_{jk} \ll 1$ implies $\Delta\tau_R \ll 1$ so we start with $J_1(\Delta\tau_R \sin \theta) \approx \frac{1}{2} \Delta\tau_R \sin \theta$ to obtain

$$\frac{\Theta_{jk}(\Delta\tau_R)}{\Delta^2 \tau_R^2 / 4} \Rightarrow 4\pi \frac{\overbrace{2\pi \int d\theta \sin^3 \theta J_0(\omega\tau_{jk} \sin \theta)}^{\Delta\tau_{jk} \cos(\Delta\tau_{jk}) - (1 - \Delta^2 \tau_{jk}^2) \sin(\Delta\tau_{jk})}}{\Delta^3 \tau_{jk}^3},$$

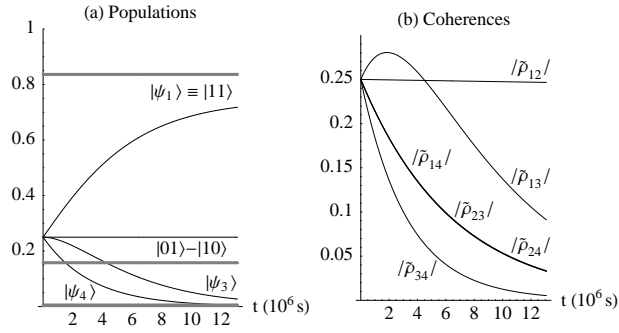


Figure 3.5: The protected singlet in two small SQUIDs dissipating collectively. $|\psi_1\rangle + |\psi_2\rangle + |\psi_3\rangle + |\psi_4\rangle$ cooling above the critical point. The singlet is an invariant subspace of both the collective interaction operator $J_z = \mathcal{X}_1 + \mathcal{X}_2$ and the Hamiltonian $H_S^{(1)}$; it is broken out of the network of allowed transitions. (a) $|\psi_4\rangle$ flows into $|\psi_3\rangle$ which flows into $|\psi_1\rangle$. $|\psi_2\rangle$ cannot give up $|\psi_1\rangle$'s usual thermal-share of its population; they do not approach their thermal (gray) levels. The collective relaxation rate from $|\psi_3\rangle$ into $|\psi_1\rangle$ is double the independent rate. (b) The coherence $\tilde{\rho}_{12}$, between $|\psi_1\rangle$ and the singlet $|\psi_2\rangle = |01\rangle - |10\rangle$, barely decays; the only mechanism for that is the $|\psi_1\rangle \rightarrow |\psi_3\rangle$ transition which is suppressed by the cold bath. Note also how $\tilde{\rho}_{13}$ grows from the decay of $\tilde{\rho}_{34}$. The subsequent decoherence rate for $\tilde{\rho}_{13}$ is double its independent dissipation rate. ($8J/h = 1.0\text{GHz}$, $2B/h = 1.5\text{GHz}$, $k_B T/h = 0.3\text{GHz}$, $R = 10\text{nm}$, $I = 0.1\mu\text{A}$).

which, to first order in $\Delta\tau_{jk}$, are identical to those of a single small SQUID

$$\frac{\gamma^2}{\hbar^2} \frac{\pi}{2} J_{j \neq k}^{(S)} \Rightarrow \frac{\gamma^2}{\hbar^2} \frac{\pi}{2} J_{jj}^{(S)}(\Delta)$$

and we may as well use the ${}_pF_q$ equivalent rates

Again, the ${}_pF_q$ equivalent-rates are the ones we use for $j = k$, and for close-together SQUIDS satisfying $\Delta\tau_{jk} \ll 1$ we also use them for the $j \neq k$ cross terms (instead of zero, which we use for $j \neq k$ whenever $\Delta\tau_{jk} \gg 1$).

This is the provenance of a collective coupling to the bath $V = \gamma(\sum_j \mathcal{X}_j)\phi_1$ whose square includes all cross terms equally. In our case, $\sum_j \mathcal{X}_j = \sum_j \sigma_j^z \equiv J_z$. For the two-SQUID chain its matrix elements in the eigenbasis are

$$J_z = \sqrt{2} \begin{pmatrix} 0 & 0 & 1 & 0 \\ 0 & 0 & 0 & 0 \\ 1 & 0 & 0 & 1 \\ 0 & 0 & 1 & 0 \end{pmatrix}$$

and the network of selection-rules becomes $|\psi_1\rangle \leftrightarrow |\psi_3\rangle \leftrightarrow |\psi_4\rangle$ while $|\psi_2\rangle$ is a protected subspace.

A collective coupling can have degenerate subspaces with which the system Hamiltonian may (or may not) cooperate, giving a decoherence- and/or relaxation-free subspace (or not) [12, 29, 79]. On the other hand, when we include all the cross terms equally, the master equation has N times as many terms, for N SQUIDS, as in the case of independent dissipation. This can scale the decoherence and relaxation rates linearly with the number of subsystems [30, 31].

3.8.3 The Markov Approximation

Instead of attempting the difficult ω integration, we instead now look at how the time-averaging samples the allowed transition frequencies from the bath. The sampling is manifested in the coefficients of diffusion, renormalization, anomalous diffusion, and damping, which convolve a $\cos \Delta\tau$ or $\sin \Delta\tau$ with the $\nu_{jk}(\tau)$ or $\mu_{jk}(\tau)$ kernels. But the only time-dependent terms in the integrands for the kernels are $\cos \omega\tau$ or $\sin \omega\tau$. Since these time-convolutions are relatively simple, in our calculation of the coefficients we switch the order of the integrals, $\int d\tau \int d\omega \Rightarrow \int d\omega \int d\tau$.

For the diffusion and damping we find that the integrations $\int_0^t d\tau \cos \omega\tau \cos \Delta\tau$ or $\int_0^t d\tau \sin \omega\tau \sin \Delta\tau$ are

$$\frac{1}{2} \left[\frac{\sin(\omega - \Delta)t}{\omega - \Delta} \pm \frac{\sin(\omega + \Delta)t}{\omega + \Delta} \right],$$

which behave, as $t \rightarrow \infty$, like Dirac delta functions: $\frac{\pi}{2} [\delta(\omega - \Delta) \pm \delta(\omega + \Delta)]$. This is because they oscillate with ω at a frequency t everywhere except at $\pm\Delta$, where they spike to a height $\sim t$ and width $\sim 1/t$. As long as the frequency of these oscillations is much faster than any features of the spectral densities (i.e. $t \gg \tau_{jk}, \tau_R$), of the cutoff (i.e. $t \gg 1/\Lambda$), and of the hyperbolic cotangent (i.e. $t \gg \hbar/k_B T$) then the only contribution to the ω integral comes from the spikes at $\pm\Delta$. Subject to these rough criteria,

$$t \gg \tau_{jk}, \tau_R \quad t \gg 1/\Lambda \quad t \gg \hbar/k_B T ,$$

the coefficients of diffusion and damping approach constant values which, thanks to

the Dirac delta functions, are easy to identify:

$$D_{jk}^\Delta \equiv \frac{\pi}{2} J_{jk}(\Delta) \coth\left(\frac{\hbar\Delta}{2k_B T}\right) e^{-|\Delta|/\Lambda} = \lim_{t \rightarrow \infty} D_{jk}^\Delta(t)$$

and

$$\gamma_{jk}^\Delta \equiv \frac{\pi}{2} J_{jk}(\Delta) e^{-|\Delta|/\Lambda} = \lim_{t \rightarrow \infty} \gamma_{jk}^\Delta(t).$$

For the renormalization and anomalous diffusion, the integrations $\int_0^t d\tau \sin \omega\tau \cos \Delta\tau$ or $\int_0^t d\tau \cos \omega\tau \sin \Delta\tau$ are

$$\frac{\sin^2 \frac{\omega+\Delta}{2} t}{\omega + \Delta} \pm \frac{\sin^2 \frac{\omega-\Delta}{2} t}{\omega - \Delta}$$

whose behavior for $t \rightarrow \infty$ is not so clear. However, for large t these terms oscillate so fast with ω that they too average away the time dependence and we can at least define constant values for the renormalization,

$$r_{jk}^\Delta \equiv \lim_{t \rightarrow \infty} \int_0^\infty d\omega J_{jk}(\omega) e^{-\omega/\Lambda} \left[\frac{\sin^2 \frac{\omega+\Delta}{2} t}{\omega + \Delta} + \frac{\sin^2 \frac{\omega-\Delta}{2} t}{\omega - \Delta} \right],$$

and anomalous diffusion,

$$A_{jk}^\Delta \equiv \int_0^\infty d\omega J_{jk}(\omega) \coth\left(\frac{\hbar\omega}{2k_B T}\right) e^{-\omega/\Lambda} \int_0^{t \rightarrow \infty} d\tau \cos \omega\tau \sin \Delta\tau,$$

which we use symbolically without actually ever evaluating them.

In principle, with time-dependent values for the coefficients we could (numerically) integrate the Born master equation 3.4 using the noises $\tilde{\mathcal{V}}_{jk}(t)$ and susceptibilities $\tilde{\mathcal{U}}_{jk}(t)$ obtained by multiplying the matrix elements of $\tilde{\mathcal{X}}_k(t)$ by *time-dependent* coefficients $(D_{jk}^\Delta(t) + iA_{jk}^\Delta(t))$ and $(r_{jk}^\Delta(t) + i\gamma_{jk}^\Delta(t))$ respectively. In this case the integrated evolution is called the “exact-Born approximation” [80].

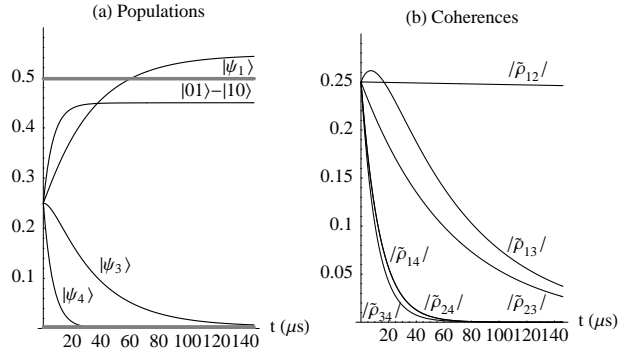


Figure 3.6: Critical behavior of two large SQUIDs. $|\psi_1\rangle + |\psi_2\rangle + |\psi_3\rangle + |\psi_4\rangle$ cooling at the critical point. The distant (e.g. $40\mu\text{m}$) SQUIDs are closely-spaced compared to the level crossing where $\Delta_{12} = 0 \ll 1/\tau_{jk}$; the $|\psi_1\rangle \leftrightarrow |\psi_2\rangle$ transitions are blocked, akin to the collective behavior of two small SQUIDs close together. (a) $|\psi_4\rangle$ flows into $|\psi_3\rangle$ and $|\psi_2\rangle = |01\rangle - |10\rangle$, whereas $|\psi_3\rangle$ flows only into $|\psi_1\rangle$, giving it an excess population over $|\psi_2\rangle$ which the chain cannot quickly resolve; the $|\psi_2\rangle \rightarrow |\psi_4\rangle \rightarrow |\psi_3\rangle \rightarrow |\psi_1\rangle$ pathway takes an extraordinarily long time (not shown). (b) The coherence $\tilde{\rho}_{12}$ barely decays; transitions $|\psi_2\rangle \leftrightarrow |\psi_1\rangle$ are blocked while transitions from $|\psi_1\rangle$ and $|\psi_2\rangle$ are suppressed by the cold bath. Some of the decaying $\tilde{\rho}_{34}$ is absorbed by $\tilde{\rho}_{13}$. ($8J/h = 1.0\text{GHz}$, $2B/h = 1.0\text{GHz}$, $k_B T/h = 0.2\text{GHz}$, $R = 10\mu\text{m}$, $I = 3\mu\text{A}$).

Instead, we will make the “Markov” approximation that just uses the constant, $t \rightarrow \infty$, coefficients in the Born master equation. In this case the integrated evolution is called the “Born-Markov approximation.” With constant coefficients, in the Schrödinger picture the noises and susceptibilities are also constant and therefore the map $\mathcal{L}(\rho) = \rho + d\rho$ is independent of time and is not conditioned on what came before, akin to the Markov chains of classical probability theory.

One could argue that, for a weak coupling to the bath, the integrated solutions, to the exact-Born and Born-Markov equations, would not differ substantially in the time that it takes the coefficients to approach their constant values. Specifically, if the SQUIDs are not too far apart and not too large, and the cutoff is high enough, and the bath is not too cold, then there is a finite time t after which the coefficients are constants; a “sufficiently” weak coupling is one where we can neglect the earlier time-dependence. Once the coefficients obtain their constant values, the exact-Born and Born-Markov equations are the same, so the Born-Markov equation is a good approximation to the exact-Born dynamics for a sufficiently weak coupling to the bath. It should be kept in mind that even the exact-Born approximation was just a plausible guess at the longer-time dynamics. Similarly the Born-Markov approximation is just a guess, whose consequences we explore.

3.9 The Born-Markov Master Equation

Now we recast our Born master equation 3.4 in a form more similar to the equation for the quantum Brownian motion of an oscillator. This brings out the

four generators of the open-system dynamics, one for each type of coefficient. We also make the Markov approximation by using the constant $t \rightarrow \infty$ coefficients.

As an alternative to calculating the noise and susceptibility in the energy eigenbasis of H_S , we can define amplitude operators $\tilde{\mathcal{X}}_k^\Delta(t)$ and $\tilde{\mathcal{P}}_k^\Delta(t)$ to be used in the Fourier expansion of the interaction operators:

$$\tilde{\mathcal{X}}_k(t - \tau) = \sum_{\Delta \geq 0} \left(\tilde{\mathcal{X}}_k^\Delta(t) \cos(\Delta\tau) - \tilde{\mathcal{P}}_k^\Delta(t) \sin(\Delta\tau) \right).$$

In the eigenbasis of H_S , the non-zero matrix elements of $\tilde{\mathcal{X}}_k^\Delta$ are just those matrix elements of $\tilde{\mathcal{X}}_k$ with energy difference $\pm\hbar\Delta$; multiplying those same matrix elements by $\mp i$ gives $\tilde{\mathcal{P}}_k^\Delta$. (This sign convention is consistent with the matrix elements of a harmonic oscillator's position, $\langle n | a^\dagger + a | n + 1 \rangle = \sqrt{n + 1}$, and momentum, $i \langle n | a^\dagger - a | n + 1 \rangle = -i\sqrt{n + 1}$.) $\tilde{\mathcal{X}}_k^0$ consists primarily of the diagonal matrix elements of $\tilde{\mathcal{X}}_k$ but also includes matrix elements between degenerate states.

By using these amplitude operators, the time-averaging of $\tilde{\mathcal{X}}_k(t')$, by the kernels, gives basis-independent expressions for the noise,

$$\tilde{V}_{jk}(t) = \sum_{\Delta \geq 0} \left(D_{jk}^\Delta(t) \tilde{\mathcal{X}}_k^\Delta(t) - A_{jk}^\Delta(t) \tilde{\mathcal{P}}_k^\Delta(t) \right),$$

and susceptibility,

$$\tilde{U}_{jk}(t) = \sum_{\Delta \geq 0} \left(r_{jk}^\Delta(t) \tilde{\mathcal{X}}_k^\Delta(t) - \gamma_{jk}^\Delta(t) \tilde{\mathcal{P}}_k^\Delta(t) \right).$$

We can now make the Markov approximation that uses the constant coefficients, in place of the time-dependent ones, and substitute these noise- and susceptibility-operators into our Born master equation 3.4 to obtain our Born-Markov master

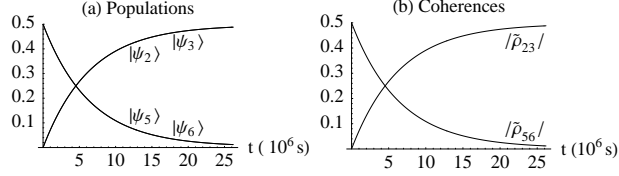


Figure 3.7: Automatic quantum error correction [48] in three small SQUIDs dissipating collectively. $|\psi_5\rangle + |\psi_6\rangle$ cooling to $|\psi_2\rangle + |\psi_3\rangle$. (a) The collective interaction operator $J_z = \mathcal{X}_1 + \mathcal{X}_2 + \mathcal{X}_3$ breaks the network of allowed transitions into three isolated pieces: $|\psi_5\rangle \leftrightarrow |\psi_2\rangle$; $|\psi_6\rangle \leftrightarrow |\psi_3\rangle$; and $|\psi_8\rangle \leftrightarrow |\psi_7\rangle \leftrightarrow |\psi_4\rangle \leftrightarrow |\psi_1\rangle$. (b) The $\tilde{\rho}_{56}$ coherence flows along with the populations into $\tilde{\rho}_{23}$ because $\Delta_{25} = \Delta_{36}$. Then $\tilde{\rho}_{23}$ never decays; transitions back into $|\psi_5\rangle$ and $|\psi_6\rangle$ are suppressed by the cold bath and are resonant (and therefore coherent) anyway. ($6J/h = 1.0\text{GHz}$, $2B/h = 1.5\text{GHz}$, $k_B T/h = 0.3\text{GHz}$, $R = 10\text{nm}$, $I = 0.1\mu\text{A}$).

equation,

$$\dot{\tilde{\rho}} = \frac{\gamma^2}{\hbar^2} \sum_{j,k=1}^N \sum_{\Delta \geq 0} \left(i r_{jk}^\Delta [\tilde{\mathcal{X}}_j, \{\tilde{\mathcal{X}}_k^\Delta, \tilde{\rho}\}] - i \gamma_{jk}^\Delta [\tilde{\mathcal{X}}_j, \{\tilde{\mathcal{P}}_k^\Delta, \tilde{\rho}\}] - D_{jk}^\Delta [\tilde{\mathcal{X}}_j, [\tilde{\mathcal{X}}_k^\Delta, \tilde{\rho}]] + A_{jk}^\Delta [\tilde{\mathcal{X}}_j, [\tilde{\mathcal{P}}_k^\Delta, \tilde{\rho}]] \right). \quad (3.5)$$

This is essentially a Fourier-series version of the Born master equation using Markov (constant) coefficients. It is reassuring that, in the limit of only one contact point (no sum over j, k) and only one energy splitting (no sum over Δ) it becomes

$$\dot{\tilde{\rho}} \sim i r [\tilde{x}, \{\tilde{x}, \tilde{\rho}\}] - i \gamma [\tilde{x}, \{\tilde{p}, \tilde{\rho}\}] - D [\tilde{x}, [\tilde{x}, \tilde{\rho}]] + A [\tilde{x}, [\tilde{p}, \tilde{\rho}]]$$

which is the well-known [76, 28] Born-Markov equation for the quantum Brownian motion of an oscillator system ($H_S = \hbar\omega_s a_s^\dagger a_s$) with a bilinear coupling ($V \sim x\phi$) to an oscillator bath.

3.10 The Four Generators

The master equation has four generators, one for each of the coefficients. We now show, for a weak coupling of our Heisenberg SQUID chain to the bath and

with J and B set close-to or far-from any resonant pairs of allowed transitions, that the renormalization and anomalous diffusion contribute effectively Hamiltonian dynamics, which can be dropped from the master equation by “renormalizing” the chain Hamiltonian, while the damping and diffusion work together to effectively decohere and thermalize the system within each network of allowed transitions.

3.10.1 The Renormalization

The renormalization’s contribution to $\dot{\tilde{\rho}}$ is

$$\dot{\tilde{\rho}}^r \equiv i \frac{\gamma^2}{\hbar^2} \sum_{j,k} \sum_{\Delta} r_{jk}^{\Delta} [\tilde{\mathcal{X}}_j, \{\tilde{\mathcal{X}}_k^{\Delta}, \tilde{\rho}\}] = i \frac{\gamma^2}{\hbar^2} \sum_{j,k} [\tilde{\mathcal{X}}_j, \{\tilde{\mathcal{U}}_{jk}^r, \tilde{\rho}\}],$$

with $\tilde{\mathcal{U}}_{jk}^r$ just that part of the susceptibility attributable to the coefficients of renormalization. Its matrix elements in the energy eigenbasis are $\langle \alpha | \tilde{\mathcal{U}}_{jk}^r | \beta \rangle = \langle \alpha | \tilde{\mathcal{X}}_k | \beta \rangle r_{jk}^{\Delta_{\alpha\beta}}$.

Expanding out the commutators gives

$$\dot{\tilde{\rho}}^r = i \frac{\gamma^2}{\hbar^2} \sum_{j,k} \left(\tilde{\mathcal{X}}_j \tilde{\mathcal{U}}_{jk}^r \tilde{\rho} + \tilde{\mathcal{X}}_j \tilde{\rho} \tilde{\mathcal{U}}_{jk}^r - \tilde{\mathcal{U}}_{jk}^r \tilde{\rho} \tilde{\mathcal{X}}_j - \tilde{\rho} \tilde{\mathcal{U}}_{jk}^r \tilde{\mathcal{X}}_j \right).$$

Working now in the energy eigenbasis by inserting resolutions of the identity, e.g. $I = \sum_{\beta} |\beta\rangle \langle \beta|$, the renormalization’s contribution to the rate of change of a density matrix element $\tilde{\rho}_{\alpha\delta} \equiv \langle \alpha | \tilde{\rho} | \delta \rangle$ is

$$\begin{aligned} \dot{\tilde{\rho}}_{\alpha\delta}^r = & i \frac{\gamma^2}{\hbar^2} \sum_{j,k} \left(\sum_{\beta\bar{\alpha}} \tilde{\mathcal{X}}_{j\alpha\beta} \tilde{\mathcal{X}}_{k\beta\bar{\alpha}} r_{jk}^{\Delta_{\beta\bar{\alpha}}} \tilde{\rho}_{\bar{\alpha}\delta} + \sum_{\beta\gamma} \tilde{\mathcal{X}}_{j\alpha\beta} \tilde{\mathcal{X}}_{k\gamma\delta} r_{jk}^{\Delta_{\gamma\delta}} \tilde{\rho}_{\beta\gamma} \right. \\ & \left. - \sum_{\beta\gamma} \tilde{\mathcal{X}}_{k\alpha\beta} \tilde{\mathcal{X}}_{j\gamma\delta} r_{jk}^{\Delta_{\alpha\beta}} \tilde{\rho}_{\beta\gamma} - \sum_{\bar{\delta}\beta} \tilde{\mathcal{X}}_{k\bar{\delta}\beta} \tilde{\mathcal{X}}_{j\beta\delta} r_{jk}^{\Delta_{\bar{\delta}\beta}} \tilde{\rho}_{\alpha\bar{\delta}} \right). \end{aligned}$$

Many terms in this sum are suppressed by selection-ruled resonance conditions. In the second term, for example, most of the $\tilde{\mathcal{X}}_{j\alpha\beta} \tilde{\mathcal{X}}_{k\gamma\delta} \sim e^{-i(\Delta_{\alpha\beta} + \Delta_{\gamma\delta})t}$ oscillate so

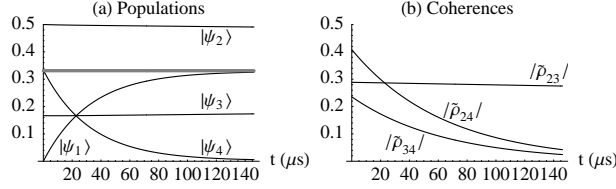


Figure 3.8: Critical behavior of three large SQUIDs dissipating independently. $|\uparrow\uparrow\downarrow\rangle$ cooling at the critical point. The distant SQUIDs are closely-spaced compared to the level crossings where $\Delta_{12} = \Delta_{13} = \Delta_{23} = 0$ and $\Delta_{45} = \Delta_{46} = \Delta_{56} = 0$. (a) The $|\psi_2\rangle \leftrightarrow |\psi_1\rangle$ and $|\psi_3\rangle \leftrightarrow |\psi_1\rangle$ transitions are cut out of the network while upward transitions are suppressed by the cold bath; therefore $|\psi_2\rangle$ and $|\psi_3\rangle$ have long-lived populations. (b) $\tilde{\rho}_{23}$ is long-lived because the transitions out of its $|\psi_2\rangle$ and $|\psi_3\rangle$ supports are so rare. ($6J/h = 1.0\text{GHz}$, $2B/h = 1.0\text{GHz}$, $k_B T/h = 0.1\text{GHz}$, $R = 10\mu\text{m}$, $I = 3\mu\text{A}$).

quickly, compared to the weak coupling between the chain and the bath, that they average to zero unless there is a near-resonance $\Delta_{\alpha\beta} \approx \Delta_{\delta\gamma}$. The second term is thus effectively a sum over nearly-resonant pairs of allowed transitions from states $|\beta\rangle$ and $|\gamma\rangle$ into $|\alpha\rangle$ and $|\delta\rangle$ respectively. So is the third term, which cancels the second term because the coefficient of renormalization is an even function of (j, k) and Δ : $r_{kj}^{\Delta_{\alpha\beta}} = r_{jk}^{\Delta_{\alpha\beta}} = r_{jk}^{\Delta_{\delta\gamma}} = r_{jk}^{\Delta_{\delta\gamma}}$ when $\Delta_{\alpha\beta} = \Delta_{\delta\gamma}$. This holds true for nearly- but not exactly-resonant pairs if the coefficient r_{jk}^{Δ} is a slowly-enough varying function of Δ . To make sure we are close-to or far-from any resonant pairs we must check the parameters J and B of the chain Hamiltonian:

$$\Delta_{\alpha\beta} - \Delta_{\delta\gamma} = (l_\beta - l_\alpha + l_\delta - l_\gamma)J - (m_\beta - m_\alpha + m_\delta - m_\gamma)B.$$

Meanwhile, the first and fourth terms are effectively sums over allowed transitions from states $|\bar{\alpha}\rangle$ near E_α ($\Delta_{\beta\bar{\alpha}} \approx \Delta_{\beta\alpha}$) and states $|\bar{\delta}\rangle$ near E_δ ($\Delta_{\beta\bar{\delta}} \approx \Delta_{\beta\delta}$) into those states $|\beta\rangle$ that are accessible by transitions from $|\alpha\rangle$ and $|\delta\rangle$ respectively. By using $r_{kj}^{\Delta_{\bar{\delta}\beta}} = r_{jk}^{\Delta_{\bar{\delta}\beta}} = r_{jk}^{\Delta_{\delta\beta}} = r_{jk}^{\Delta_{\beta\delta}}$ we rearrange the fourth term into

$-\sum_{\bar{\delta}\beta} \tilde{\rho}_{\alpha\bar{\delta}} \tilde{\mathcal{X}}_{j\bar{\delta}\beta} \tilde{\mathcal{X}}_{k\beta\delta} r_{jk}^{\Delta\beta\delta}$ to arrive at

$$\dot{\tilde{\rho}}^r = i \frac{\gamma^2}{\hbar^2} \sum_{j,k} [\tilde{\mathcal{X}}_j \tilde{\mathcal{U}}_{jk}^r, \tilde{\rho}] = -\frac{i}{\hbar} [\tilde{R}_S'', \tilde{\rho}]$$

which is just an additional Hamiltonian dynamics in the interaction picture with an effectively Hermitian

$$\tilde{R}_S'' \equiv -(\gamma^2/\hbar) \sum_{j,k} \tilde{\mathcal{X}}_j \tilde{\mathcal{U}}_{jk}^r = -\sum_{j,k} \tilde{\mathcal{X}}_j \sum_{\Delta} \frac{\gamma^2}{\hbar} r_{jk}^{\Delta} \tilde{\mathcal{X}}_k^{\Delta}.$$

3.10.2 The Anomalous Diffusion

The anomalous diffusion's contribution to $\dot{\tilde{\rho}}$ is

$$\dot{\tilde{\rho}}^A \equiv \frac{\gamma^2}{\hbar^2} \sum_{j,k} \sum_{\Delta} A_{jk}^{\Delta} [\tilde{\mathcal{X}}_j, [\tilde{\mathcal{P}}_k^{\Delta}, \tilde{\rho}]] = -\frac{\gamma^2}{\hbar^2} \sum_{j,k} [\tilde{\mathcal{X}}_j, [\tilde{\mathcal{V}}_{jk}^A, \tilde{\rho}]],$$

for which we use $\langle \alpha | \tilde{\mathcal{V}}_{jk}^A | \beta \rangle = \langle \alpha | \tilde{\mathcal{X}}_k | \beta \rangle i A_{jk}^{\Delta\alpha\beta}$, i.e. the matrix elements of that part of the noise attributable to the anomalous diffusion. The expansion of $\dot{\tilde{\rho}}^A$ in the energy eigenbasis is thus

$$\begin{aligned} \dot{\tilde{\rho}}_{\alpha\delta}^A = & -i \frac{\gamma^2}{\hbar^2} \sum_{j,k} \left(\sum_{\beta\bar{\alpha}} \tilde{\mathcal{X}}_{j\alpha\beta} \tilde{\mathcal{X}}_{k\beta\bar{\alpha}} A_{jk}^{\Delta\beta\bar{\alpha}} \tilde{\rho}_{\bar{\alpha}\delta} - \sum_{\beta\gamma} \tilde{\mathcal{X}}_{j\alpha\beta} \tilde{\mathcal{X}}_{k\gamma\delta} A_{jk}^{\Delta\gamma\delta} \tilde{\rho}_{\beta\gamma} \right. \\ & \left. - \sum_{\beta\gamma} \tilde{\mathcal{X}}_{k\alpha\beta} \tilde{\mathcal{X}}_{j\gamma\delta} A_{jk}^{\Delta\alpha\beta} \tilde{\rho}_{\beta\gamma} + \sum_{\bar{\delta}\beta} \tilde{\mathcal{X}}_{k\bar{\delta}\beta} \tilde{\mathcal{X}}_{j\beta\delta} A_{jk}^{\Delta\bar{\delta}\beta} \tilde{\rho}_{\alpha\bar{\delta}} \right). \end{aligned}$$

The selection-ruled resonance conditions are the same as before, but the coefficient of anomalous diffusion, while still an even function of (j, k) , is an odd function of Δ and we now use $A_{kj}^{\Delta\alpha\beta} = A_{jk}^{\Delta\alpha\beta} = A_{jk}^{\Delta\delta\gamma} = -A_{jk}^{\Delta\gamma\delta}$ to cancel the second term with the third. Similarly, we use $A_{kj}^{\Delta\bar{\delta}\beta} = A_{jk}^{\Delta\bar{\delta}\beta} = A_{jk}^{\Delta\delta\beta} = -A_{jk}^{\Delta\beta\delta}$ to arrange the fourth term into $-\sum_{\bar{\delta}\beta} \tilde{\rho}_{\alpha\bar{\delta}} \tilde{\mathcal{X}}_{j\bar{\delta}\beta} \tilde{\mathcal{X}}_{k\beta\delta} A_{jk}^{\Delta\beta\delta}$ and arrive at

$$\dot{\tilde{\rho}}^A = -\frac{\gamma^2}{\hbar^2} \sum_{j,k} [\tilde{\mathcal{X}}_j \tilde{\mathcal{V}}_{jk}^A, \tilde{\rho}] = -\frac{i}{\hbar} [\tilde{A}_S'', \tilde{\rho}]$$

which is again just an additional Hamiltonian dynamics in the interaction picture with an effectively Hermitian

$$\tilde{A}_S'' \equiv (\gamma^2/i\hbar) \sum_{j,k} \tilde{\mathcal{X}}_j \tilde{\mathcal{V}}_{jk}^A = \sum_{j,k} \tilde{\mathcal{X}}_j \sum_{\Delta} \frac{\gamma^2}{\hbar} A_{jk}^{\Delta} i \tilde{\mathcal{P}}_k^{\Delta}.$$

It is temperature dependent because (recall)

$$A_{jk}^{\Delta} = \int_0^{\infty} d\omega J_{jk}(\omega) \coth\left(\frac{\hbar\omega}{2k_B T}\right) e^{-\omega/\Lambda} \int_0^{t \rightarrow \infty} d\tau \cos \omega\tau \sin \Delta\tau.$$

3.10.3 Renormalizing the Chain

We now show that, to second order in the coupling, the effective Hamiltonian dynamics of the combined renormalization and anomalous diffusion can be removed from the master equation by adding them into a renormalized chain Hamiltonian $H_S^{(1)} = H_S + H_S''$ in which

$$H_S'' \equiv R_S'' + A_S'' = \sum_{j,k} \mathcal{X}_j \mathcal{W}_{jk},$$

and $\langle \alpha | \mathcal{W}_{jk} | \beta \rangle \equiv \langle \alpha | \mathcal{X}_k | \beta \rangle \left(\frac{\gamma^2}{\hbar} A_{jk}^{\Delta\alpha\beta} - \frac{\gamma^2}{\hbar} r_{jk}^{\Delta\alpha\beta} \right)$. We can think of this as a shift to the chain Hamiltonian. If H_S'' commutes with H_S then the shift just alters the chain's energies, whereas if they don't commute then the chain's eigenstates are also perturbed by the bath (in the sense that shifted chain eigenstates are needed to describe the oscillatory portion of the chain's open-system dynamics).

When we include the shift in a new Hamiltonian for the chain we must exclude it from the coupling, $V^{(1)} \equiv V - H_S'' \otimes I_B$, so that the total Hamiltonian $H = H_S^{(1)} + H_B + V^{(1)}$ remains the same as before. The renormalized chain Hamiltonian $H_S^{(1)}$ redefines the interaction picture. Specifically, we use $H_1 \equiv H_S^{(1)} + H_B$ to

define the new interaction picture coupling $\tilde{V}^{(1)}(t) \equiv e^{iH_1 t/\hbar}(V - H_S'')e^{-iH_1 t/\hbar}$, where $\tilde{\mathcal{O}}(t) = e^{iH_1 t/\hbar}\mathcal{O}e^{-iH_1 t/\hbar}$ now denotes an operator \mathcal{O} in this new interaction picture. Then we proceed exactly as before, and discard the third and fourth order terms (i.e. $\tilde{V}\tilde{H}_S''$, $\tilde{H}_S''\tilde{V}$, and $\tilde{H}_S''^2$) that arise from the nested commutators, to arrive again at our Born-Markov master equation, but this time in the interaction picture of $H_S^{(1)}$ with its concomitant new energies, transition frequencies, and eigenstates. The master equation is augmented this time by the non-vanishing single commutator,

$$-\frac{i}{\hbar}\text{Tr}_B[\tilde{V}^{(1)}(t), \tilde{w}(0)] = -\frac{i}{\hbar}[-\tilde{H}_S'', \rho(0)] \neq 0.$$

This appearance of $-\tilde{H}_S'' = -\tilde{R}_S'' - \tilde{A}_S''$ in the new interaction picture serves to cancel, to second order, the effective Hamiltonian dynamics $\tilde{H}_S''^{(1)} = \tilde{R}_S''^{(1)} + \tilde{A}_S''^{(1)}$ that results from the renormalization and anomalous diffusion in this second iteration of the derivation. Only the damping and diffusion remain in the Born-Markov master equation.

This renormalized Hamiltonian is the one we observe when we study a system in its environment. In quantum process tomography, for example, one prepares a variety of initial states and then studies, at a variety of times, their evolving expectation values for a complete set of incompatible observables. In this way one can reconstruct the evolution of the initial states. Some have oscillating expectation values (perhaps with a decaying envelope) while others do not (although they may still relax and thermalize). The latter may be interpreted as the stationary eigenstates, while the oscillation frequencies give the energies. These eigenstates and energies are those of the shifted Hamiltonian, since the system was observed

during its interaction with its environment.

We would like now to concentrate on the damping and diffusion. Later on, to make concrete sense of these two generators, our examples use the familiar and useful energies and eigenstates of the Heisenberg SQUID Chain. In other words, we assume that the renormalized Hamiltonian is

$$H_S^{(1)} = \sum_{j=1}^N (J\vec{\sigma}_j \cdot \vec{\sigma}_{j+1} - B\sigma_j^x),$$

as though the “bare” SQUIDs were engineered with a slightly different original Hamiltonian H_S , including a “counter term” that happens to cancel the renormalization and anomalous diffusion caused by their crystal environment. This engineering may actually be quite difficult, relying perhaps on many trials and errors. In any case, our general discussion of the damping and diffusion is in terms of the renormalized energies and the matrix elements in the renormalized eigenbasis.

3.10.4 The Damping and Diffusion

The effect of the remaining diffusion and damping is

$$\dot{\tilde{\rho}} = -\frac{\gamma^2}{\hbar^2} \sum_{j,k=1}^N \left([\tilde{\mathcal{X}}_j, [\tilde{\mathcal{V}}_{jk}^D, \tilde{\rho}]] - i[\tilde{\mathcal{X}}_j, \{\tilde{\mathcal{U}}_{jk}^\gamma, \tilde{\rho}\}] \right)$$

with $\langle \alpha | \tilde{\mathcal{V}}_{jk}^D | \beta \rangle = \langle \alpha | \tilde{\mathcal{X}}_k | \beta \rangle D_{jk}^{\Delta\alpha\beta}$ and with $\langle \alpha | \tilde{\mathcal{U}}_{jk}^\gamma | \beta \rangle = \langle \alpha | \tilde{\mathcal{X}}_k | \beta \rangle i\gamma_{jk}^{\Delta\alpha\beta}$, again just those parts of the noise and susceptibility attributable to the diffusion and damping.

We can combine the two coefficients into a rate

$$\Gamma_{jk}^{\alpha\beta} \equiv \frac{\gamma^2}{\hbar^2} (\gamma_{jk}^{\Delta\alpha\beta} + D_{jk}^{\Delta\alpha\beta}) = \frac{\gamma^2}{\hbar^2} \frac{\pi}{2} J_{jk}(\Delta) [1 + \coth(\frac{\hbar\Delta}{2k_B T})]$$

(apart from a factor $e^{-|\Delta|/\Lambda} \approx 1$ when $\Lambda \gg \Delta$). Then in terms of the coherences $\tilde{\rho}_{\alpha\delta} \equiv \langle \alpha | \tilde{\rho} | \delta \rangle$ and populations $\tilde{\rho}_{\alpha\alpha}$ the expansion of $\dot{\tilde{\rho}}$ in the eigenbasis of $H_S^{(1)}$ is a matrix element equation for

$$\begin{aligned} \dot{\tilde{\rho}}_{\alpha\delta} = & - \sum_{j,k} \left(\sum_{\beta\bar{\alpha}} \tilde{\mathcal{X}}_{j\alpha\beta} \tilde{\mathcal{X}}_{k\beta\bar{\alpha}} \Gamma_{jk}^{\beta\bar{\alpha}} \tilde{\rho}_{\bar{\alpha}\delta} - \sum_{\beta\gamma} \tilde{\mathcal{X}}_{j\alpha\beta} \tilde{\mathcal{X}}_{k\gamma\delta} \Gamma_{jk}^{\delta\gamma} \tilde{\rho}_{\beta\gamma} \right. \\ & \left. - \sum_{\beta\gamma} \tilde{\mathcal{X}}_{k\alpha\beta} \tilde{\mathcal{X}}_{j\gamma\delta} \Gamma_{jk}^{\alpha\beta} \tilde{\rho}_{\beta\gamma} + \sum_{\bar{\delta}\beta} \tilde{\mathcal{X}}_{k\bar{\delta}\beta} \tilde{\mathcal{X}}_{j\beta\delta} \Gamma_{jk}^{\beta\bar{\delta}} \tilde{\rho}_{\alpha\bar{\delta}} \right), \end{aligned}$$

where we have used the evenness of D_{jk}^{Δ} and oddness of γ_{jk}^{Δ} with respect to Δ to combine the two generators into this one expression.

With the rate $\Gamma_{jk}^{\alpha\beta}$ neither an even nor odd function of $\Delta_{\alpha\beta}$ there are no more index gymnastics with which to cancel terms, although the selection-ruled resonance conditions are the same as before and eliminate many of the $\tilde{\mathcal{X}}_{j\alpha\beta} \tilde{\mathcal{X}}_{k\gamma\delta}$. In the first and fourth terms, the remaining transitions from states near E_{α} ($\Delta_{\beta\bar{\alpha}} \approx \Delta_{\beta\alpha}$) and E_{δ} ($\Delta_{\beta\bar{\delta}} \approx \Delta_{\beta\delta}$) tend to decrease $\tilde{\rho}_{\alpha\delta}$ in proportion to $\tilde{\rho}_{\alpha\delta}$ as well as in proportion to nearby (in energy) matrix elements $\tilde{\rho}_{\bar{\alpha}\delta}$ (in the same column) and $\tilde{\rho}_{\alpha\bar{\delta}}$ (in the same row). In the second and third terms, the remaining nearly-resonant pairs of transitions from $|\beta\rangle$ and $|\gamma\rangle$ into $|\alpha\rangle$ and $|\delta\rangle$ ($\Delta_{\alpha\beta} \approx \Delta_{\delta\gamma}$) tend to increase $\tilde{\rho}_{\alpha\delta}$ in proportion to those matrix elements $\tilde{\rho}_{\beta\gamma}$ within, and/or nearly within, the diagonal that includes $\tilde{\rho}_{\alpha\delta}$ (when the density matrix is stretched to be linearly spaced with increasing energy). When $\delta = \alpha$ this diagonal is the central diagonal, sometimes called *the* diagonal.

Two general features of these coupled first order differential equations are decoherence and relaxation. Decoherence is caused by transitions from $|\alpha\rangle$ and $|\delta\rangle$,

$$\frac{\partial \dot{\tilde{\rho}}_{\alpha\delta}}{\partial \tilde{\rho}_{\alpha\delta}} = - \sum_{j,k} \left(\sum_{\beta} \tilde{\mathcal{X}}_{j\alpha\beta} \tilde{\mathcal{X}}_{k\beta\alpha} \Gamma_{jk}^{\beta\alpha} - \overbrace{\tilde{\mathcal{X}}_{j\alpha\alpha} \tilde{\mathcal{X}}_{k\delta\delta} \Gamma_{jk}^{\delta\delta}}^0 \right)$$

$$\frac{d \tilde{\rho}_{\alpha\delta}}{dt} = - \left[\begin{array}{c} \tilde{\rho}_{\alpha\delta}^- \\ \tilde{\rho}_{\alpha\delta} \end{array} \right] + \left[\begin{array}{c} \tilde{\rho}_{\beta\gamma} \\ \tilde{\rho}_{\alpha\delta} \end{array} \right]$$

Figure 3.9: A cartoon of the matrix element equation for damping and diffusion. When the density matrix elements are arranged by increasing energy: $\tilde{\rho}_{\alpha\delta}$ decreases in proportion to nearby matrix elements in the same row, $\tilde{\rho}_{\alpha\bar{\delta}}$, and column $\tilde{\rho}_{\bar{\alpha}\delta}$; and it increases in proportion to matrix elements $\tilde{\rho}_{\beta\gamma}$ within, and/or nearby within, the diagonal that includes $\tilde{\rho}_{\alpha\delta}$.

$$- \underbrace{\tilde{\chi}_{k\alpha\alpha} \tilde{\chi}_{j\delta\delta} \Gamma_{jk}^{\alpha\alpha}}_0 + \sum_{\beta} \tilde{\chi}_{k\delta\beta} \tilde{\chi}_{j\beta\delta} \Gamma_{jk}^{\beta\delta}) \equiv -\bar{\Gamma}_{\alpha\delta}$$

(here the second and third terms vanished because of our specific selection rules), and is exacerbated by transitions from nearby states. Setting $\delta = \alpha$ we see the relaxation dynamics, in that the population $\tilde{\rho}_{\alpha\alpha}$ is flowing to and from the $\tilde{\rho}_{\beta\beta}$ at the selection-ruled transition rates $2 \sum_{jk} \tilde{\chi}_{j\alpha\beta} \tilde{\chi}_{k\beta\alpha} \Gamma_{jk}^{\beta\alpha} \tilde{\rho}_{\alpha\alpha}$ and $2 \sum_{jk} \tilde{\chi}_{j\alpha\beta} \tilde{\chi}_{k\beta\alpha} \Gamma_{jk}^{\alpha\beta} \tilde{\rho}_{\beta\beta}$. A stationary (and thermal) balance is eventually reached at $\tilde{\rho}_{\beta\beta} / \tilde{\rho}_{\alpha\alpha} = \Gamma_{jk}^{\beta\alpha} / \Gamma_{jk}^{\alpha\beta} = e^{-\hbar\Delta_{\alpha\beta}/k_B T}$ (at which point the populations' effect on the off-diagonal coherences $\tilde{\rho}_{\alpha\delta}$,

$$- \sum_{j,k,\beta} \tilde{\chi}_{j\alpha\beta} \tilde{\chi}_{k\beta\delta} \left(\underbrace{\Gamma_{jk}^{\beta\delta} \tilde{\rho}_{\delta\delta}}_{\bar{\alpha}=\delta} - \underbrace{\Gamma_{jk}^{\delta\beta} \tilde{\rho}_{\beta\beta}}_{\gamma=\beta} - \underbrace{\Gamma_{jk}^{\alpha\beta} \tilde{\rho}_{\beta\beta}}_{\gamma=\beta} + \underbrace{\Gamma_{jk}^{\beta\alpha} \tilde{\rho}_{\alpha\alpha}}_{\bar{\delta}=\alpha} \right),$$

also vanishes). The decay of the coherences allows the relaxation to proceed to a thermal equilibrium $\rho_T \equiv e^{-H_S^{(1)}/k_B T} / Z_S$ provided the network of selection-ruled transitions does not isolate any subspace(s). For isolated networks each subspace will obtain its own a stationary thermal balance of populations constrained by the

total available initial probability to be in that subspace.

Remarkably, the decay of $\tilde{\rho}_{\alpha\delta}$ is offset, as it is on the central diagonal, by the nearly-resonant pairs of transitions into $|\alpha\rangle$ and $|\delta\rangle$ from any matrix elements $\tilde{\rho}_{\beta\gamma}$ within, and/or nearly within, the off-center diagonal that includes $\tilde{\rho}_{\alpha\delta}$. Indeed, a population-like coherence flow is established between $\tilde{\rho}_{\alpha\delta}$ and $\tilde{\rho}_{\beta\gamma}$ that is primarily into the lower energy subspace when the temperature is low; quantum oscillations which are decaying in one subspace can in principle emerge in a lower energy subspace.

3.11 Numerical Simulations

We simulate the effects of the matrix element equation in a variety of scenarios for two- and three-SQUID chains. In all cases we choose J and B to set the chain close-to or far-from resonant pairs of transitions (we can run at the critical point because of its exactly-resonant pairs). That way we can and do discard the oscillating coefficients from the equation, since their effect would average to zero anyway. The matrix element equation becomes a coupled first order differential equation with constant coefficients which we numerically integrate [81].

We consider large SQUIDs, $R = 10\mu\text{m}$ with $I = 3\mu\text{A}$, and small SQUIDs, $R = 10\text{nm}$ with $I = 0.1\mu\text{A}$. In both cases we imagine them to be spaced $4R$ apart in a solid crystal with mass density $\rho = 5\text{g/cm}^3$ and sound velocity 5km/s . We set the Heisenberg splitting at $1.0\text{GHz} = 8J/h$ for a two-SQUID chain and $1.0\text{GHz} = 6J/h$ for a three-SQUID chain. We then choose SQUIDs with frequencies of

$2B/h = 0.5, 1.0,$ or 1.5 GHz (below, at, or above the chain's critical point). We set the temperature to be $1/5$ the SQUID frequencies, i.e. $k_B T/h = 0.1, 0.2,$ or 0.3 GHz.

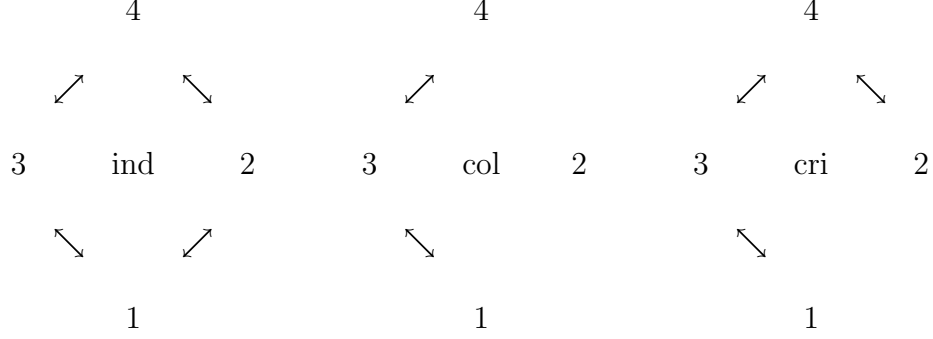
Although larger SQUIDs are possible, these parameters keep the photon-induced decoherence rates [75], in the absence of shielding, well below our phonon-induced rates. But still these SQUIDs' $4R$ separation is large enough to discard the $j \neq k$ cross terms. At the critical point, where $\Delta = 0 \ll 1/\tau_{jk}$, the cross term rates $\Gamma_{jk}^{\Delta=0}$ are identical to the $j = k$ rates. They also vanish, because of the super-ohmic spectral densities which decrease, as $\Delta \rightarrow 0$ faster than $\coth(\hbar\Delta/2k_B T) \rightarrow \infty$. On the other hand, the small SQUIDs' $4R$ separation is small enough to achieve a collective coupling to the bath for all Δ .

In either case the matrix elements of the interaction operators are used to calculate all the constant coefficients in the matrix element equation and we then proceed with the numerical simulations for any initial state $\rho(0)$.

3.12 Discussion

The relaxation and decoherence will thermalize the SQUIDs when the network of selection-rules is complete. For example, for two large SQUIDs dissipating independently, the matrix elements of the interaction operators show that the network of selection-rules is $|\psi_1\rangle \leftrightarrow |\psi_2\rangle$, $|\psi_1\rangle \leftrightarrow |\psi_3\rangle$, $|\psi_2\rangle \leftrightarrow |\psi_4\rangle$, and $|\psi_3\rangle \leftrightarrow |\psi_4\rangle$. There is a reasonable pathway from any eigenstate to any other and these examples lead to thermalization. However, in the case of small SQUIDs close together there is a col-

lective coupling J_z and the network (for two SQUIDs) becomes $|\psi_1\rangle \leftrightarrow |\psi_3\rangle \leftrightarrow |\psi_4\rangle$ while $|\psi_2\rangle$ is a protected subspace. We attempt to summarize with a schematic:



in which the first and second networks are those of independent and collective dissipation. The third network is at the critical point $\Delta_{12} = 0$ for which the network is $|\psi_1\rangle \leftrightarrow |\psi_3\rangle \leftrightarrow |\psi_4\rangle \leftrightarrow |\psi_2\rangle$. Being at the critical point severs the $|\psi_1\rangle \leftrightarrow |\psi_2\rangle$ link, as was done in the collective case, for $\Delta_{12}\tau_{jk} = 0 \ll 1$, but not the $|\psi_2\rangle \leftrightarrow |\psi_4\rangle$ link for which $\Delta_{14}\tau_{jk} \gg 1$. The only allowed transitions out of $|\psi_1\rangle$ and $|\psi_2\rangle$ are suppressed by the cold bath which is loath to supply the necessary energy. This helps to protect the population of $|\psi_2\rangle$ and the coherence $\tilde{\rho}_{12}$.

3.13 Conclusion

A chain of a few coupled SQUIDs exchanging their angular momenta with a phonon bath can be studied, in the Born-Markov approximation, with master equation techniques from the quantum Brownian motion model. The renormalization and temperature-dependent anomalous diffusion can be used to renormalize the Hamiltonian for the chain. In the new eigenbasis the damping and diffusion give a matrix element equation showing decoherence, relaxation, and the possibility for

decaying quantum oscillations to emerge in a lower energy subspace. The relaxation adjusts the populations of the eigenstates and undermines their support for any superposition (coherence) between them, leading to decoherence.

The cascade of populations can occupy entangled states of intermediate energy, resulting in a surge of the entanglement of formation that indicates the number of singlets needed to form, from local operations and classical communication, an ensemble of SQUID pairs $\rho(t)$ [82]. The entanglement is induced even though the SQUIDS are dissipating independently.

The level spacings in the Heisenberg SQUID chain include pairs of resonant transitions which are necessary for coherent oscillations to decay into a lower energy subspace where they can decohere more slowly. In this phenomenon, a superposition of two eigenstates relaxes coherently into a superposition of two lower-energy eigenstates with the same energy difference as the upper two.

Small SQUIDS close together exhibit a collective coupling to the bath which can give a protected subspace and enhanced or suppressed transition and decoherence rates. In effect, the network of selection-ruled transitions is broken into isolated pieces. When the level spacings cooperate to allow coherence flow in these sufficiently isolated pieces, decaying quantum information can reappear and be sustained in a lower energy subspace; this is the idea behind “automatic quantum error correction” [48].

Another feature of the Heisenberg SQUID chain is the critical point level crossings where an allowed transition vanishes along with its frequency. The network of selection-rules in effect acquires some features of the collective behavior as $\Delta\tau_{jk} \rightarrow$

$0 \ll 1$; even large SQUIDs spaced well apart, when tuned to the critical point, can have extended coherence times.

Chapter 4

Damping and Diffusion of A Heisenberg Few-Spin Chain in a Phonon Bath

4.1 Abstract

We apply the chain-Boson model of Chapter 3 to the case of a few spins whose exchange coupling is strained by quantized lattice distortions. Here we use the generators of renormalization and anomalous diffusion to renormalize the chain, although our emphasis is still on the damping and diffusion which together cause relaxation and decoherence. The exchange-strain operators sum to zero, so a collective coupling vanishes. We consider a strong exchange coupling between the spins so that the bath wavelengths that interact with the chain are much shorter than the inter-spin distance and the chain behaves as if it is dissipating into independent baths at each site. But the introduction of next nearest-neighbor exchange, or “frustration,” presents a critical point energy level crossing where even distant spins obtain the collective coupling which protects states from decay.

4.2 Introduction

A pair of magnetic ions in a crystal experience an exchange coupling which arises from Coulomb interaction and the Pauli exclusion principle. The anti-symmetric

spin configuration $|\uparrow\downarrow\rangle - |\downarrow\uparrow\rangle$ requires a symmetric charge configuration, and vice-versa. The charge configurations have distinct “overlap integrals” and there is a concomitant energy difference between the spin configurations. The coupling thereby causes coherent quantum oscillations between, for example, $|\uparrow\downarrow\rangle$ and $|\downarrow\uparrow\rangle$.

Several spins can be uniformly spaced in a line with spin-spin couplings to form a spin-chain. The coupling between nearest-neighbor spins can be “frustrated” by an exchange-like coupling between next-nearest-neighbors. If the frustration increases beyond a critical point then it, instead of the nearest-neighbor exchange, will determine the ground state. For four spins with periodic boundary conditions, there is a complete dimerization of the ground state, in which next-nearest-neighbor spins pair up in singlets:

$$|\uparrow\uparrow\downarrow\downarrow\rangle - |\uparrow\downarrow\downarrow\uparrow\rangle - |\downarrow\uparrow\uparrow\downarrow\rangle + |\downarrow\downarrow\uparrow\uparrow\rangle = (|\uparrow_1\downarrow_3\rangle - |\downarrow_1\uparrow_3\rangle)(|\uparrow_2\downarrow_4\rangle - |\downarrow_2\uparrow_4\rangle).$$

In this paper we consider some open-system effects of the spin-chain’s coupling to phonons. When the spins are magnetic ions in a crystal lattice the overlap integral will diminish with the distance between them [83]. The nearest-neighbor exchange coupling is strained by the distortion of the lattice and therefore the evolution of the spin-chain depends on the lattice configuration, and vice versa. Exchange-strained spins have a long history in Spin-Peierls phase transitions [83] and are relevant to the decoherence of spin qubits in quantum dots [84].

Our system is loosely modeled on the inorganic spin chain CuGeO_3 . We assume our magnetic ions are 0.3 nm apart, and their nearest neighbor exchange is strained by 7.166 meV/nm; a 10% change in the spins’ separation would change the

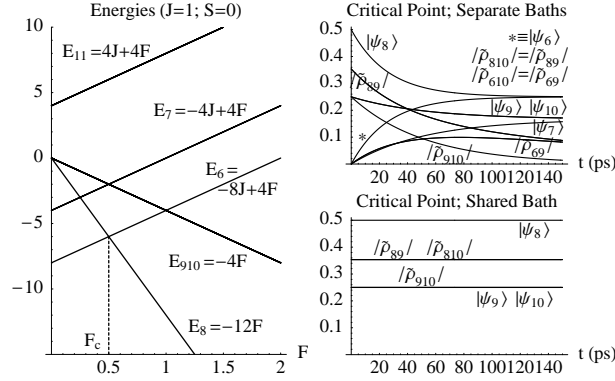


Figure 4.1: A Heisenberg four-spin chain at the critical point cooling from $\sqrt{2} |\psi_8\rangle + |\psi_9\rangle + |\psi_{10}\rangle$. At the critical point there is an energy level crossing where $\Delta \rightarrow 0$ and the bath wavelengths which interact with the chain are longer than the inter-spin spacings. This gives a collective coupling to the bath, which vanishes for exchange-strained spins; the open-system dynamics are dramatically different from the separate-baths approximation normally used for distant qubits. E_8 and $E_{9,10}$ are not degenerate; the state is evolving in the Schrödinger picture. ($J_0 = 103.4$ meV, $F_0 = J_0/2$, $\gamma' = 5.238 \times 10^{-7}$ meV ps, $\hbar\Lambda = 6.582 \times 10^5$ meV, $k_B T = 41.36$ meV).

exchange strength by 0.22 meV. We choose a nearest neighbor exchange of 103.4 meV, much stronger than CuGeO_3 's approximately 7 – 11 meV [85, 86]. In this way we avoid the complications of intermediate bath wavelengths interacting with the chain; our point that there is an advantage to being at the critical point would be true in either case. We run our simulations at $k_B T = 41.36$ meV, which is cold compared to the strong exchange coupling.

As in chapter 3, we work from the total Hamiltonian $H = H_S + H_B + V$, describing the spins, the bath, and their coupling, and apply master equation techniques from the quantum Brownian motion model [76, 28], in the Born-Markov approximation. In this chapter the *inter-qubit* coupling is strained by the phonon heat bath (as opposed to the environment's perturbation of *individual-qubit* dynamics in chapter

3). The renormalization and anomalous diffusion are used to renormalize the chain, introducing and/or modifying the frustration, as well as introducing other less significant temperature dependent terms. Again we use the damping and diffusion together to develop a matrix element equation for the populations and coherences, and it gives the relaxation and decoherence rates. But in the case of exchange-strained spins there are isolated networks of exchange-strain selection rules so that, rather than complete thermalization, a relative thermalization occurs in each subspace. The collective exchange-strain vanishes. This is relevant to the critical point open-system dynamics, for which even distant spins acquire the collective behavior and are protected from decay.

4.3 The Heisenberg Spin Chain

The bath-free evolution of our Heisenberg chain of N spins is described by its system Hamiltonian,

$$H_S = \sum_{j=1}^N (J_0 \vec{\sigma}_j \cdot \vec{\sigma}_{j+1} + F_0 \vec{\sigma}_{j-1} \cdot \vec{\sigma}_{j+1}).$$

We will consider cases with and without the bath-free frustration F_0 . In anticipation of the renormalized energies and eigenstates we begin by discussing

$$H_S^{(1)} = \sum_{j=1}^N (J \vec{\sigma}_j \cdot \vec{\sigma}_{j+1} + F \vec{\sigma}_{j-1} \cdot \vec{\sigma}_{j+1} + S \vec{\sigma}_{j-1} \cdot \vec{\sigma}_j \vec{\sigma}_{j+1} \cdot \vec{\sigma}_{j+2} - S \vec{\sigma}_{j-1} \cdot \vec{\sigma}_{j+1} \vec{\sigma}_j \cdot \vec{\sigma}_{j+2}),$$

in which we use a renormalized exchange J and frustration F as well as a third term S which will also arise from the interaction with the bath. Again we assume periodic boundary conditions.

For four spins the J , F , and S sums commute and their respective quantum numbers l , f , and s determine the energy spectrum $\{lJ + fF + sS\}$ (up to some remaining degeneracies). These terms commute also with the magnetic sum $J_z = \sum_j \sigma_j^z$ so that each eigenstate is a linear combination of states with the same number $m \equiv N_\uparrow - N_\downarrow$ of $|\uparrow\rangle$ vs. $|\downarrow\rangle$ spins and is typically entangled, with the exception of the extremal m states $|\uparrow\uparrow\dots\rangle$ and $|\downarrow\downarrow\dots\rangle$. Increasing F relative to fixed J causes energy-level crossings. At a critical value, F_c , the ground state changes.

We use the four-spin chain for our numerical simulations. The $m = \pm 4$ eigenstates are

$$|\psi_1\rangle = |\uparrow\uparrow\uparrow\uparrow\rangle \text{ and } |\psi_{16}\rangle = |\downarrow\downarrow\downarrow\downarrow\rangle.$$

In the $m = 2$ subspace we use

$$\begin{aligned} |\psi_2\rangle &\equiv |\uparrow\uparrow\uparrow\downarrow\rangle - |\uparrow\uparrow\downarrow\uparrow\rangle + |\uparrow\downarrow\uparrow\uparrow\rangle - |\downarrow\uparrow\uparrow\uparrow\rangle \\ |\psi_{3,4}\rangle &\equiv |\uparrow\uparrow\uparrow\downarrow\rangle \mp |\uparrow\uparrow\downarrow\uparrow\rangle - |\uparrow\downarrow\uparrow\uparrow\rangle \pm |\downarrow\uparrow\uparrow\uparrow\rangle \\ |\psi_5\rangle &\equiv |\uparrow\uparrow\uparrow\downarrow\rangle + |\uparrow\uparrow\downarrow\uparrow\rangle + |\uparrow\downarrow\uparrow\uparrow\rangle + |\downarrow\uparrow\uparrow\uparrow\rangle. \end{aligned}$$

The $m = -2$ states $|\psi_{12}\rangle$ thru $|\psi_{15}\rangle$, which have the same energies, can be obtained by flipping every spin, $\uparrow \leftrightarrow \downarrow$. In the $J_z = 0$ subspace, with $|\psi_\pm\rangle \equiv |\uparrow\downarrow\uparrow\downarrow\rangle \pm |\downarrow\uparrow\downarrow\uparrow\rangle$, we use

$$\begin{aligned} |\psi_6\rangle &\equiv |\uparrow\uparrow\downarrow\downarrow\rangle + |\uparrow\downarrow\downarrow\uparrow\rangle + |\downarrow\uparrow\uparrow\downarrow\rangle + |\downarrow\downarrow\uparrow\uparrow\rangle - 2|\psi_+\rangle \\ |\psi_7\rangle &\equiv |\psi_-\rangle \\ |\psi_8\rangle &\equiv |\uparrow\uparrow\downarrow\downarrow\rangle - |\uparrow\downarrow\downarrow\uparrow\rangle - |\downarrow\uparrow\uparrow\downarrow\rangle + |\downarrow\downarrow\uparrow\uparrow\rangle \\ |\psi_9\rangle &\equiv |\uparrow\downarrow\downarrow\uparrow\rangle - |\downarrow\uparrow\uparrow\downarrow\rangle \\ |\psi_{10}\rangle &\equiv |\uparrow\uparrow\downarrow\downarrow\rangle - |\downarrow\downarrow\uparrow\uparrow\rangle \\ |\psi_{11}\rangle &\equiv |\uparrow\uparrow\downarrow\downarrow\rangle + |\uparrow\downarrow\downarrow\uparrow\rangle + |\downarrow\uparrow\uparrow\downarrow\rangle + |\downarrow\downarrow\uparrow\uparrow\rangle + |\psi_+\rangle. \end{aligned}$$

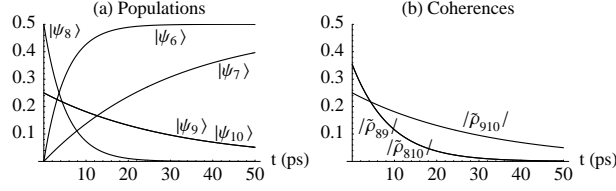


Figure 4.2: Relaxing from a nearly-degenerate subspace into a mix of distinct energies ($E_{9,10}$ and E_7). $\sqrt{2}|\psi_8\rangle + |\psi_9\rangle + |\psi_{10}\rangle$ cooling below the critical point. ($J_0 = 103.4$ meV, $F_0 = 0$).

Their various quantum numbers and energies are

m	$\alpha \Rightarrow \psi_\alpha\rangle$	l	f	s	E_α
± 4	1, 16	4	4	0	$4J + 4F$
	2, 12	-4	4	-16	$-4J + 4F - 16S$
± 2	3, 4, 13, 14	0	-4	8	$-4F + 8S$
	5, 15	4	4	0	$4J + 4F$
	6	-8	4	24	$-8J + 4F + 24S$
	7	-4	4	-16	$-4J + 4F - 16S$
0	8	0	-12	-24	$-12F - 24S$
	9, 10	0	-4	8	$-4F + 8S$
	11	4	4	0	$4J + 4F$

The critical point level crossing between $|\psi_6\rangle$ and $|\psi_8\rangle$ occurs at $F_c = J/2 - 3S \approx J/2$ assuming S is small. When J dominates the Hamiltonian, $|\psi_6\rangle$ is the ground state whereas when F dominates, the ground state is the completely dimerized $|\psi_8\rangle$.

Keep in mind, however, that it is H_S , with the same eigenstates but different energies, i.e. with $J \rightarrow J_0$, $F \rightarrow F_0$, and $S = 0$, that we use to describe the

chain's free evolution as we develop the master equation. From it we will derive the renormalized $H_S^{(1)}$ with the frustration F and other term S induced by the interaction with the bath.

4.4 The Harmonic Phonon Bath

The harmonic crystal Hamiltonian is very similar to what we used in the SQUID chain example. But for frequencies below a cutoff frequency Λ we assume linear and isotropic dispersions, $\omega_s(\vec{k}) = c|\vec{k}|$ for polarizations $\hat{e}_s(\vec{k}) = \{\hat{k}_{\perp 1}, \hat{k}_{\perp 2}, \hat{k}_{\parallel}\}$. (Introducing distinct transverse and longitudinal sound speeds would just result in a complicated geometric factor in the spectral densities.) The displacement at site \vec{x}_j is

$$\vec{u}(\vec{x}_j) = \frac{1}{\sqrt{V}} \sum_{\vec{k}s} \frac{\hat{e}_s(\vec{k})\sqrt{\hbar}}{\sqrt{2\rho\omega_s(\vec{k})}} \left(a_{\vec{k}s} e^{i\vec{k}\cdot\vec{x}_j} + a_{\vec{k}s}^\dagger e^{-i\vec{k}\cdot\vec{x}_j} \right)$$

with V and ρ the volume and mass density of the crystal and the $\vec{x}_j = d(j-1)\hat{x}$ are the spins' equilibrium positions spaced a distance d apart along the x -axis.

4.5 The Chain-Bath Coupling

The overlap integral diminishes with the distance between the spins and we must therefore alter the exchange coupling J_0 to account for the displacements of the nearest-neighbor spins from their equilibrium positions. The distance between adjacent spins grows by $u_{j+1}^x - u_j^x$, to first order in the displacements, where u_j^x is the displacement of the j^{th} spin in the \hat{x} direction (along the chain). We keep the

equilibrium J_0 in the chain Hamiltonian H_S and add the coupling

$$V = J' \sum_{j=1}^N \vec{\sigma}_j \cdot \vec{\sigma}_{j+1} (u_{j+1}^x - u_j^x)$$

with J' the sensitivity of the exchange energy to a change in the adjacent spins' separation. We assume that the longer-range frustration is less sensitive to strain and neglect it altogether. This is especially valid in the absence of any bath-free frustration ($F_0 = 0$), but we also consider $F_0 \approx J_0/2$ and $F_0 \approx J_0$ for which our results are an approximation only to those cases where the frustration strain is much less than the exchange strain, $F' \ll J'$.

We can rewrite the exchange-strain coupling as

$$V = J' \sum_{j=1}^N \underbrace{(\vec{\sigma}_{j-1} \cdot \vec{\sigma}_j - \vec{\sigma}_j \cdot \vec{\sigma}_{j+1})}_{\mathcal{X}_j} u_j^x = J' \sum_{j=1}^N \mathcal{X}_j u_j^x \quad (4.1)$$

to emphasize the bi-linear form, as we did in Chapter 3. The chain operators $\mathcal{X}_j \equiv \vec{\sigma}_{j-1} \cdot \vec{\sigma}_j - \vec{\sigma}_j \cdot \vec{\sigma}_{j+1}$ interact with the bath operators u_j^x .

Note the selection rules: $\langle l'm' | \mathcal{X}_j | lm \rangle \sim \delta_{m',m}$. The “interaction operator” \mathcal{X}_j does not drive transitions between distinct m, m' . This is because the $\vec{\sigma}_j \cdot \vec{\sigma}_{j\pm 1}$ commute with J_z and, since we order our eigenstates with decreasing m , the \mathcal{X}_j are block-diagonal in the energy eigenbasis of H_S . On the other hand there can be transitions between distinct l, l' .

For example, in the $m = \pm 2$ subspaces the interaction operators for a four

spin chain are

$$\mathcal{X}_{1,2} = \begin{pmatrix} 0 & \mp 2 & -2 & 0 \\ \mp 2 & \pm 2 & 0 & 0 \\ -2 & 0 & \mp 2 & 0 \\ 0 & 0 & 0 & 0 \end{pmatrix}; \quad \mathcal{X}_{3,4} = \begin{pmatrix} 0 & \pm 2 & 2 & 0 \\ \pm 2 & \pm 2 & 0 & 0 \\ 2 & 0 & \mp 2 & 0 \\ 0 & 0 & 0 & 0 \end{pmatrix}.$$

The \mathcal{X}_j vanish in the $m = \pm 4$ (one-dimensional) subspaces, while in the $J_z = 0$ subspace they are

$$\mathcal{X}_{1,2} = \begin{pmatrix} 0 & 0 & \mp 2\sqrt{3} & 0 & 0 & 0 \\ 0 & 0 & 0 & \pm 2 & -2 & 0 \\ \mp 2\sqrt{3} & 0 & 0 & 0 & 0 & 0 \\ 0 & \pm 2 & 0 & \pm 2 & 0 & 0 \\ 0 & -2 & 0 & 0 & \mp 2 & 0 \\ 0 & 0 & 0 & 0 & 0 & 0 \end{pmatrix}$$

and

$$\mathcal{X}_{3,4} = \begin{pmatrix} 0 & 0 & \mp 2\sqrt{3} & 0 & 0 & 0 \\ 0 & 0 & 0 & \mp 2 & 2 & 0 \\ \mp 2\sqrt{3} & 0 & 0 & 0 & 0 & 0 \\ 0 & \mp 2 & 0 & \pm 2 & 0 & 0 \\ 0 & 2 & 0 & 0 & \mp 2 & 0 \\ 0 & 0 & 0 & 0 & 0 & 0 \end{pmatrix}$$

satisfying $\mathcal{X}_1 + \mathcal{X}_2 + \mathcal{X}_3 + \mathcal{X}_4 = 0$. These interaction operators present separate “networks” of selection-ruled transitions: within the $m = 2$ subspace,

$$\{|\psi_2\rangle \leftrightarrow |\psi_3\rangle, |\psi_2\rangle \leftrightarrow |\psi_4\rangle\},$$

and this is isolated from an identical $|\psi_{\alpha+10}\rangle$ network in the $m = -2$ subspace, both of which are isolated from the $J_z = 0$ subspace in which

$$|\psi_6\rangle \leftrightarrow |\psi_8\rangle$$

is isolated from

$$\{|\psi_7\rangle \leftrightarrow |\psi_9\rangle, |\psi_7\rangle \leftrightarrow |\psi_{10}\rangle\}.$$

Given these selection rules, the only non-vanishing transition energies are $\hbar\Delta_1 = 4J_0 - 8F_0$ and $\hbar\Delta_2 = 8J_0 - 16F_0$; With more general values for J , F , and S (i.e. after we renormalize), they would be $\hbar\Delta_1 \equiv 4J - 8F + 24S$ and $\hbar\Delta_2 \equiv 8J - 16F - 48S$.

It is always true that, for these exchange-strained interaction operators, a collective coupling vanishes: $\sum_j \mathcal{X}_j = 0$. In this case the exchange-strain does not disturb the chain at all. A collective coupling arises when the spins are very close together compared to the bath wavelengths that interact with the chain; the adjacent spins are pushed to and fro in tandem by the long-wavelength passing phonons and their separation does not change appreciably.

4.6 The Formalism

The formalism is very much the same as in the SQUID chain, only we are using u_j^x in place of ϕ_j and the interaction operators \mathcal{X}_j are also different from those of the SQUID chain.

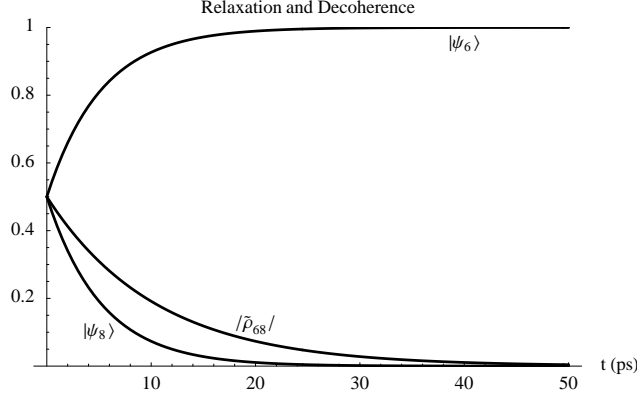


Figure 4.3: Decoherence and Relaxation in a Heisenberg four-Spin Chain. $|\psi_6\rangle + |\psi_8\rangle$ cooling below the critical point. ($J_0 = 103.4$ meV, $F_0 = 0$).

4.7 The Coefficients

4.7.1 The Bath Correlator

To evaluate the correlator we (again) perform the trace in the bath's energy eigenbasis by summing over the diagonal matrix elements:

$$\begin{aligned}
\text{Tr}_B[\tilde{u}_j^x(t) \tilde{u}_j^x(t') \rho_B] &= \frac{1}{V} \sum_n \sum_{\vec{k}_s, \vec{k}'_{s'}} \frac{e_s^x(\vec{k}) e_{s'}^x(\vec{k}') \hbar}{2\rho \sqrt{\omega_s(\vec{k}) \omega_{s'}(\vec{k}')}} \\
&\times \langle n | \left(\tilde{a}_{\vec{k}_s}(t) e^{i\vec{k} \cdot \vec{x}_j} + \tilde{a}_{\vec{k}_s}^\dagger(t) e^{-i\vec{k} \cdot \vec{x}_j} \right) \left(\tilde{a}_{\vec{k}'_{s'}}(t') e^{i\vec{k}' \cdot \vec{x}_k} + \tilde{a}_{\vec{k}'_{s'}}^\dagger(t') e^{-i\vec{k}' \cdot \vec{x}_k} \right) \frac{e^{-E_n/k_B T}}{Z_B} | n \rangle \\
&= \frac{1}{V} \overbrace{\left(\sum_{\vec{k}} \int_0^\infty \frac{d\omega \omega^2}{c^3} \int_0^\pi d\theta \sin \theta \int_0^{2\pi} d\phi \sum_s e_s^x(\vec{k})^2 \right)}^1 \frac{\hbar}{2\rho\omega} \\
&\times \underbrace{\left[\coth\left(\frac{\hbar\omega}{2k_B T}\right) \cos(\omega\tau) - i \sin(\omega\tau) \right]}_{(N_\omega+1)e^{-i\omega\tau} + N_\omega e^{i\omega\tau}} \underbrace{\cos(\omega\tau_{jk} \sin \theta \cos \phi)}_{\Re[e^{\pm i\vec{k} \cdot (\vec{x}_j - \vec{x}_k)}]}.
\end{aligned}$$

The double sum $\sum_{\vec{k}_s \vec{k}'_{s'}}$ collapses to a single sum $\sum_{\vec{k}_s}$ (which we convert to a \vec{k} -space integral, in spherical coordinates, of the sum over s) because the only non-zero cross-

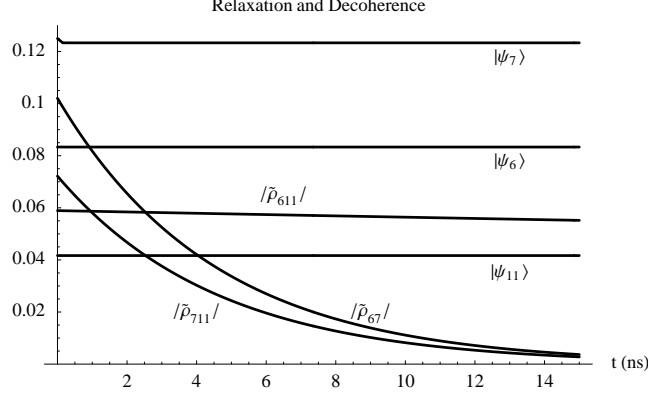


Figure 4.4: Extended coherence and relaxation times for low-lying states; times are in nanoseconds, not picoseconds. $|\uparrow \rightarrow \uparrow \rightarrow \rangle$ cooling below the critical point. Only the $J_z = 0$ subspace is shown. It is isolated from the others. Also, $|\psi_6\rangle$, $|\psi_7\rangle$, and $|\psi_{11}\rangle$ lie at the bottom of their mutually-isolated networks of allowed transitions. Upward transitions are suppressed by the cold bath. ($J_0 = 103.4$ meV, $F_0 = 0$).

terms $\sim \delta_{\vec{k}\vec{k}'} \delta_{ss'}$. They are

$$\langle n | \tilde{a}_{\vec{k}s} e^{i\vec{k}\cdot\vec{x}_j} \tilde{a}_{\vec{k}'s'}^\dagger e^{-i\vec{k}'\cdot\vec{x}_k} | n \rangle = (n_{\vec{k}s} + 1) \delta_{\vec{k}\vec{k}'} \delta_{ss'} e^{-i\omega\tau} e^{i\vec{k}\cdot\vec{x}_{jk}}$$

and

$$\langle n | \tilde{a}_{\vec{k}s}^\dagger e^{-i\vec{k}\cdot\vec{x}_j} \tilde{a}_{\vec{k}'s'} e^{i\vec{k}'\cdot\vec{x}_k} | n \rangle = n_{\vec{k}s} \delta_{\vec{k}\vec{k}'} \delta_{ss'} e^{i\omega\tau} e^{-i\vec{k}\cdot\vec{x}_{jk}},$$

The isotropy of the linear dispersions simplifies the sum of the squares of the x -components of the (orthonormal) polarization vectors: $\sum_s e_s^x(\vec{k})^2 = 1$.

To complete our analysis of the bath correlator we must integrate over the \vec{k} -space. It is relatively easy to perform the ϕ integration, $\int_0^{2\pi} d\phi \cos(\omega\tau_{jk} \sin\theta \cos\phi) = 2\pi J_0(\omega\tau_{jk} \sin\theta)$, and the θ integration

$$\Theta_{jk} \equiv 2\pi \int_0^\pi d\theta \sin\theta J_0(\omega\tau_{jk} \sin\theta) = 4\pi \frac{\sin(\omega\tau_{jk})}{\omega\tau_{jk}},$$

leaving only the integration over bath frequencies ω :

$$\text{Tr}_B[\tilde{u}_j^x(t) \tilde{u}_j^x(t') \rho_B] = \underbrace{\int_0^\infty d\omega J_{jk}(\omega) \coth\left(\frac{\hbar\omega}{2k_B T}\right) \cos(\omega\tau)}_{\nu_{jk}(\tau)} - i \underbrace{\int_0^\infty d\omega J_{jk}(\omega) \sin(\omega\tau)}_{\mu_{jk}(\tau)},$$

characterized by the spectral densities

$$J_{jk}(\omega) = \underbrace{\frac{\hbar}{4\pi^2 \rho c^3}}_{\gamma} \omega \frac{\sin(\omega\tau_{jk})}{\omega\tau_{jk}} \frac{\Lambda^2}{\Lambda^2 + \omega^2}$$

which vanish for $\omega\tau_{jk} \gg 1$ or, on the other hand, become identical for $\omega\tau_{jk} \ll 1$:

$$J_{jk}(\omega) \Rightarrow J_{jj}(\omega) \equiv \gamma \omega \frac{\Lambda^2}{\Lambda^2 + \omega^2},$$

where for convenience we use the coupling constant $\gamma \equiv \hbar/4\pi^2 \rho c^3$.

In this case of the spins' exchange-strained coupling to the bath we use a different form of cutoff, $\frac{\Lambda^2}{\Lambda^2 + \omega^2}$, than in the SQUID-chain. For the spin-chain the spectral densities are only linear in ω and this cutoff is strong enough for, and popular for, ohmic (linear in ω) spectral densities [76].

4.7.2 The Markov Approximation

Again we rely on the Dirac delta function behavior of the $\int_0^t d\tau \cos \omega\tau \cos \Delta\tau$ and $\int_0^t d\tau \sin \omega\tau \sin \Delta\tau$ to pick out the constant coefficients of diffusion and damping. We discard the factor $\Lambda^2/(\Lambda^2 + \Delta^2) \approx 1$ for our high cutoff frequency $\Lambda \gg \Delta$. Then we assume we are either close-to or far-from any level crossings. For $\Delta\tau_{jk} \gg 1$ we use

$$D_{jj}^\Delta \equiv \frac{\pi}{2} \gamma \Delta \coth\left(\frac{\hbar\Delta}{2k_B T}\right); \quad D_{j \neq k}^\Delta = 0 = \gamma_{j \neq k}^\Delta; \quad \gamma_{jj}^\Delta \equiv \frac{\pi}{2} \gamma \Delta,$$

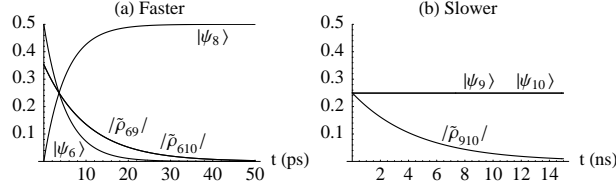


Figure 4.5: Two time-scales for decay; picoseconds vs. nanoseconds. $\sqrt{2}|\psi_6\rangle + |\psi_9\rangle + |\psi_{10}\rangle$ cooling above the critical point. Transitions out of $|\psi_9\rangle$ and $|\psi_{10}\rangle$ are suppressed by the cold bath, while those from $|\psi_6\rangle$ are enhanced. ($J_0 = 103.4$ meV, $F_0 = J_0$).

neglecting the cross terms $D_{j\neq k}^\Delta \approx 0 \approx \gamma_{j\neq k}^\Delta$ which vanished with $\sin(\Delta\tau_{jk})/\Delta\tau_{jk} \ll$

1. For $\Delta\tau_{jk} \ll 1$ we use, correct to first order in $\Delta\tau_{jk}$,

$$D_{j\neq k}^\Delta = D_{jj}^\Delta = \frac{\pi}{2}\gamma \Delta \coth\left(\frac{\hbar\Delta}{2k_B T}\right); \quad \gamma_{j\neq k}^\Delta = \gamma_{jj}^\Delta = \frac{\pi}{2}\gamma \Delta ,$$

i.e. the collective coupling case with the $j \neq k$ cross terms equal to the $j = k$ ones.

Because the spectral density is only ohmic, i.e. growing linearly with Δ , we cannot throw out the cross terms even for a critical point because $\coth(\hbar\Delta/2k_B T) \rightarrow \infty$ as fast as $\Delta \rightarrow 0$. For the exchange-strained chain the collective coupling vanishes (in effect the $j \neq k$ cross terms cancel the $j = k$ terms); we expect at least some protection from decoherence at the critical point.

These approximations are only valid near-to and far-from a level crossing, whereas the intermediate Δ would require the $\sin(\Delta\tau_{jk})/\Delta\tau_{jk}$ factors.

For the renormalization and anomalous diffusion, by contour integration in the complex ω -plane, we obtain long-time principal values:

$$r_{jj}^\Delta = \frac{\pi}{2}\gamma \Lambda$$

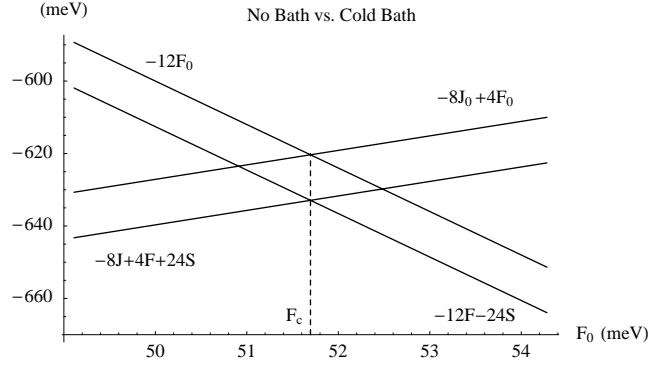


Figure 4.6: Bath-free and renormalized energies of $|\psi_6\rangle$ and $|\psi_8\rangle$. ($J_0 = 103.4$ meV).

and

$$A_{jj}^\Delta = \frac{\pi}{2} \gamma \frac{\Delta}{\pi} \left[2\Re[\Psi(\frac{i\hbar\Delta/\pi}{2k_B T})] - 2\Psi(\frac{\hbar\Lambda/\pi}{2k_B T}) - \frac{2k_B T}{\hbar\Lambda/\pi} \right].$$

Here $\Psi(z)$ is the digamma function and $\Re[\Psi(z)]$ is the real part of it. Again we discard the factor $\Lambda^2/(\Lambda^2 + \Delta^2) \approx 1$. We also neglect the $j \neq k$ cross terms on the grounds that these integrals go to much higher frequencies than the damping and diffusion do, and the cross term integrals are thus suppressed by their $\frac{\sin(\omega\tau_{jk})}{\omega\tau_{jk}}$ kernel.

4.8 The Four Generators

We now show, for a weak coupling of our Heisenberg spin chain to the bath and with J , F , and S set near-to or far-from any resonant pairs of allowed transitions, that the renormalization and anomalous diffusion contribute effectively Hamiltonian dynamics, which can be dropped from the master equation by “renormalizing” the chain Hamiltonian, while the damping and diffusion work together to effectively decohere and thermalize the system within each network of allowed transitions.

4.8.1 The Renormalization

Recall the renormalization's contribution to the rate of change of a density matrix element $\tilde{\rho}_{\alpha\delta} \equiv \langle \alpha | \tilde{\rho} | \delta \rangle$ is

$$\begin{aligned} \dot{\tilde{\rho}}_{\alpha\delta}^r = & i \frac{J^2}{\hbar^2} \sum_{j,k} \left(\sum_{\beta\bar{\alpha}} \tilde{\mathcal{X}}_{j\alpha\beta} \tilde{\mathcal{X}}_{k\beta\bar{\alpha}} r_{jk}^{\Delta\beta\bar{\alpha}} \tilde{\rho}_{\bar{\alpha}\delta} + \sum_{\beta\gamma} \tilde{\mathcal{X}}_{j\alpha\beta} \tilde{\mathcal{X}}_{k\gamma\delta} r_{jk}^{\Delta\gamma\delta} \tilde{\rho}_{\beta\gamma} \right. \\ & \left. - \sum_{\beta\gamma} \tilde{\mathcal{X}}_{k\alpha\beta} \tilde{\mathcal{X}}_{j\gamma\delta} r_{jk}^{\Delta\alpha\beta} \tilde{\rho}_{\beta\gamma} - \sum_{\bar{\delta}\beta} \tilde{\mathcal{X}}_{k\bar{\delta}\beta} \tilde{\mathcal{X}}_{j\beta\delta} r_{jk}^{\Delta\bar{\delta}\beta} \tilde{\rho}_{\alpha\bar{\delta}} \right). \end{aligned}$$

By the selection-ruled resonance conditions of Chapter 3, the third term cancels the second term as long as the coefficient r_{jk}^{Δ} is a slowly-enough varying function of Δ . In our case of exchange-strained interaction operators, the coefficients $r_{jj}^{\Delta} = \frac{\pi}{2}\gamma\Lambda$ and $r_{j\neq k}^{\Delta} \approx 0$ are independent of Δ . But the other coefficients, A_{jk}^{Δ} , D_{jk}^{Δ} , and γ_{jk}^{Δ} , do vary with Δ and thus for those generators, to make use of these resonance conditions, we must check that the parameters J , F , and S of the chain Hamiltonian are set either near-to or far-from any resonant pairs of transitions.

Then the first and fourth terms give the additional Hamiltonian dynamics in the interaction picture with an effectively Hermitian

$$\tilde{R}_S'' \equiv -(J^2/\hbar) \sum_{j,k} \tilde{\mathcal{X}}_j \tilde{\mathcal{U}}_{jk}^r = - \sum_{j,k} \tilde{\mathcal{X}}_j \sum_{\Delta} \frac{J^2}{\hbar} r_{jk}^{\Delta} \tilde{\mathcal{X}}_k^{\Delta}.$$

With $r_{j\neq k}^{\Delta} \approx 0$ and $r_{jj}^{\Delta} = \frac{\pi}{2}\gamma\Lambda$ independent of Δ we have

$$R_S'' = -\frac{J^2}{\hbar} \frac{\pi}{2} \gamma \Lambda \sum_j \underbrace{(\vec{\sigma}_{j-1} \cdot \vec{\sigma}_j - \vec{\sigma}_j \cdot \vec{\sigma}_{j+1})^2}_{\mathcal{X}_j}.$$

We then use $(\vec{\sigma}_j \cdot \vec{\sigma}_{j+1})^2 = -2\vec{\sigma}_j \cdot \vec{\sigma}_{j+1}$ and $\{\vec{\sigma}_{j-1} \cdot \vec{\sigma}_j, \vec{\sigma}_j \cdot \vec{\sigma}_{j+1}\} = -2\vec{\sigma}_{j-1} \cdot \vec{\sigma}_{j+1}$ to obtain

$$R_S'' = \sum_j (J_r \vec{\sigma}_j \cdot \vec{\sigma}_{j+1} + F_r \vec{\sigma}_{j-1} \cdot \vec{\sigma}_{j+1})$$

in which there is a bath-induced exchange coupling, $J_r \equiv \frac{J'^2}{\hbar} \frac{\pi}{2} \gamma 4\Lambda$, and frustration, $F_r \equiv \frac{J'^2}{\hbar} \frac{\pi}{2} \gamma 2\Lambda$.

4.8.2 The Anomalous Diffusion

The anomalous diffusion's contribution is again just an additional Hamiltonian dynamics in the interaction picture with an effectively Hermitian

$$\tilde{A}_S'' \equiv \frac{J'^2}{i\hbar} \sum_{j,k} \tilde{\chi}_j \tilde{\mathcal{V}}_{jk}^A = \sum_{j,k} \tilde{\chi}_j \sum_{\Delta} \frac{J'^2}{\hbar} A_{jk}^{\Delta} i\tilde{\mathcal{P}}_k^{\Delta}.$$

For the purposes of calculation we define $\vec{\sigma}_j \cdot \vec{\sigma}_{j+1}^A$ to be the operator that results from multiplying the eigenbasis matrix elements of $\vec{\sigma}_j \cdot \vec{\sigma}_{j+1}$ by the A_{jj}^{Δ} coefficients. Then, by throwing out the cross terms ($A_{j \neq k}^{\Delta} \approx 0$) and re-summing various terms, we can write

$$A_S'' = -\frac{J'^2}{\hbar} \sum_j \vec{\sigma}_j \cdot \vec{\sigma}_{j+1} (\vec{\sigma}_{j-1} \cdot \vec{\sigma}_j^A - 2\vec{\sigma}_j \cdot \vec{\sigma}_{j+1}^A + \vec{\sigma}_{j+1} \cdot \vec{\sigma}_{j+2}^A).$$

A representative summand is, for example,

$$\mathcal{A}_{23} = -\vec{\sigma}_2 \cdot \vec{\sigma}_3 (\vec{\sigma}_1 \cdot \vec{\sigma}_2^A - 2\vec{\sigma}_2 \cdot \vec{\sigma}_3^A + \vec{\sigma}_3 \cdot \vec{\sigma}_4^A).$$

Like $\vec{\sigma}_j \cdot \vec{\sigma}_{j+1}$, the operator in parentheses only drives transitions of one or two rungs on the ladder of exchange energies, e.g. $\hbar\Delta_1 = 4J_0 - 8F_0$ and $\hbar\Delta_2 = 8J_0 - 16F_0$ for a four spin chain, and its non-vanishing matrix elements are proportional to either $\frac{\pi}{2}\gamma a_1 \equiv A_{jj}^{\Delta_1}$ or $\frac{\pi}{2}\gamma a_2 \equiv A_{jj}^{\Delta_2}$. The Hermitian part of our representative summand, $(\mathcal{A}_{23} + \mathcal{A}_{23}^{\dagger})/2$, apart from a factor $\frac{\pi}{2}\gamma$, can be expanded as

$$(a_1 + a_2)(\vec{\sigma}_1 \cdot \vec{\sigma}_2 + \vec{\sigma}_3 \cdot \vec{\sigma}_4) - (a_1 + a_2)(\vec{\sigma}_1 \cdot \vec{\sigma}_3 + \vec{\sigma}_2 \cdot \vec{\sigma}_4) + (a_1 - a_2)[\vec{\sigma}_1 \cdot \vec{\sigma}_2 \vec{\sigma}_3 \cdot \vec{\sigma}_4 - \vec{\sigma}_1 \cdot \vec{\sigma}_3 \vec{\sigma}_2 \cdot \vec{\sigma}_4]$$

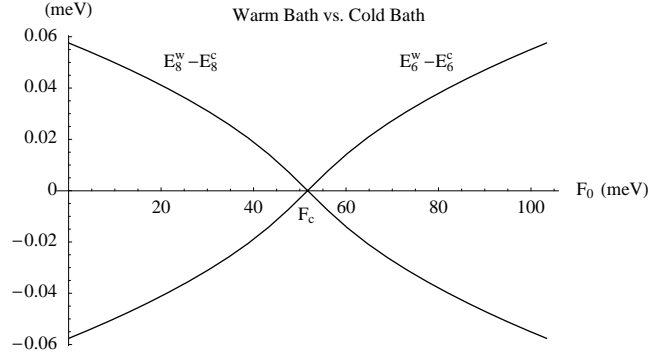


Figure 4.7: Changing the chain's spectrum by warming the bath. Energy shifts for $|\psi_6\rangle$ and $|\psi_8\rangle$. ($J_0 = 103.4$ meV, $k_B T = 41.36$ meV (cold) and $k_B T = 4136$ meV (warm)).

From this we conclude that

$$A''_S = \sum_j \left(J_A \vec{\sigma}_j \cdot \vec{\sigma}_{j+1} + F_A \vec{\sigma}_{j-1} \cdot \vec{\sigma}_{j+1} + S_A \vec{\sigma}_{j-1} \cdot \vec{\sigma}_j \vec{\sigma}_{j+1} \cdot \vec{\sigma}_{j+2} - S_A \vec{\sigma}_{j-1} \cdot \vec{\sigma}_{j+1} \vec{\sigma}_j \cdot \vec{\sigma}_{j+2} \right)$$

(which we have checked explicitly for four spins) and obtain, again, a bath-induced exchange, $J_A \equiv \frac{J'^2}{\hbar} \frac{\pi}{2} \gamma 2(a_1 + a_2)$, and frustration, $F_A \equiv -J_A$, and additional term $S_A = \frac{J'^2}{\hbar} \frac{\pi}{2} \gamma (a_1 - a_2)$.

They are temperature dependent because (recall A_{jj}^Δ)

$$a_i = \frac{\Delta_i}{\pi} \left[2\Re[\Psi(\frac{i\hbar\Delta_i/\pi}{2k_B T})] - 2\Psi(\frac{\hbar\Lambda/\pi}{2k_B T}) - \frac{2k_B T}{\hbar\Lambda/\pi} \right].$$

4.8.3 The Damping and Diffusion

We would like now to concentrate on the damping and diffusion. From now on, and in all our numerical simulations, we use the renormalized Hamiltonian $H_S^{(1)}$ with, to summarize,

$$J = J_0 + \underbrace{4\gamma'\Lambda}_{J_r} + \underbrace{2\gamma'(a_1 + a_2)}_{J_A};$$

$$F = F_0 + \underbrace{2\gamma'\Lambda}_{F_r} - \underbrace{2\gamma'(a_1 + a_2)}_{-F_A};$$

$$S = \underbrace{\gamma'(a_1 - a_2)}_{S_A},$$

where, with $\Delta_2 = 2\Delta_1 = 8J_0/\hbar - 16F_0/\hbar$,

$$a_i = \frac{\Delta_i}{\pi} \left[2\Re[\Psi(\frac{i\hbar\Delta_i/\pi}{2k_B T})] - 2\Psi(\frac{\hbar\Lambda/\pi}{2k_B T}) - \frac{2k_B T}{\hbar\Lambda/\pi} \right],$$

and $\gamma' \equiv \frac{J'^2}{\hbar} \frac{\pi}{2} \gamma$.

Again the decoherence is caused by transitions from $|\alpha\rangle$ and $|\delta\rangle$,

$$\frac{\partial \dot{\tilde{\rho}}_{\alpha\delta}}{\partial \tilde{\rho}_{\alpha\delta}} = - \sum_{j,k} \left(\sum_{\beta} \tilde{\chi}_{j\alpha\beta} \tilde{\chi}_{k\beta\alpha} \Gamma_{jk}^{\beta\alpha} - \overbrace{\tilde{\chi}_{j\alpha\alpha} \tilde{\chi}_{k\delta\delta} \Gamma_{jk}^{\delta\delta}}^0 \right. \\ \left. - \underbrace{\tilde{\chi}_{k\alpha\alpha} \tilde{\chi}_{j\delta\delta} \Gamma_{jk}^{\alpha\alpha}}_0 + \sum_{\beta} \tilde{\chi}_{k\delta\beta} \tilde{\chi}_{j\beta\delta} \Gamma_{jk}^{\beta\delta} \right) \equiv -\bar{\Gamma}_{\alpha\delta}$$

only in this case of exchange-strained spins the second and third terms vanish because, for the exchange-strained interaction operators, the zero-frequency diffusion vanishes as does the damping coefficient $\gamma_{jk}^0 = 0$.

4.9 Numerical Simulations

We simulate the effects of the matrix element equation in a variety of scenarios for four-spin chains. In all cases we choose J_0 and F_0 to be close-to or far-from any resonant pairs of allowed transitions (we can run at the critical point because of its exactly-resonant pairs). That way we can and do discard the oscillating coefficients from the equation, since their effect would average to zero anyway. The matrix element equation becomes a coupled first order differential equation with constant coefficients which we numerically integrate [81].

We consider an initial exchange frequency of 100 THz, with $J_0 = 103.4$ meV, and run scenarios without any bath-free frustration, $F_0 = 0$, and with frustration at the critical point $F_0 = J_0/2$ as well as twice that. We use a cold bath $k_B T = 4J_0/10 = 41.36$ meV. We assume our spins are a few angstroms apart and experience an exchange strain of $J' = 7.166$ meV/nm which results in an overall coupling $\gamma' \equiv \frac{J'^2}{\hbar} \frac{\pi}{2} \gamma = 5.238 \times 10^{-7}$ meV ps, in which we used a lattice mass density of $\rho = 5 \times 10^3$ kg/m and sound speed of $c = 5 \times 10^3$ m/s. This gives a quality factor for the 100 THz exchange splitting of 10^5 . The renormalization and anomalous diffusion depend slightly on temperature and greatly on the cutoff frequency for which we use $\Lambda = 10^6$ ps $^{-1}$. We use J_0 and F_0 to obtain the renormalized values J , F , and S with which we then study the damping and diffusion.

At the critical point, where $\Delta = 0$, the cross term rates $\Gamma_{jk}^{\Delta=0} = 0$ do not vanish; our spectral densities are only ohmic. Instead they become identical for all j, k . Whenever $\Delta < 0.1/\tau_c$, with τ_c the phonon transit time between most distant sites (the length of the chain) we set the $j \neq k$ cross terms equal to the $j = k$ ones. And whenever $\Delta\tau_{jk} > 10/\tau_c$ we set the cross terms to zero. We have avoided the more complicated intermediate cases.

The matrix elements of the interaction operators are used to calculate all the constant coefficients in the matrix element equation and we then proceed with the numerical simulations for any initial state $\rho(0)$.

4.10 Discussion

The extra term S introduced by the temperature dependent anomalous diffusion is very small (but we include it anyway in our simulations), whereas the changes from J_0 to J and from F_0 to F of about 2 and 1 meV, respectively, are more dramatic because they are proportional to the large cutoff Λ . The renormalizing will not take F to, or past, the critical point $J/2 - 3S$ unless F_0 was already there, at $F_0 = J_0/2$.

The interaction operators do not drive transitions between subspaces of distinct J_z , so there is no point in including a magnetic field in these examples. We work primarily in the $J_z = 0$ subspace as there are more states and networks there. There are no pairs of nearly-resonant allowed transitions so we do not see decaying oscillations emerging in lower energy subspaces.

The relaxation and decoherence will thermalize the spins only within each isolated network, and in proportion to the total initial probability to be in that subspace. Upward transitions are suppressed by the cold bath; low-lying states spanning isolated networks are protected by the cold bath. Downward transitions are enhanced. The larger the energy given off to the bath, the faster the rate. Starting in a degenerate but higher-energy subspace does not necessarily protect the state.

We are working with distant spins, relative to the few-spin chain's frequencies, so ordinarily we could not take advantage of the vanishing collective exchange strain. But the spectrum of the frustrated Heisenberg spin chain does present a critical point

level crossing where in fact all the allowed transitions have $\Delta \rightarrow 0$ and the collective coupling is relevant. Strikingly, this protects eigenstates and superpositions from decay. The decoherence free subspace is non-degenerate, even though it obtains at a level crossing, and therefore the protected superpositions evolve and continue to evolve.

4.11 Conclusion

A chain of a few Heisenberg coupled spins whose exchange is strained by a phonon bath can be studied with master equation techniques, in the Born-Markov approximation, from the model for quantum Brownian motion. The renormalization and temperature-dependent anomalous diffusion can be used to renormalize the chain Hamiltonian. This shifts the energies but not the eigenstates. It can introduce frustration, but not enough to get to the critical point, for which the critical frustration must already be present. The damping and diffusion give a matrix element equation showing decoherence, relaxation, and the possibility for decaying oscillations to emerge in a lower energy subspace. However, this possibility is not allowed by the chain's spectrum, and the disjoint network of allowed transitions prevent the total thermalization. Instead there is a relative thermalization within each network. The relaxation adjusts the populations of the eigenstates and undermines their support for any superposition (coherence) between them, leading to decoherence.

An important feature of the frustrated Heisenberg spin chain is the critical

point level crossing where some allowed transitions vanish along with their frequency thanks to the vanishing property of a collective strain. The networks of selection-rules in effect acquire the feature of the collective behavior as $\Delta\tau_{jk} \rightarrow 0 \ll 1$; even a chain with well-spaced spins will have extended coherence and relaxation times when tuned to the critical point.

Chapter 5

Summary

In this dissertation we looked at three solid state qubit encoding schemes from two perspectives. We first proposed that a hydrogenic spin qubit could remove some of the obstacles to quantum computing with P donor spins in Si. We then developed a chain-boson model for the decoherence of a chain of qubits embedded in a bosonic bath and applied it to a few coupled SQUIDs' exchanging their angular momenta with a phonon bath as well as a few coupled spins-1/2 whose exchange strength is strained by a phonon bath.

5.1 P donor spins in Si

Consideration of a simple encoding scheme for the Kane quantum computer has led to a modified architecture which overcomes many obstacles to the original proposal. Resonant hyperfine stepping provides digital control with an extremely well defined and stable parameter; there is no tuning of the hyperfine strength and there is no qubit specific tuning; we can optimize the fidelity of the entire computer by tuning the clock frequency (and thus the bit pulse width) of the bit trains. Effectively, we have replaced the AC magnetic field with a digital electric field.

Digital shuttling of electrons removes the need for the complicated and difficult exchange mediated coupling and overcomes the nearest neighbor restrictions. It also

makes the computer easier to fabricate since the donors can be irregularly spaced and further apart, allowing for larger gate electrodes, and malfunctioning donor sites can be diagnosed and ignored, provided there is enough S gate capability to shuttle other qubits' electrons around the misbehaving donor.

There is a natural data-bus to a nuclear spin-pair quantum memory or electron spin-pairs for projective measurement beneath a Single Electron Transistor. The availability of a projective measurement means we can initialize 50% of the qubits at higher temperatures, and electron shuttling can then pool initialized qubits into the working part of the computer. These many benefits were obtained at the cost of coupling to an auxiliary subspace outside the logical subspace. The fidelity depends crucially on tuning the clock frequency and the global magnetic field. We have investigated the sensitivity of the computer and found that less than one error per 10^5 gate operations is attainable even for relative variations in field and frequency as large as 10^{-5} .

5.2 The Chain-Boson Model

The chain-boson model is a natural extension of the spin-boson model. It places a chain of two-level systems in a bath in such a way that there are position-dependent system-bath couplings. This makes it possible to clarify the role of bath “correlation lengths” in the decoherence of encoded qubits. We followed master equation techniques from the model for quantum Brownian motion to obtain the generators of the open system dynamics. We concentrated mainly on the generators

associated with the coefficients of damping and diffusion, which we calculated for small ($\Delta \ll 1/\tau_{jk}$) and large ($\Delta \gg 1/\tau_{jk}$) transition frequencies in the Born-Markov approximation.

We then obtained a matrix element equation in the chain's energy eigenbasis similar to what one would obtain with a Bloch-Redfield approach [87], but in the interaction picture. This allowed us to discard rapidly oscillating terms, assuming our system Hamiltonian is set close-to or far-from pairs of resonant transitions, leaving an easily-integrated system of coupled first order differential equations, with constant coefficients, for the evolution of $\tilde{\rho}(t)$. This matrix equation shows the relaxation, decoherence, and thermalization, subject to selection-ruled networks of allowed transitions.

The matrix equation also reveals the possibility for coherent oscillations to move from one subspace, where they are decaying, to another, where they can decay more slowly. This is dependent on pairs of resonant allowed transitions in the chain's spectrum, so that a superposition of two eigenstates can relax coherently into a superposition of two lower-energy eigenstates with the same energy difference as the upper two. We observed this in the chain of Heisenberg-coupled SQUIDs exchanging their angular momentum with the phonon bath.

Despite individual qubit transition frequencies that imply the independent dissipation of well-spaced qubits, the inter-qubit coupling can provide a critical point level crossing where one or more transition frequencies vanish and the low-frequency portion of the collective coupling operator becomes relevant to some system transitions. In fact, in the SQUID chain, we found that transitions between the lowest

two states were blocked at their degeneracy point, helping to protect some superpositions. In the exchange-strained spin-chain the situation was even more dramatic. A *non-degenerate* subspace became decoherence-free so that coherent oscillations could persist indefinitely.

5.3 Relevance

The promising theoretical results for hydrogenic spin quantum computing should motivate further research on the coherent shuttling and measurement of electron spins, extremely pure Si fabrication, optimal control sequences, and the spin-orbit and dipole-dipole interactions during realistic electrode driven switching and shuttling.

Decoherence is a major obstacle to quantum computation. The possibility of augmenting qubit encoding schemes with an inter-qubit coupling to obtain some or all of the benefits of a collective coupling, as found in this work with two model studies, is worth consideration in a variety of implementations and quantum error correction and prevention protocols. Also, the movement of coherent oscillations from one subspace to another suggests that carefully timed changes to the system Hamiltonian could help maintain the quantum information, even though our methods are not appropriate to a time-dependent Hamiltonian.

BIBLIOGRAPHY

- [1] M. Friesen, R. Joynt, and M. A. Eriksson, *Appl. Phys. Lett.* **81**, 4619 (2002).
- [2] B. E. Kane, *Nature* **393**, 133 (1998).
- [3] Y. Nakamura, Y. A. Pashkin, and J. S. Tsai, *Nature* **398**, 786 (1990).
- [4] J. R. Friedman, V. Patel, W. Chen, S. K. Tolpygo, and J. E. Lukens, *Nature* **406**, 43 (2000).
- [5] C. H. van der Wal, A. C. J. ter Haar, F. K. Wilhelm, R. N. Schouten, C. J. P. M. Harmans, T. P. Orlando, S. Lloyd, and J. E. Mooij, *Science* **290**, 773 (2000).
- [6] D. A. Lidar and L.-A. Wu, *Phys. Rev. Lett.* **88**, 17905 (2002).
- [7] D. P. DiVincenzo, D. Bacon, J. Kempe, G. Burkard, and K. B. Whaley, *Nature* **408**, 339 (2000).
- [8] M. A. Nielsen and I. L. Chuang, *Quantum Computation and Quantum Information* (Cambridge University Press, Cambridge, UK, 2000).
- [9] D. Kribs, R. Laflamme, and D. Poulin, *Phys. Rev. Lett.* **94**, 180501 (2005).
- [10] L.-M. Duan and G.-C. Guo, *Phys. Rev. A* **57**, 737 (1998).
- [11] D. A. Lidar, I. L. Chuang, and K. B. Whaley, *Phys. Rev. Lett.* **81**, 2594 (1998a).
- [12] P. Zanardi and M. Rasetti, *Mod. Phys. Lett. B* **11**, 1085 (1997a).

- [13] A. J. Skinner, M. E. Davenport, and B. E. Kane, Phys. Rev. Lett. **90**, 087901 (2003).
- [14] G. Burkard, D. Loss, and D. P. DiVincenzo, Phys. Rev. B **59**, 2070 (1999).
- [15] X. Hu and S. Das Sarma, Phys. Rev. A **61**, 062301 (2000).
- [16] K. Andres, R. N. Bhatt, P. Goalwin, T. M. Rice, and R. E. Walstedt, Phys. Rev. B **24**, 244 (1981).
- [17] B. Koiller, X. Hu, and S. Das Sarma, Phys. Rev. Lett. **88**, 027903 (2002).
- [18] B. E. Kane, N. S. McAlpine, A. S. Dzurak, R. G. Clark, G. J. Milburn, H. B. Sun, and H. Wiseman, Phys. Rev. B **61**, 2961 (2000).
- [19] P. Recher, E. Sukhorukov, and D. Loss, Phys. Rev. Lett. **85**, 1962 (2000).
- [20] J. Levy, Phys. Rev. Lett. **89**, 147902 (2002).
- [21] S. Benjamin, [quant-ph/0104034](#).
- [22] J. M. Kikkawa and D. D. Awschalom, Nature **397**, 139 (1999).
- [23] A. Fujiwara and Y. Takahashi, Nature **410**, 560 (2001).
- [24] J. I. Cirac and P. Zoller, Nature **404**, 579 (2000).
- [25] D. Kielpinski, C. Monroe, and D. J. Wineland, Nature **417**, 709 (2002).
- [26] A. J. Leggett, S. Chakravarty, A. T. Dorsey, M. P. A. Fisher, A. Garg, and W. Zwerger, Rev. Mod. Phys. **59**, 1 (1987).

- [27] G. W. Ford, M. Kac, and P. Mazur, *J. Math. Phys.* **6**, 504 (1965).
- [28] B.-L. Hu, J. P. Paz, and Y. Zhang, *Phys. Rev. D* **45**, 2843 (1992).
- [29] L.-M. Duan and G.-C. Guo, *Phys. Rev. Lett.* **79**, 1953 (1997).
- [30] R. H. Dicke, *Phys. Rev.* **93**, 99 (1954).
- [31] E. M. Chudnovsky and D. A. Garanin, *Phys. Rev. Lett.* **93**, 257205 (2004).
- [32] M. Thorwart and P. Hänggi, *Phys. Rev. A* **65**, 012309 (2001).
- [33] D. Ahn, J. H. Oh, K. Kimm, and S. W. Hwang, *Phys. Rev. A* **61**, 052310 (2000).
- [34] X. X. Yi, H. T. Cui, and X. G. Wang, *Phys. Lett. A* **306**, 285 (2003).
- [35] T. Yu and J. H. Eberly, *Phys. Rev. B* **68**, 165322 (2003).
- [36] M. Governale, M. Grifoni, and G. Schön, *Chem. Phys.* **268**, 273 (2001).
- [37] M. J. Storcz and F. K. Wilhelm, *Phys. Rev. A* **67**, 042319 (2003).
- [38] A. Abliz, S.-S. Li, L.-L. Sun, S.-L. Feng, and H.-Z. Zheng, *Phys. Rev. A* **69**, 052309 (2004).
- [39] M. J. Storcz, U. Hartmann, S. Kohler, and F. K. Wilhelm, *Phys. Rev. B* **72**, 235321 (2005a).
- [40] M. J. Storcz, F. Hellmann, C. Hrelescu, and F. K. Wilhelm, *Phys. Rev. A* **72**, 052314 (2005b).

- [41] I. A. Grigorenko and D. V. Khveshchenko, Phys. Rev. Lett. **94**, 040506 (2005).
- [42] J. Q. You, X. Hu, and F. Nori, Phys. Rev. B **72**, 144529 (2005).
- [43] G. M. Palma, K.-A. Suominen, and A. K. Ekert, Proc. R. Soc. London, Ser. A **452**, 567 (1996).
- [44] J. H. Reina, L. Quiroga, and N. F. Johnson, Phys. Rev. A **65**, 032326 (2002).
- [45] B. Ischi, M. Hilke, and M. Dubé, Phys. Rev. B **71**, 195325 (2005).
- [46] F. Benatti, R. Floreanini, and M. Piani, Phys. Rev. Lett. **91**, 070402 (2003).
- [47] D. Braun, Phys. Rev. Lett. **89**, 277901 (2002).
- [48] J. P. Barnes and W. S. Warren, Phys. Rev. Lett. **85**, 856 (2000).
- [49] M. Dubé and P. C. E. Stamp, Int. J. Mod. Phys. B **12**, 1191 (1998).
- [50] F. de Pasquale, G. L. Giorgi, and S. Paganelli, Phys. Rev. A **71**, 042304 (2005).
- [51] P. Zanardi and M. Rasetti, Phys. Rev. Lett. **79**, 3306 (1997b).
- [52] D. Bacon, J. Kempe, D. A. Lidar, and K. B. Whaley, Phys. Rev. Lett. **85**, 1758 (2000).
- [53] J. Kempe, D. Bacon, D. A. Lidar, and K. B. Whaley, Phys. Rev. A **63**, 042307 (2001).
- [54] G. Feher, Phys. Rev. **103**, 834 (1959).
- [55] G. Burkard and D. Loss, Phys. Rev. Lett. **88**, 047903 (2002).

- [56] N. E. Bonesteel, D. Stepanenko, and D. P. DiVincenzo, Phys. Rev. Lett. **87**, 207901 (2001).
- [57] E. I. Rashba, Fiz. Tverd. Tela (Leningrad) **2**, 1224 (1960).
- [58] B. E. Kane, Fortschritte der Physik **48**, 1023 (2000).
- [59] L. S. Levitov, T. P. Orlando, J. B. Majer, and J. E. Mooij, cond-mat/0108266.
- [60] A. Lyakhov and C. Bruder, New J. Phys. **7**, 181 (2005).
- [61] D. Bacon, K. R. Brown, and K. B. Whaley, Phys. Rev. Lett. **87**, 247902 (2001).
- [62] T. J. Osborne and N. Linden, quant-ph/0312141.
- [63] V. Subrahmanyam, Phys. Rev. A **69**, 034304 (2004).
- [64] M. Christandl, N. Datta, A. Ekert, and A. J. Landahl, Phys. Rev. Lett. **92**, 187902 (2004).
- [65] D. Burgarth and S. Bose, Phys. Rev. A **71**, 052315 (2005).
- [66] T. S. Cubitt, F. Verstraete, and J. I. Cirac, quant-ph/0404179.
- [67] J. S. Pratt and J. H. Eberly, Phys. Rev. B **64**, 195314 (2001).
- [68] L. Amico, A. Osterloh, F. Plastina, R. Fazio, and G. M. Palma, Phys. Rev. A **69**, 022304 (2004).
- [69] D. Bruss, N. Datta, A. Ekert, L. C. Kwek, and C. Macchiavello, quant-ph/0411080.

- [70] A. Osterloh, L. Amico, G. Falci, and R. Fazio, *Nature* **416**, 608 (2002).
- [71] T. J. Osborne and M. A. Nielsen, *Phys. Rev. A* **66**, 032110 (2002).
- [72] L.-A. Wu, M. S. Sarandy, and D. A. Lidar, *Phys. Rev. Lett.* **93**, 250404 (2004).
- [73] M. C. Arnesen, S. Bose, and V. Vedral, *Phys. Rev. Lett.* **87**, 017901 (2001).
- [74] M. Asoudeh and V. Karimpour, [quant-ph/0405060](#).
- [75] E. M. Chudnovsky and A. B. Kuklov, *Phys. Rev. B* **67**, 064515 (2003).
- [76] J. P. Paz and W. H. Zurek, in *Coherent Atomic Matter Waves: Les Houches-Ecole d'Été de Physique Théorique 72*, edited by R. Kaiser, C. Westbrook, and F. David (Springer-Verlag, Berlin/Heidelberg, 2000).
- [77] M. H. Devoret, A. Walraff, and J. M. Martinis, [cond-mat/0411174](#).
- [78] J. E. Mooij, T. P. Orlando, L. Levitov, L. Tian, C. H. V. der Wal, and S. Lloyd, *Science* **285**, 1036 (1999).
- [79] D. A. Lidar, I. L. Chuang, and K. B. Whaley, *Phys. Rev. Lett.* **81**, 2594 (1998b).
- [80] D. P. DiVincenzo and D. Loss, *Phys. Rev. B* **71**, 035318 (2005).
- [81] Wolfram, *Mathematica* 5.0.1.
- [82] W. K. Wootters, *Phys. Rev. Lett.* **80**, 2245 (1998).
- [83] E. Pytte, *Phys. Rev. B* **10**, 4637 (1974).
- [84] X. Hu and S. Das Sarma, *Phys. Rev. Lett.* **96**, 100501 (2006).

- [85] K. Fabricius, A. Klumper, U. Löw, B. Büchner, and T. Lorenz,
`cond-mat/9705036`.
- [86] W. Geertsma and D. Khomskii, `cond-mat/0007421`.
- [87] A. G. Redfield, *Adv. Magn. Reson.* **1**, 1 (1965).